(12)

AD

AD-E402 385

Technical Report ARAED-TR-92019

MODELING AND OPTIMIZATION OF SHAPED CHARGE LINER COLLAPSE AND JET FORMATION

Ernest L. Baker

January 1993

US ARMY
ARMAMENT MUNITIONS
& CHEMICAL COMMAND
ARMAMENT RDE CENTER

U.S. ARMY ARMAMENT RESEARCH, DEVELOPMENT AND ENGINEERING CENTER

Armament Engineering Directorate

Picatinny Arsenal, New Jersey

The views, opinions, and/or findings contained in this report are those of the authors(s) and should not be construed as an official Department of the Army position, policy, or decision, unless so designated by other documentation.

The citation in this report of the names of commercial firms or commercially available products or services does not constitute official endorsement by or approval of the U.S. Government.

Destroy this report when no longer needed by any method that will prevent disclosure of its contents or reconstruction of the document. Do not return to the originator.

REPORT DOCUMENTATION PAGE

Form Approved OMB No. 0704-0188

1. AGENCY USE ONLY (Leave blank)	2. REPORT DATE	3. REPORT TYPE AND DATES COVERED
	January 1993	

4. TITLE AND SUBTITLE
MODELING AND OPTIMIZATION OF SHAPED CHARGE LINER COLLAPSE AND JET FORMATION

5. FUNDING NUMBERS

6. AUTHOR(S)

Ernest L. Baker

7. PERFORMING ORGANIZATION NAME(S) AND ADDRESSES(S)

ARDEC, AED
Energetics and Warheads Divsion (SMCAR-AEE-WW)
Picatinny Arsenal, NJ 07806-5000

8. PERFORMING ORGANIZATION REPORT NUMBER

Technical Report ARAED-TR-92019

9.SPONSORING/MONITORING AGENCY NAME(S) AND ADDRESS(S)

ARDEC, IMD
STINFO Br (SMCAR-IMI-I)
Picatinny Arsenal, NJ 07806-5000

10. SPONSORING/MONITORING AGENCY REPORT NUMBER

11. SUPPLEMENTARY NOTES

12a. DISTRIBUTION/AVAILABILITY STATEMENT

Approved for public release, distribution is unlimited.

12b. DISTRIBUTION CODE

13. ABSTRACT (Maximum 200 words)

This research project concentrates on the modeling and optimization of shaped charge liner collapse and jet formation. The research has produced an improved analytical model of shaped charge liner collapse and subsequent jet formation. The improved model was used to investigate the direct distributed parameter optimization of a nonlinear dynamic system using variable metric nonlinear programming. This investigation consisted of optimizing the liner contour required to produce a desired jet profile in the least squares sense. Additionally, a very practical discrete optimization problem was chosen so that the continuum modeling and experimentation could be used to verify the optimization results.

Analytical shaped charge mathematical models have proven very useful in the prediction of shaped charge characteristics while requiring minimal computer time and memory, as well as conservative user effort. Therefore, parametric investigation using analytical shaped charge modeling is both practical and economically feasible. Unfortunately, current analytical models rely on many empirical relationships and do not incorporate constitutive relationships for the various materials. To predict shaped charge characteristics over a broader range of materials and geometries, a more fundamental analytical model was developed.

When parametric investigation becomes practical, the question of parametric optimization naturally arises. The process of shaped charge liner collapse and jet formation is normally modeled as a distributed parameter nonlinear dynamic system. Optimization of distributed parameter systems has traditionally been very difficult. Nonlinear dynamic system behavior adds more complication to an already difficult optimization problem. Recent advances of numerical methods for discrete parametric optimization provide dramatic increases in efficiency and reliability. The application of these new variable metric sequential quadratic programming algorithms to distributed parameter nonlinear dynamic systems should prove to be a significant contribution to the technology base.

14. SUBJECT TERMS

Warheads Explosives Detonation

15. NUMBER OF PAGES
180

16. PRICE CODE

17. SECURITY CLASSIFICATION OF REPORT	18. SECURITY CLASSIFICATION OF THIS PAGE	19. SECURITY CLASSIFICATION OF ABSTRACT	20. LIMITATION OF ABSTRACT
UNCLASSIFIED	UNCLASSIFIED	UNCLASSIFIED	SAR

ACKNOWLEDGMENTS

I am grateful to all my colleagues at Washington State University. I am particularly grateful to Walter Grantham, not only for his guidance and instruction in the areas of controls, optimization, and games theory, but also for his encouragement. I would like to acknowledge the many hours of assistance provided by Hussein Zbib, contributing greatly to the continuum modeling and material acceleration models. I am grateful to Robert Mifflin for providing excellent guidance, personal time, and many publications on nonlinear optimization. Yogendra Gupta provided much of the inspiration for my research on detonation products equations of state.

CONTENTS

CONTENTS (cont)

TABLES

FIGURES

FIGURES

FIGURES

INTRODUCTION

Research Objectives

Mathematical modeling of dynamic systems requires a balance between the opposing factors of model complexity and computational feasibility. To properly predict system behavior, appropriate system complexities must be included in the model. Paradoxically, increased model complexity increases computational requirements and user demands. This paradox is relevant to parametric investigation and becomes extremely crucial in parametric optimization. Because of the iterative nature of parametric optimization, a small increase in model complexity can lead to a large increase in computational demand.

From an optimization standpoint, increased model complexity can be accommodated by decreasing the number of model evaluations required. Therefore, optimization efficiency can be measured in terms of the number of model evaluations required to achieve an optimum. Recent advances of numerical methods for discrete parametric optimization provide dramatic increases in efficiency and reliability. In particular, variable metric sequential quadratic programming has proven to be a particularly successful method for discrete parametric optimization of nonlinear systems. The application of these new variable metric sequential quadratic programming algorithms to distributed parameter nonlinear dynamic systems is expected to yield considerable increases of optimization efficiency.

Shaped charge liner collapse and jet formation is a distributed parameter dynamic system that exemplifies the opposing factors of model complexity and computational feasibility. Two major approaches were taken to the problem of modeling shaped charges. These two approaches are commonly known as continuum modeling and analytic modeling. The first approach involves the direct integration of the conservation equations and is extremely computationally intensive. In the second method mathematical models of separate portions of the liner collapse and jet formation are pieced together to form one final model. This second method is much less computationally intensive, but current analytical models relay on many empirical relationships and do not incorporate constitutive relationships for the various materials. To predict shaped charge characteristics over a broader range of materials and geometries, a more fundamental analytical model was developed.

The research concentrates on the modeling and optimization of shaped charge liner collapse and jet formation. The research objectives are:

- Provide an improved analytical model of shaped charge liner collapse and subsequent jet formation.

- Provide a state of the art variable metric nonlinear optimization program appropriate for the direct distributed parameter optimization.

- Investigate the direct distributed parameter optimization of nonlinear dynamic systems using variable metric nonlinear programming. This investigation was done using the shaped charge analytical model and the state-of-the-art variable metric nonlinear optimization program.

Significance and Justification

Primary motivation for this research project comes from the desire to overcome the impracticalities of distributed parameter nonlinear dynamic systems numerical optimization of shaped charge systems. Currently, such systems are commonly optimized manually using mathematical models or through experimentation. The ability to perform practical numerical optimization on such systems should yield better designs, reduce design time and associated cost, as well as providing a larger variety of design choices. This research demonstrates that both the modeling methodology and the optimization methodology should complement each other to achieve practical distributed parameter nonlinear dynamic system optimization.

Further justification for the research lies in the benefits of an improved analytical shaped charge liner collapse and jet formation model. The inclusion of constitutive relationships for the various materials, as well as a more fundamental approach, should yield more generally applicable shaped charge predictions. Therefore, shaped charge parametric investigations can be performed over a broader range of materials and geometries.

Physical Description

The term "shaped charge" refers to a high explosive charge with a lined cavity. The liner is typically a hollow metal cone or wedge. The high explosive charge is used to collapse the liner in such a way that a high velocity jet is produced from the collapse point. This jet typically stretches to several times its original length before it breaks up into small particles. An illustration of the liner collapse and jetting process is presented in figures 1 and 2. The shaped charge is useful for many applications because of its penetration capability. Armor piercing conventional weapons applications have traditionally provided much of the impetus for the research and development of the shaped charge (ref 1). Shaped charges find use in many industrial applications including wellbore perforation, underwater trenching and demolition, and mining (refs 2 and 3). Any situation where cutting or perforation in a precise and directed manner is essential may be appropriate for shaped charge application.

Shaped Charge Modeling

Typically, two approaches were taken to the problem of modeling shaped charges. The first approach involves the use of finite element or finite difference programs which directly integrate the conservation equations to compute a continuum solution of the explosive detonation, shaped charge liner collapse, and jet formation (ref 1). This approach has the advantage of allowing the analyst to apply many of the known physical properties of different materials and explosives in the modeling scheme. Equation-of-state properties and material strength effects are taken into account. The disadvantage is that a single computation requires a great deal of computer time and memory. The computations involve explosive detonation, as well as extremely high strain and strain rates in the jetting region, normally requiring the addition of numerical artifices to ensure stable numerical solutions. In addition, the preparation of every computer run requires considerable user time and effort. Parametric investigation can be impractical and economically unacceptable. A continuum solution of the Ballistic Research Laboratory (BRL) 81-mm precision shaped charge using the dynamic arbitrary Lagrange Eulerian (ALE) program CALE (ref 4) is presented in figure 3. This calculation took approximately 7 hr on a high performance Silicon Graphics 4D computer work station.

A second approach abandons the idea of directly integrating the conservation equations. Instead, mathematical models describing separate portions of the liner collapse and jet formation are pieced together. The first attempt of this type appears to be the work of Pugh, Eichelberger, and Rostoker (ref 5) who applied the basic jetting theory of Birkhoff, MacDougall, Pugh, and Taylor (ref 6) to the nonsteady collapse phenomena. The resulting formulation is commonly known as the P-E-R jet formation theory (ref 7). The same basic conceptual approach was used in almost all analytical shaped charge models to date. The major impetus has been toward a better understanding and modeling of various processes of the shaped charge phenomena. None the less, current analytical models rely on many empirical fits and do not incorporate constitutive relationships for the various materials (explosive, liner, and confinement) (ref 7). In addition, detailed shock wave propagation, wave interactions, and all other related shock physics are not included in analytical models. However, this method has the obvious advantage of requiring much less computer time and memory, as well as greatly reduced user effort. Thus, parametric investigation becomes both practical and economically feasible.

Parametric Optimization

From the ability to perform parametric investigation, the question of parametric optimization naturally arises. Analytical shaped charge models are distributed parameter nonlinear dynamic systems. Optimization of distributed parameter systems has traditionally been very difficult (ref 8). Nonlinear dynamic system behavior adds

more complication to an already difficult optimization problem. Within the last two decades, there has been a dramatic increase in the efficiency and reliability of optimization methods for almost all discrete parameter problem categories (ref 9). Improvements of discrete nonlinear parametric optimization methods were primarily based on the rigorous application of optimization theory, as well as increased use of numerically stable linear algebraic methods (ref 10). In particular, variable metric sequential quadratic programming has proven to be a particularly successful method for discrete parametric optimization of nonlinear systems (ref 11). This method successively minimizes a quadratic subproblem with linearized constraints. The quadratic cost function matrix (variable metric matrix) is updated for each quadratic subproblem. Currently, the most widely accepted variable metric matrix update is the Broyden, Fletcher, Goldfarb, and Shanno (BFGS) update (refs 10 and 12). The application of a BFCS variable metric sequential quadratic programming algorithm to distributed parameter nonlinear dynamic systems should contribute significantly to the technology base.

Shaped Charge Optimization

Currently, shaped charge design is accomplished through manual iterations using mathematical models and experimentation. This manual process can be extremely time consuming and expensive. The application of parametric numerical optimization to shaped charge modeling should prove to be a valuable contribution to shaped charge technology.

SHAPED CHARGE MODELING

Technical Background

Technical Description

Explosive devices with lined cavities are generally divided into three categories: explosively formed penetrators (EFP), hemispherical shaped charges (Hemi), and conical shaped charges (shaped charge). An EFP consists of a shallow metal plate that is explosively launched. The metal plate is designed to subsequently fold into a penetrator geometry during flight. A Hemi consists of a hemispherical metal liner that is explosively launched and imploded into a penetrator geometry through a squashing process. The term shaped charge is used to designate devices that induce severe liner jetting; whereas, the other categories characterize less severe forms of liner distortion. The idealized phenomena of shaped charge liner collapse and jet formation is described by the separate processes of explosive detonation behavior, liner collapse, collapse point jetting, and jet stretching. An idealized description follows:

- The first state of the functioning of a shaped charge is the explosive detonation (fig. 1). The explosive is detonated at the apex end of the shaped charge device. The explosive may be point initiated, plane wave initiated, or ring initiated by a wave shaper. The explosive detonation front propagates through the explosive with some velocity D. The detonation sweeps across the liner surface with a tangential sweep velocity U_{det} which is greater than D due to the angle of incidence φ.

- The second stage of the process is the interaction of the explosive with a liner. The explosive products high pressures accelerates successive liner elements, effectively bending or turning the liner contour. Each liner element accelerates towards the centerline axis with some changing velocity v and velocity vector angle δ. The velocity vector of the element changes both in magnitude and direction during the acceleration.

- As the liner element reaches the axis, it enters a jetting region. The center of this jetting region on the axis is known as the collapse point. The collapse point moves along the axis at some velocity V_{cl} which changes during the entire jet formation process. Referenced to the collapse point, the liner element enters the jetting region at some angle β with a velocity V_{in}. The liner element mass separates into two parts, each part moving in opposite directions along the axis away from the collapse point. The mass along the axis forward of the collapse point is known as the jet, and the mass along the axis behind the collapse point is known as the slug.

- The induced velocities of the jet V_j and slug V_s change during the entire formation process; therefore, velocity gradients exist along both the jet and slug. In the case of the jet, a negative velocity gradient causes jet stretching and a positive velocity gradient, known as an inverse velocity gradient, causes mass accumulation. This type of mass accumulation typically occurs only at the tip of shaped charge jets, and the rest of the jet stretches at a high rate. The jet will stretch to several times its original length and eventually break up into small particles.

Shaped Charge Modeling

The terms "analytical" shaped charge model or "one-dimensional" shaped charge model (ref 5) are currently used to specify a complete mathematical shaped charge model that incorporates smaller separate mathematical models describing different portions or phenomena of the liner collapse and jet formation. Typically an analytical shaped charge model is divided into separate models describing explosive detonation behavior, liner velocity and acceleration, liner angular projection, collapse point jetting, sonic criterion, jet tip formation, and jet stretching

behavior (refs 13 through 16). A solution is achieved by treating the liner as a set of discrete mass elements, each initially the thickness of the liner. The effects of the model on each of the liner elements are calculated to predict the final jet characteristics.

Explosive Detonation Behavior. Classical detonation theory (refs 17 and 18) provides a stable constant detonation velocity solution for a jump discontinuity from unreacted explosive to completely reacted detonation products. The theory assumes that the detonation products are in thermodynamic equilibrium, and is described by a thermodynamic equation of state. The solution is known as a Chapman-Jouguet detonation, after the first two men to propose such a solution (refs 19 and 20). Chapman and Jouguet independently hypothesized that the flow at the fully reacted state, just behind the detonation front, is sonic with respect to the detonation velocity. Experimentation verifies that on a macroscopic level, Chapman-Jouguet detonations are often rapidly approached after explosive initiation. Normally, detonation behavior modeling in analytical shaped charge models is limited to steady Chapman-Jouguet detonations, and any transient detonation behavior is ignored. The constant Chapman-Jouguet detonation velocities are either derived from experimentation (ref 21) or are calculated using a thermochemical equation of state (refs 22 and 23). When a constant Chapman-Jouguet detonation velocity is assumed, both the time t_o that the detonation reaches each element and the liner sweep velocity at each element $U_{det} = D/\sin\varphi$ can be easily calculated from the initiation and liner geometries.

Liner Acceleration. By assuming a final linear distribution of radial gas velocity, constant radial density distribution, and no axial effect, Gurney (ref 24) derived formulas for the final velocity v_o for exploding cylindrical or spherical shells. These simple formulas can be expressed in the general form

$$v_o = \sqrt{2E_{gur}f(\mu)} = \sqrt{2E_{gur}}\left(\frac{C}{M} + \frac{n}{n+2}\right)^{-\frac{1}{2}}$$

where C is the charge mass, M is the shell mass, n is a spatial geometry constant (0 for rectilinear, 1 for cylindrical, and 2 for spherical), and $\mu \equiv C/M$ is the charge to mass ratio. The value of the Gurney energy E_{gur} is taken as an explosive property and represents the explosive's available specific kinetic energy (normally about 70% of the heat of detonation). This same general approach has been maintained and applied to many different explosives and geometries over the years (refs 7 and 25 through 27). However, it was not until 1983 that formulation was derived for cylindrical imploding geometries. Chou et al. (ref 28) and Hennequin (ref 29) independently derived formulas of the form

$$v_o = \sqrt{2E_{gur}}f(\mu, r_i/ro, l)$$

where v_o is the liner velocity as the liner reaches the axis. r_i and ro are the explosive charge inside the outside radii, respectively. In addition, the total explosive impulse I is taken as a function of r_i and ro for a particular explosive. The parameter I was empirically determined using finite element calculation results. By making the additional assumptions that the detonation products pressure is uniformly distributed, and that there exists at some radius r_x a cylindrical surface within the explosive that never moves, Chanteret (ref 30) developed an equation for the total explosive impulse I. The resulting Gurney formulation is

$$v_o = \sqrt{2E_{gur}} f(\mu, r_i/ro) = \sqrt{2E_{gur}} \left(\frac{r_o^2 - r_i^2}{r_x^2 - r_i^2} \frac{M}{C} + \frac{1}{6} \right)^{-\frac{1}{2}}$$

A determination of r_x, based on a momentum balance across the unmoving cylindrical surface, is also presented (ref 30).

These final velocity forms do not explicitly treat liner acceleration. In the simplest treatment of liner explosive interaction, the acceleration is ignored and the liner velocity is treated as constant. More often, empirical relationships for the liner acceleration are incorporated with a final velocity model. The most commonly used acceleration form, proposed by Randers-Pehrson (ref 31), is exponential

$$v(t) - v_o \left[1 - \exp\left(- \frac{t - t_o}{\tau} \right) \right]$$

Based on initial momentum considerations, Chou et al. (ref 28) suggests the following form for the time constant τ

$$\tau = C_1 \frac{M v_o}{P_{cj}} + C_2$$

The constants C_1 and C_2 are taken as intrinsic explosive parameters and were determined empirically from finite element calculations. Jacobs (ref 32), as well as Jones et al. (ref 33), have developed theoretical acceleration formulas based on ideal gas expansion. No axial effects are included in the formulations and the original Gurney assumptions are included. The relatively simple result of Jones et al., used in the shaped charge model of Baker (ref 16), is

$$v = \sqrt{\frac{2E_{gur}}{B}} \left[1 - \left(\frac{r_m}{r_{mo}} (A - 1) - A \right)^{-BC(\gamma - 1)/M(A + 1)} \right]^{\frac{1}{2}}$$

$$A = \frac{2M/C + 1}{2N/C + 1}, \quad B = \frac{N}{C} A^2 + \frac{M}{C} + \frac{1}{3} \frac{1 + A^3}{1 + A}$$

where r_{mo} is the original charge thickness, $r_m - r_{mo}$ is the distance traveled by the liner, N is the charge case or tamping mass, and γ is the polytropic gas exponent for the detonation products.

Liner Angular Projection. During the liner collapse process, the liner element velocity vector makes an angle δ with the normal to the original liner. Taylor (ref 34) developed a formula relating the projection angle δ with the liner velocity v and the speed U_{det} with which the detonation sweeps across the liner surface

$$\sin \delta = v/2U_{det}$$

In deriving this formula it was assumed that the process was steady-state in a coordinate system moving at the sweep velocity U_{det}. The effect of nonsteady conditions on the projection angle was first addressed empirically by Randers-Pehrson (ref 31). His resulting formula is

$$\delta = \frac{v_o}{2U} - \frac{1}{2}v_o'\tau + \frac{1}{5}(v_o'\tau)^2$$

where the prime denotes differentiation with respect to distance along the axis. Chou et al. (ref 28) derived formulation for the projection angle based purely on liner collapse kinematics. The resulting formulation is

$$\delta = \frac{v_o}{2U} - \frac{1}{2}v_o'\tau + \frac{1}{4}\tau \cdot v_o$$

Both formulas were found to agree well with finite element calculations.

An alternate approach to liner velocity estimation is to produce a projection angle formula based on explosive properties and calculate the liner velocity using the Taylor angle formula (ref 34). Using this approach and assuming steady conditions, Deforneaux and Didler (ref 35) derived a formula for the final projection angle in plane geometry. Kerdraon (ref 36) developed an empirically based final projection angle formula for imploding cylindrical charges of the form

$$2\delta = \frac{1}{1/\varphi + K\rho_o\mu}\, e^{-a\mu/r^2}$$

where φ, K, and a are empirical explosive constants, ρ_o is the initial explosive density, and r is the liner radius.

Collapse Point Jetting. Birkhoff, MacDougall, Pugh, and Taylor (ref 6) published the first theory of shaped charge jet formation in 1948. Recognizing that very high pressures are produced, they neglected liner strength and treated the liner as a nonviscous fluid. Furthermore, they treated the jet formation as a steady-state incompressible hydrodynamic event, producing a constant velocity jet. By applying the steady-state incompressible irrotational Bernoulli equation and momentum conservation in the axial direction to a constant angle liner, they derived the following formulation

$$v_{cl} = v_o \cos\left(\frac{\beta - \alpha}{2}\right) / \sin\beta,\ v_{in} = v_o \cos\left(\frac{\beta + \alpha}{2}\right) / \sin\beta$$

$$v_j = v_{in} + v_{cl},\ v_s = v_{in} - v_{cl}$$

$$m_j = \frac{m}{2}(1 - \cos\beta),\ m_s = \frac{m}{2}(1 - \sin\beta)$$

They noted that although experimental observation agreed qualitatively with many aspects of their theory, constant velocity jets were not observed. In fact, most shaped charges produce a large jet velocity gradient, causing the jet to stretch and eventually break up.

Pugh, Eichelberger, and Rostoker (ref 5) modified the steady-state theory to account for the jet velocity gradient. The resulting theory, known as the P-E-R theory, is based on the same assumptions as the steady-state theory, except that the final collapse velocities of various liner elements are not the same for all elements, but depend on the original element position. Therefore, the liner velocity vector angle β are no longer constants. The resulting formulation is given by

$$v_{cl} = v_o \cos(\beta - \alpha - \delta)/\sin\beta,\ v_{in} = v_o \cos(\alpha + \delta)/\sin\beta$$

$$v_j = v_{in} + v_{cl},\ v_s = v_{in} - v_{cl}$$

$$\frac{dm_j}{dm} = \frac{1}{2}(1 - \cos\beta),\ \frac{dm_s}{dm} = \frac{1}{2}(1 - \sin\beta)$$

The jet and slug velocities may be expressed as

$$v_j = v_o \cos(\alpha + \delta - \beta/2),\ v_s = v_o \cos(\alpha + \delta - \beta/2)/\cos(\beta/2)$$

Normally, from apex to base, the collapse velocity v_o and collapse velocity vector angle δ decrease, whereas the collapse angle β increases. The jet velocity is normally predicted to decrease from tip to tail, causing jet elongation. The P-E-R theory still serves as the basis for almost all current implemented analytical shaped charge models. Several attempts were made to test the P-E-R theory experimentally. Allison and Vitali (ref 37) obtained excellent results using a novel radioactive tracer technique. Eichelberger (ref 38) showed evidence of a systematic discrepancy between theoretical and experimental results. He attributes possible sources of the small discrepancy to finite acceleration, liner collapse internal interaction, and errors in the basic hydrodynamic theory because of the nonsteady character of the phenomenon.

Sonic Criterion. Extremely high velocity shaped charge jets are radially dispersed in fine particulation, instead of continuous and coherent. This effect, known as overdriving, was observed experimentally for shaped charges with small liner angles and large collapse velocities (ref 39). Because the effect occurs at high collapse velocities, compressible effects have long been suspected. Walsh et al. (ref 40) addressed limiting conditions for jet formation by considering supersonic collapse velocities. They concluded that jetting will not occur below some critical turning angle, β_c. The critical turning angle is the angle above which an oblique attached shock cannot form, as proposed by von Neumann (ref 41). This theory predicts when a jet will not be formed, but does not predict the quality of formed jets. Chou et al. (refs 42 and 43) investigated the onset of radial jet dispersion and theorized that supersonic jetting produces radially dispersed jets. Their theory is commonly called the sonic criterion, and is expressed as

$v_{in} < c$	a solid coherent jet occurs
$v_{in} > c,\ \beta > \beta_c$	jetting occurs, but the jet is not coherent
$v_{in} > c,\ \beta < \beta_c$	jetting does not occur

where c is the local speed of sound at the collapse point. The sonic criterion is normally used as a general principle. In practice, it was found that the value of the critical Mach number, based on the speed of sound in the liner material under ambient conditions, is about 1.2 for copper.

Jet Tip Formation. Generally, the induced liner collapse velocity decreases from the liner apex to the liner base, causing a negative jet velocity gradient and consequent jet stretching. However, near the liner apex, liner elements are not at sufficient distances from the axis to accelerate considerably. Consequently, there often exists a region of liner near the apex that produces a positive velocity gradient, due to the increasing element acceleration distances (refs 44 and 45). The positive jet velocity gradient causes jet mass to accumulate at the jet tip. This accumulation is commonly called the jet tip formation process. For purely conical charges, the first 20% to 30% of the liner, from the apex, forms the jet tip which has a much larger radius than the rest of the jet. Carleone et al. (ref 45) suggests that a modified jet tip velocity V_{tip} should be calculated by summing the shaped charge jet momentum and mass, until the newly formed jet velocity equals the summed momentum divided by the summed mass

$$v_{tip} = v_j, \text{ where } v_j = \frac{\int_0^{m_j} v_j dm_j}{\int_0^{m_j} dm_j}$$

Most current analytical shaped charge programs incorporate this shaped charge tip formula.

Jet Stretching Behavior. When a negative jet velocity gradient exists, the shaped charge jet stretches at a high rate. Analytical shaped charge models normally assume that strength effects are negligible and calculate the jet strain based upon the initial jet velocity distribution and Lagrangian mass distribution (ref 45). The position z of each Lagrangian jet element is normally expressed in terms of the initial element jetting position z_o, the current time t, the initial element jetting time t_o, and the element jet velocity V_j

$$z(x,t) = z_o(x) + (t - t_o)v_j(x)$$

The term x represents the liner position of the Lagrangian element. Using the above expression and assuming jet incompressibility, the time dependent jet radius distribution can be determined.

Research

Current analytical shaped charge models rely on many empirical fits and do not incorporate constitutive relationships for the various materials (explosive, liner, and confinement). To predict shaped charge characteristics over a broader range of materials and geometries, a more fundamental shaped charge model (PASCC1 version 3.0) was developed. Research has focused on the development of an improved liner collapse velocity and acceleration model using equation-of-state relationships for the high explosive detonation products. The ability to use the Gurney formulation for the collapse velocity and acceleration modeling was retained for use when desired. In addition, an improved detonation products equation of state was developed and used for both analytic shaped charge and continuum shaped charge modeling.

Explosive Detonation Behavior

The explosive detonation behavior is described by an explosive detonation velocity and detonation products equation of state. The explosive detonation velocity is required to determine initial acceleration times along the shaped charge liner. The detonation products equation is used in the liner acceleration modeling. The Jones-Wilkens-Lee-Baker (JWLB) equation of state was researched, developed, and implemented into the liner acceleration modeling. The JWLB equation of state is also applicable to continuum modeling, and is currently available in several dynamic finite element and finite difference programs including DYNA2D, DYNA3D (ref 46), and CALE (ref 4).

Explosive Detonation Velocity. The explosive detonation velocity is described as a third order polynomial function of axial distance. However, a constant detonation velocity based on the Chapman-Jouguet state is normally assumed. A variable detonation velocity can be used to describe either detonation buildup or explosive composition and density gradient effects (ref 47). The time t_o that the detonation reaches each element and the liner sweep velocity at each element $U_{det} = D/\sin\varphi$ are calculated from the initiation and liner geometries. Currently implemented initiation geometries include point, plane, and peripheral initiation. Currently implemented liner geometries include linear, trumpet, biconic, polynomial, and sinusoid geometries.

Detonation Products Equation of State. Many explosive modeling applications require detonation products equations of state. Modern finite element and finite difference modeling applications often require both overdriven detonation and lower pressure detonation products expansion. Large detonation wave shaping and multiple point initiation are typical overdriven detonation applications. Lower pressure detonation products expansion is required for material acceleration

applications, such as explosively formed penetrators and shaped charges. Current thermodynamic equation of states used in dynamic finite element and finite difference programs are either parameterized to give agreement with thermochemical potential calculations (ref 48) or experimental copper cylinder explosive expansion experiments (refs 49 and 50). Thermochemical potential calculations have proven to be very useful for the prediction of explosive products properties, particularly near and above the Chapman-Jouguet state (refs 22 and 23). Unfortunately, they do not reproduce the products expansion behavior accurately enough for typical warheads design. Currently, thermodynamic equations of state [Jones-Wilkens-Lee (JWL), refs 48 and 49] used for warheads design are normally calibrated to give agreement with copper cylinder explosive expansion experiments. These equations of state have not been calibrated for high pressures above the Chapman-Jouguet state. Experimentation (ref 51) and comparison with thermochemical calculations (figs. 4 through 6) have demonstrated that a poor description of the high pressure region exists. To achieve a suitable equation of state for both overdriven and lower pressure products expansion, an appropriate equation-of-state form has been derived, implemented, and parameterized for a large variety of military explosives (refs 52 and 53).

Equation-of-state Formulation. The equation-of-state form was chosen so as to adequately describe the high pressure regime produced by overdriven detonation, and yet retain the low pressure expansion behavior required for standard material acceleration modeling. To this end, the derived form is based on the JWL equation of state (ref 49) due to its computational robustness, and asymptotic approach to an ideal gas at high expansions. Additional exponential terms and a variable Gruneisen parameter have been added to adequately describe the high pressure region above the Chapman-Jouguet state. The resulting equation-of-state form, named Jones-Wilkens-Lee-Baker (JWLB), is

$$P = \sum_i A_i\left(1 - \frac{\lambda}{R_i V}\right)e^{-R_i V} + \frac{\lambda E}{V} + C\left(1 - \frac{\lambda}{\omega}\right)V^{-(\omega+1)} \qquad (1)$$

where

$$\lambda \equiv \sum_i (A_{\lambda i} V + B_{\lambda i})e^{-R_{\lambda i} V} + \omega \qquad (2)$$

For consistency with the JWL equation of state, V is defined as a specific volume ratio, $V \equiv \rho_o/\rho$ and E is defined as $E \equiv \rho_o e$ where e is the specific internal energy. The JWLB equation-of-state form is based on a first order expansion around the principle isentrope

$$P_s \equiv \sum_i A_i e^{-R_i V} + C V^{-(\omega+1)} \tag{3}$$

Using the Gruneisen parameter

$$\lambda \equiv V \left.\frac{\partial P}{\partial E}\right|_V \tag{4}$$

the isentropic identity

$$P = - \left.\frac{\partial E}{\partial V}\right|_S \tag{5}$$

$$\Rightarrow E_s - E_{cj} = \sum_i \frac{A_i}{R_i} e^{-R_i V} + \frac{C}{\omega} V^{-\omega} - \sum_i \frac{A_i}{R_i} e^{-R_i V_{cj}} - \frac{C}{\omega} V_{cj}^{-\omega} \tag{6}$$

and the Chapman-Jouguet condition

$$E_{cj} = E_o + \frac{1}{2}(P_{cj} + P_o)(V_o - V_{cj}) \equiv \sum_i \frac{A_i}{R_i} e^{-R_i V} - \frac{C}{\omega} V_{cj}^{-\omega} \tag{7}$$

the final form may be derived

$$P = \frac{\lambda}{V}(E - E_s) + P_s$$

$$= \frac{\lambda}{V}\left(E - \sum_i \frac{A_i}{R_i} e^{-R_i V} - \frac{C}{\omega} V^{-\omega}\right) + \sum_i A_i e^{-R_i V} + C V^{-(\omega+1)} \tag{8}$$

$\Rightarrow$ Final form

Some important characteristics of the equation of state are that the Gruneisen parameter λ, is represented as an analytic function of specific volume, V. $\lambda + 1$ approaches a constant adiabatic gamma, $\frac{V}{P}\left.\frac{\partial P}{\partial P}\right|_S = \omega + 1$ for large V, so that ideal gas

behavior is asymptotically approached. The principle isentrope description is essentially identical to JWL, with the exception of an increased number of exponential terms. It was found that for most explosives, three exponential terms (instead of two in JWL) are adequate to describe the principle isentrope over both the high pressure region above the Chapman-Jouguet state and the lower pressure expansion region. It is important to note that the internal energy referencing is defined by equation 7. The value of E_o must be consistent so that

$$E_o = \sum_i \frac{A_i}{R_i} e^{-R_i V_{cj}} + \frac{C}{\omega} V_{cj}^{-\omega} - \frac{1}{2}(P_{cj} + P_o)(V_o - V_{cj}) \tag{9}$$

Normally, the equation-of-state parameters are chosen so the E_o had the value $E_o = \rho_o \Delta H$, where ΔH is the heat of detonation. This is consistent with the initial internal energy of the unreacted material having a value of zero.

Speed of Sound. The generalized speed of sound is often required for implementation into a finite element of finite difference program. The speed of sound may be easily derived as follows

$$\frac{\partial P}{\partial V} = \sum_i A_i \left(\frac{\lambda}{R_i V^2} - \frac{\frac{\partial \lambda}{\partial V}}{R_i V} \right) e^{-R_i V} - \sum_i A_i \left(1 - \frac{\lambda}{R_i V} \right) R_i e^{-R_i V}$$

$$+ C \left(- \frac{\frac{\partial \lambda}{\partial V}}{\omega} \right) V^{-(\omega+1)} - C(\omega + 1) \left(1 - \frac{\lambda}{\omega} \right) V^{-(\omega+2)}$$

$$- \frac{E\lambda}{V^2} + \frac{\lambda}{V} \frac{\partial E}{\partial E} + \frac{E}{V} \frac{\partial \lambda}{\partial V} \tag{10}$$

$$(5),\ (10)\Rightarrow \left.\frac{\partial P}{\partial V}\right|_S = \sum_i A_i \left(\frac{\lambda}{R_i V^2} - \frac{\frac{\partial \lambda}{\partial V}}{R_i V} - R_i + \frac{\lambda}{V} \right) e^{-R_i V}$$

$$-C\left[(\omega + 1)\left(1 - \frac{\lambda}{\omega}\right) + V\frac{\frac{\partial \lambda}{\partial V}}{\omega} \right] V^{-(\omega+2)}$$

$$- \frac{E\lambda}{V^2} - \frac{\lambda}{V} P + \frac{E}{V}\frac{\partial \lambda}{\partial V} \qquad (11)$$

$$c^2 = \left.\frac{\partial P}{\partial \rho}\right|_S \Rightarrow \rho_o c^2 = -V^2 \left.\frac{\partial P}{\partial V}\right|_S \qquad (12)$$

$$\Rightarrow \rho_o c^2 = \sum_i A_i \left(V\frac{\frac{\partial \lambda}{\partial V}}{R_i} - \frac{\lambda}{R_i} + R_i V^2 - \lambda V \right) e^{-R_i V}$$

$$+ C\left[(\omega + 1)\left(1 - \frac{\lambda}{\omega}\right) + V\frac{\frac{\partial \lambda}{\partial V}}{\omega} \right] V^{-\omega} + E\lambda + \lambda V P - EV\frac{\partial \lambda}{\partial V} \qquad (13)$$

$$\frac{\partial \lambda}{\partial V} = \sum_i A_{\lambda i} e^{-R_{\lambda i} V} - \sum_i (A_{\lambda i} V + B_{\lambda i}) R_{\lambda i} e^{-R_{\lambda i} V} \qquad (14)$$

Adiabatic Gamma. Another useful quantity is the generalized adiabatic gamma. The adiabatic gamma may also be easily derived

$$\gamma \equiv -\left.\frac{\partial \ln P}{\partial \ln V}\right|_S = -\frac{V}{P}\left.\frac{\partial P}{\partial V}\right|_S \tag{15}$$

$$(11),\ (15) \Rightarrow \gamma = \frac{1}{P}\sum_i A_i\left(\frac{\partial \lambda}{\partial V}\frac{}{R_i} - \frac{\lambda}{R_i V} + R_i V - \lambda\right)e^{-R_i V}$$

$$+ \frac{C}{P}\left[(\omega+1)\left(1-\frac{\lambda}{\omega}\right) + V\frac{\frac{\partial \lambda}{\partial V}}{\omega}\right]V^{-(\omega+1)} + \frac{E\lambda}{VP} + \lambda - \frac{E}{P}\frac{\partial \lambda}{\partial V} \tag{16}$$

$$(14) \Rightarrow \frac{\partial \lambda}{\partial V} = \sum_i A_{\lambda i} e^{-R_{\lambda i} V} - \sum_i (A_{\lambda i} V + B_{\lambda i}) R_{\lambda i} e^{-R_{\lambda i} V}$$

Principle Isentrope Properties. Often, properties along the isentrope that passes through the Chapman-Jouguet state are of particular interest. The Gruneisen parameter is given by equation 2. The adiabatic gamma is given by

$$(3) \Rightarrow \frac{\partial P_s}{\partial V} = -\sum_i A_i R_i e^{-R_i V} - C(\omega+1)V^{-(\omega+2)} \tag{17}$$

$$(3),(15) \Rightarrow \gamma_S = \frac{V\sum_i A_i R_i e^{-R_i V} + C(\omega+1)V^{-(\omega+1)}}{\sum_i A_i e^{-R_i V} + CV^{-(\omega+1)}} \tag{18}$$

The speed of sound along the principle isentrope is given by

$$(12) \Rightarrow \rho_o c^2 = \sum_i A_i R_i V^2 e^{-R_i V} + C(\omega+1)V^{-\omega} \tag{19}$$

Reacted Products Hugoniot. Another often used state space locus is the reacted products Hugoniot. Assuming the initial pressure to be zero, conservation gives

Mass: $\rho_o D = \rho(D - u)$ (20)

Momentum: $P = \rho_o D u$ (21)

Energy: $$\frac{D^2}{2} + \frac{E_o}{\rho_o} = \frac{P}{\rho} + \frac{(D-u)^2}{2} + \frac{E}{\rho_o} \tag{22}$$

$$(20) \Rightarrow u = \frac{\rho - \rho_o}{\rho} D = (1 - V)D \tag{23}$$

$$(23), (20) \Rightarrow P = \rho_o (1 - V) D^2 = \frac{P}{\rho_o (1 - V)} \tag{24}$$

$$(22),(24) \Rightarrow \frac{P}{2\rho_o(1-V)} + \frac{E_o}{\rho_o} = \frac{P}{\rho} + V^2 \frac{P}{2\rho_o(1-V)} + \frac{E}{\rho_o} \tag{25}$$

$$\Rightarrow E = E_o + \frac{P}{2(1-V)} - V^2 \frac{P}{2(1-V)} - PV$$

$$= E_o + \frac{P}{2(1-V)}\left(1 - V^2 - 2V + 2V^2\right) = E_o \frac{P}{2(1-V)}\left(v^2 - 2V + 1\right)$$

$$= E_o + \frac{P(1-V)}{2} \tag{26}$$

$$(1),(26) \Rightarrow E\left[1 - \frac{\lambda(1-V)}{2V}\right]$$

$$= E_o + \left[\sum_i A_i \left(1 - \frac{\lambda}{R_i V}\right) e^{-R_i V} + C\left(1 - \frac{\lambda}{\omega}\right) V^{-(\omega+1)}\right] \frac{(1-V)}{2} \tag{27}$$

$$\Rightarrow E = \frac{E_o + \left[\sum_i A_i\left(1 - \frac{\lambda}{R_i V}\right)e^{-R_i V} + C\left(1 - \frac{\lambda}{\omega}\right)V^{-(\omega+1)}\right]\frac{(1 - V)}{2}}{\left[1 - \frac{\lambda(1 - V)}{2V}\right]} \qquad (28)$$

Equation-of-State Calibration. A generalized method of parameterization was developed using a nonlinear optimization program (NLQPEB), thermochemical potential calculations (TIGER), and a mathematical cylinder test model (CYLTEST). The NLQPEB program was developed for the solution of generalized nonlinear optimization problems with equality and inequality constraints. The program uses sequential quadratic programming, with a Broyden-Fletcher-Goldfarb-Shanno (BFGS) variable metric update and a modified merit function based on the Kuhn-Tucker (ref 54) first order necessary conditions. NLQPEB is used to solve for a set of JWLB parameters that reproduce the predicted pressure, volume, and Gruneisen parameter principle isentrope behavior in the least squares sense. Additional equality constraints are imposed so that the predicted Chapman-Jouguet state be reproduced, and that CYLTEST reproduces the experimental cylinder expansion test results at prescribed cylinder inside area expansions. The pressure, volume, Gruneisen parameter principle isentrope behavior, and the Chapman-Jouguet state are predicted using the computer program TIGER. Either the Becker-Kistiakowsky-Wilson (BKW) or the Jacobs-Cowperthwaite-Zwisler (JCZ3) (refs 23 and 32) thermochemical equations of state can be used for the calculations. The mathematical cylinder expansion test model, implemented into the program CYLTEST, is a modification of the model suggested by G.I. Taylor (ref 34) using Reynolds hydraulic treatment. The modification includes radial flow and cylinder wall thinning considerations. The copper cylinder expansion tests normally consist of an oxygen free copper tube [10 in. high x 1 in. outside diameter (OD), x 3/4 in. inside diameter (ID)] filled with an explosive charge. The oxygen free copper tube is machined to very precise tolerances, the explosive charge density is carefully measured, and at least two experiments are done to access reproducibility. The explosive charge is detonated from one end and the cylinder wall movement is measured using an ultrahigh speed smear camera. The resulting film record is carefully digitized using a film display digitization unit. The cylinder wall displacement versus time is fit from the digitized results using a polynomial. Normally, the cylinder wall velocity at three and seven inside area expansions is calculated from the polynomial fit, and used for the equation-of-state parameterization routine. The velocity at other area expansions can be calculated and included in the parameterization if deemed important. BKWR and JWLB calculations for octol 75/25 after JWLB parameterization are compared in figures 7 through 9. The resulting JWLB parameters are used to perform dynamic finite element computation of the cylinder expansion experiment. The dynamic finite element results are subsequently

compared to digitized experimental data. DYNA2D cylinder test modeling at 6 μs intervals is shown in figure 10. The material boundaries and computational mesh of the computations is clearly seen. Normally, the Johnson-Cook material model and the Mie-Gruneisen equation of state are used for the copper material description. An experimental streak photography result of displacement versus time for an octol 75/25 cylinder expansion test is presented in figure 11. A comparison of DYNA2D finite element and experimental cylinder expansion test results for octol 75/25 is presented in figure 12. The cylinder test dynamic finite element results agree very closely with the experimental results.

Equation-of-State Parameters. A variety of military explosives were parameterized for the JWLB equation of state. The JWLB parameters presented in table 1 were calibrated using BKW thermochemical potential calculations with the LLNL revised BKW parameters (BKWR) along with ARDEC cylinder test results.

Liner Acceleration

Gurney formulation has often been used for high explosive material acceleration modeling, particularly for liner acceleration applications. A Gurney formulation for liner acceleration option is available in PASCC1. The work of Taylor (ref 34) provides a more fundamental methodology for modeling exploding cylinders, including axial flow effects. His treatment uses Reynolds hydraulic formulation. A modification of his method to include radial detonation products flow effects and cylinder thinning was developed. It was found to give better agreement with cylinder expansion finite element modeling. The model was extended to slab and imploding cylindrical geometries for use in shaped charge analytical modeling. This type of methodology requires an equation of state for the expanding high explosive products. Based on the earlier JWL (ref 49) thermodynamic equation of state, the JWLB thermodynamic equation of state for explosive products was developed to accurately predict the acceleration of metals in finite element and finite difference programs (ref 53). The various equation-of-state constants exist for a large range of common high explosives. The JWLB equation of state provides a convenient constitutive relationship for the explosive products.

Cylinder Expansion. The Taylor (ref 34) long bomb model neglects radial detonation flow effects that can become significant for thin walled cylinders. To include radial flow effects, two models based on the Taylor long bomb model were developed. The first of the two models is based on a products linear radial velocity distribution assumption. The second model is based on a products constant spherical surfaces distribution assumption. The two models were compared to the Taylor long bomb model, as well as to dynamic finite element modeling using the same detonation products JWLB equation of state. The two models reproduce the finite element predictions surprisingly well.

Taylor Heavy Long Cylindrical Bomb Model. Based on the assumption of heavy confinement, Taylor (ref 34) proposed the use of Reynolds hydraulic treatment and isentropic detonation products flow to model a heavy long cylindrical bomb expansion. The model is very similar to the Delaval nozzle theory (ref 17), but includes the momentum of the cylinder wall. A diagram of a Taylor heavy long cylinder expansion due to high explosive detonation is presented in figure 13. It should be noted that flow velocities are relative to the detonation velocity, D. The Taylor heavy long cylindrical bomb model can be represented as follows

Mass: $$\rho_o D r_o^2 = \rho U r^2 \tag{29}$$

Liner momentum: $$2\pi r P = mD\frac{d\Theta}{dt} \tag{30}$$

Energy: $$\rho_o D r_o^2\left(\frac{d^2}{2} + e_o\right) = \rho U r^2\left(\frac{U^2}{2} + e\right) + P U r^2 \tag{31}$$

Principle isentrope: $$P = \sum_i A_i e^{-R_i \rho_o/\rho} + C\,(\rho_o/\rho)^{-(\omega+1)}$$

$$de = -Pd\left(\frac{1}{\rho}\right) \tag{32}$$

Taylor angle: $$v = 2D\sin\frac{\Theta}{2} \tag{33}$$

Based on the assumption of heavy confinement, this model neglects radial flow effects in the detonation products. Additionally, the detonation products flow is assumed to be isentropic from the Chapman-Jouguet state and cylinder strength is neglected. To achieve an easier computational form, the following reduction is made

$$C \equiv \rho_o \pi r_0^2$$

$$(29) \Rightarrow \left(\frac{r}{r_o}\right)^2 = \frac{\rho_o D}{\rho U} \tag{34}$$

$$v_r \equiv \frac{dr}{dt} = D\sin\Theta,\ (2) \Rightarrow 2\pi rP = -mD^2\frac{d\cos\Theta}{dr} = mD^2 2\frac{d\sin^2\frac{\Theta}{2}}{dr}$$

$$(33) \Rightarrow \frac{d\frac{v^2}{2}}{dr} = \frac{2\pi r}{M}P \Rightarrow d\frac{v^2}{2} = \frac{C}{m}\frac{P}{\rho_o}d\left(\frac{r}{r_o}\right)^2$$

$$= \frac{C}{m}d\left[\frac{P}{\rho_o}\left(\frac{r}{r_o}\right)^2\right] - \frac{C}{m}\left(\frac{r}{r_o}\right)^2\frac{1}{\rho_o}dP$$

$$(34) \Rightarrow d\frac{v^2}{2} = \frac{C}{m}D\left[d\left(\frac{P}{\rho U}\right) - \frac{1}{\rho U}dP\right] \qquad (35)$$

$$(31) \Rightarrow \frac{D^2}{2} + e_o = \frac{U_{cj}^2}{2} + \frac{P_{cj}}{\rho_{cj}} + e_{cj} = \frac{U^2}{2} + \frac{P}{\rho} + e$$

$$\Rightarrow \frac{U^2}{2} - \frac{U_{cj}^2}{2} = -\left(\frac{P}{\rho} - \frac{P_{cj}}{\rho_{cj}}\right) - (e - e_{cj}) \qquad (36)$$

$$(32) \Rightarrow de = -Pd\left(\frac{1}{\rho}\right),\ (8) \Rightarrow d\frac{U^2}{2} = -d\frac{P}{\rho} + Pd\frac{1}{\rho} = -\frac{1}{\rho}dP$$

$$\Rightarrow -\frac{1}{\rho U}dP = dU,\ (7) \Rightarrow d\frac{v^2}{2} = \frac{C}{m}D\left[d\left(\frac{P}{\rho U}\right) + dU\right]$$

$$\Rightarrow \frac{v^2}{2} = \frac{C}{m}D\left(\frac{P}{\rho U} - \frac{P_{cj}}{P_{cj}U_{cj}} + U - U_{cj}\right) \qquad (37)$$

$$P_{cj} = \rho_o D\,(D - U_{cj}) = \rho_{cj}U_{cj}(D - U_{cj})$$

$$(37) \Rightarrow \frac{v^2}{2} = \frac{C}{m}D\left[\frac{P}{\rho U} - (D - U)\right] \qquad (38)$$

The final form is as follows

$$P = \sum_i A_i e^{-R_i \rho_o/\rho} + C\,(\rho_o/\rho)^{-(\omega+1)} \tag{39}$$

$$e_{cj} - e = \sum_i \frac{A_i}{\rho_o R_i}\left(e^{-R_i\rho_o/\rho_{cj}} - e^{-R_i\rho_o/\rho}\right)$$

$$+ \frac{C}{\omega\rho_o}\left[(\rho_o/\rho_{cj})^{-\omega} - (\rho_o/\rho)^{-\omega}\right] \tag{40}$$

$$\frac{U^2}{2} = \frac{U_{cj}^2}{2} + \frac{P_{cj}}{\rho_{cj}} - \frac{P}{\rho} + (e_{cj} - e) \tag{41}$$

$$\frac{v^2}{2} = \frac{C}{m} D\left[\frac{P}{\rho U} - (D - U)\right] \tag{42}$$

$$\rho = \frac{\rho_o D}{\left(\frac{r}{r_o}\right)^2} \tag{43}$$

In the case of lighter confinement, radial flow effects can become significant. Therefore, two different methods of radial flow treatment were investigated.

Products Linear Radial Velocity Distribution. One method of including radial flow effects is to assume a linear radial velocity gas distribution along cross sectional planes of the detonation products. A diagram of a products linear radial velocity distribution cylinder expansion due to high explosive detonation is presented in figure 14. Again, it should be noted that flow velocities are relative to the detonation velocity, D. If a linear radial velocity gas distribution is assumed to exist in the detonation products, the following model results

Mass: $$\rho_{cj}U_{cj}r_\delta^2 = \rho U r^2 \tag{44}$$

Axial momentum: $$P_{cj}r_\delta^2 - Pr^2 = \frac{m}{\pi}D^2\cos\Theta - \frac{m}{\pi}D^2 + \rho U^2 r^2 - \rho_{cj}U_{cj}^2 r_\delta^2 \tag{45}$$

Energy: $$\rho_{cj}U_{cj}r_\delta^2\left(\frac{U_{cj}^2}{2} + e_{cj}\right) + P_{cj}U_{cj}r_\delta^2$$

$$= \rho U r^2\left(\frac{U^2}{2} + \frac{v_r^2}{4} + e\right) + PUr^2 \tag{46}$$

Principle isentrope: $$P = \sum_i A_i e^{-R_i\rho_o/\rho} + C\left(\rho_o/\rho\right)^{-(\omega+1)}$$

$$de = -Pd\left(\frac{1}{\rho}\right) \tag{47}$$

Taylor angle: $$v = 2D\sin\frac{\Theta}{2} \tag{48}$$

Tangency: $$\frac{v_r}{U} = \tan\Theta \tag{49}$$

To achieve an easier computational form the following reduction is made

$$(48)\Rightarrow\cos\Theta = 1 - \frac{(v/D)^2}{2},\ \sin\Theta = \left[(v/D)^2 - \frac{(v/D)^4}{4}\right]^{\frac{1}{2}} \tag{50}$$

$$(44)\Rightarrow U = \frac{\rho_{cj}U_{cj}}{\rho(r/r_o)^2} \tag{51}$$

$$(42),\ (50)\Rightarrow P_{cj}r_\delta^2 - Pr^2 = -\frac{m}{\pi}D^2\frac{(v/D)^2}{2} - \rho_{cj}U_{cj}^2 r_\delta^2 + \rho U^2 r^2$$

$$\Rightarrow\frac{v^2}{2} = \left[P(r/r_o)^2 - P_{cj} + \rho(r/r_o)^2U^2 - \rho_{cj}U_{cj}^2\right]\frac{C}{m\rho_o} \tag{52}$$

$$(46)\Rightarrow \frac{U_{cj}^2}{2} + e_{cj} + \frac{P_{cj}}{\rho_{cj}} = \frac{U^2}{2} + \frac{v_r^2}{4} + e + \frac{P}{\rho} \tag{53}$$

$$(53)\Rightarrow \rho = \frac{P}{\frac{U_{cj}^2}{2} + e_{cj} + \frac{P_{cj}}{\rho_{cj}} - \frac{U^2}{2} - \frac{v_r^2}{4} - e} \tag{54}$$

$$(49),(50)\Rightarrow v_r = U\frac{\sin\Theta}{\cos\Theta} = U\frac{\left[(v/D)^2 - \frac{(v/D)^4}{4}\right]^{\frac{1}{2}}}{1 - \frac{(v/D)^2}{2}} \tag{55}$$

The final form is as follows

$$(47)\Rightarrow P = \sum_i A_i e^{-R_i\rho_o/\rho} + C\,(\rho_o/\rho)^{-(\omega+1)} \tag{56}$$

$$(47)\Rightarrow e_{cj} - e = \sum_i \frac{A_i}{\rho_o R_i}\left(e^{-R_i\rho_o/\rho_{cj}} - e^{-R_i\rho_o/\rho}\right) + \frac{C}{\omega\rho_o}\left[(\rho_o/\rho_{cj})^{-\omega} - (\rho_o/\rho)^{-\omega}\right] \tag{57}$$

$$(51)\Rightarrow U = \frac{\rho_{cj}U_{cj}}{\rho(r/r_o)^2} \tag{58}$$

$$(52)\Rightarrow \frac{v^2}{2} = \left[P(r/r_o)^2 - P_{cj} + \rho(r/r_o)^2U^2 - \rho_{cj}U_{cj}^2\right]\frac{C}{m\rho_o} \tag{59}$$

$$(55)\Rightarrow v_r = U\frac{\left[(v/D)^2 - \frac{(v/D)^4}{4}\right]^{\frac{1}{2}}}{1 - \frac{(v/D)^2}{2}} \tag{60}$$

$$(54)\Rightarrow \rho = \frac{P}{\left(\frac{U_{cj}^2}{2} + e_{cj} + \frac{P_{cj}}{\rho_{cj}} - \frac{U^2}{2} - \frac{v_r^2}{4} - e\right)} \tag{61}$$

Products Constant Spherical Surfaces. Another method of including radial flow effects is to assume spherical surfaces of constant thermodynamic properties and mass flow in the detonation products. The detonation products mass flow is assumed to be in a perpendicular direction to the spherical surfaces. A diagram of a products constant spherical surfaces cylinder expansion due to high explosive detonation is presented in figure 15. Again, it should be noted that flow velocities are relative to the detonation velocity, D. If constant detonation product properties are assumed across spherical surfaces, the following model results

Mass: $$\rho_{cj} U_{cj} A_o = \rho U A \tag{62}$$

Axial momentum: $$P_{cj} r_\delta^2 - P r^2 = \frac{m}{\pi} D^2 \cos\Theta - \frac{m}{\pi} D^2 + \rho U^2 r^2 - \rho_{cj} U_{cj}^2 r_\delta^2 \tag{63}$$

Energy: $$\rho_{cj} U_{cj} A_o \left(\frac{U_{cj}^2}{2} + e_{cj}\right) + P_{cj} U_{cj} A_o = \rho U A \left(\frac{U^2}{2} + e\right) + P U A \tag{64}$$

Principle isentrope: $$P = \sum_i A_i e^{-R_i \rho_o/\rho} + C\left(\rho_o/\rho\right)^{-(\omega+1)},\ de = -Pd\left(\frac{1}{\rho}\right) \tag{65}$$

Taylor angle: $$v = 2D\sin\frac{\Theta}{2} \tag{66}$$

Spherical area: $$A = \pi r^2 \frac{2\left(1 - \cos\Theta\right)}{\sin^2\Theta} \tag{67}$$

To achieve an easier computational form, the following reduction is made

$$(66)\Rightarrow \cos\Theta = 1 - 2\sin^2\frac{\Theta}{2} = 1 - 2\left(\frac{v}{2D}\right)^2 = 1 - \frac{(v/D)^2}{2} \tag{68}$$

$$(67),(68)\Rightarrow A = 2\pi r^2 \frac{\frac{(v/D)^2}{2}}{1-\left[1-\frac{(v/D)^2}{2}\right]^2} = \frac{\pi r^2}{1-\left(\frac{v}{2D}\right)^2} \tag{69}$$

$$(62),(69)\Rightarrow \rho = \frac{\rho_{cj}U_{cj}\pi r_\delta^2}{U\pi r^2}\left[1-\left(\frac{v}{2D}\right)^2\right] = \frac{\rho_{cj}U_{cj}}{U(r/r_o)^2}\left[1-\left(\frac{v}{2D}\right)^2\right] \tag{70}$$

$$(63)\Rightarrow P_{cj}r_\delta^2 - Pr^2 = -\frac{m}{\pi}D^2\frac{(v/D)^2}{2} - \rho_{cj}U_{cj}^2 r_\delta^2 + \rho U^2 r^2$$

$$\Rightarrow \frac{v^2}{2} = \left[P(r/r_o)^2 - P_{cj} + \rho(r/r_o)^2U^2 - \rho_{cj}U_{cj}^2\right]\frac{C}{m\rho_o} \tag{71}$$

$$(64)\Rightarrow \frac{U_{cj}^2}{2} + e_{cj} + \frac{P_{cj}}{\rho_{cj}} = \frac{U^2}{2} + e + \frac{P}{\rho}$$

$$\Rightarrow \frac{U^2}{2} = \frac{U_{cj}^2}{2} + e_{cj} + \frac{P_{cj}}{\rho_{cj}} - e - \frac{P}{\rho} \tag{72}$$

The final form is as follows

$$(65)\Rightarrow P = \sum_i A_i e^{-R_i\rho_o/\rho} + C(\rho_o/\rho)^{(\omega+1)} \tag{73}$$

$$(65)\Rightarrow e_{cj} - e = \sum_i \frac{A_i}{\rho_o R_i}\left(e^{-R_i\rho_o/\rho_{cj}} - e^{-R_i\rho_o/\rho}\right)$$

$$+ \frac{C}{\omega\rho_o}\left[(\rho_o/\rho_{cj})^{-\omega} - (\rho_o/\rho)^{-\omega}\right] \tag{74}$$

$$(72)\Rightarrow \frac{U^2}{2} = \frac{U_{cj}^2}{2} + \frac{P_{cj}}{\rho_{cj}} - \frac{P}{\rho} + e_{cj} - e \tag{75}$$

$$(71)\Rightarrow \frac{v^2}{2} = \left[P(r/r_o)^2 - P_{cj} + \rho(r/r_o)^2U^2 - \rho_{cj}U_{cj}^2\right]\frac{C}{m\rho_o} \tag{76}$$

$$(70)\Rightarrow \rho = \frac{\rho_{cj}U_{cj}}{U(r/r_o)^2}\left[1 - \left(\frac{v}{2D}\right)^2\right] \tag{77}$$

Cylinder Model Results Comparison. The three models were solved at a given radial expansion using a second order single variable minimizer (Brent's Algorithm) with the difference of the chosen density (optimization variable) and the calculated density as the optimization cost function. This solution method proved to be extremely fast at all chosen cylinder expansions. The three models were compared using charge to mass ratios of 0.1, 1.0, and 10.0 using the JWLB equation of state and the same octol 75/25 parameters. The resulting plots of cylinder wall velocity versus cylinder radius divided by original radius is presented in figures 16 through 18.

From figure 16 it is clear that the two new models agree very closely with the Taylor (ref 34) long bomb model for thick wall cylinders. This is expected, as radial flow effects should become negligible when the charge to mass ratio becomes small. For the more typical charge to mass ratio of 1.0, the radial flow effects are more significant in figure 17. The two models that include radial flow effects agree very closely, predicting a velocity about 25% lower than Taylor long bomb predicted velocity. Radial flow effects became very significant for very thin walled cylinders as clearly shown in figure 18. Continuum modeling of 1 in. outside diameter, 3/4 in. inside diameter, 10 in. higher copper cylinder tests were done using the explicit second order dynamic Lagrangian finite element program DYNA2D (ref 46). The explosive was modeled using a constant velocity detonation and the JWLB equation of state using the same octol 75/25 parameters used for the analytic cylinder test modeling. The copper cylinder was modeled using the Johnson-Cook strength model and the Mie-Gruneisen equation of state. The finite element mesh size was chosen by increasing the mesh resolution until no noticeable change in cylinder wall velocity histories were noted. A comparison of the finite element predicted inside cylinder wall velocity versus inside cylinder wall radius with the three analytic cylinder model results is presented in figure 19. The two new analytic models agree much better with the finite element predictions than the Taylor (ref 34) long bomb model. The finite element

results clearly show a large initial shock and subsequent cylinder wall ringing not predicted by the analytic models. This difference is expected, as the analytic models do not include any type of shock behavior. Inspection of the finite element flow fields revealed that the detonation products Lagrangian elements tend to remain nearly planar, rather than spherical, indicating that the linear radial velocity distribution assumption tends to be more consistent with the finite element predictions. The inside cylinder wall velocity versus cylinder radius at 1 1/2 in., 5 in. , and 2 in. heights is presented in figure 20. The linear velocity distribution model results are included on the same plot. The velocity histories at the three locations agree very closely with each other, indicating that the cylinder is long enough that a nearly steady process is occurring.

The analytic cylinder models as expressed do not consider the fact that the cylinders thin during radial expansion. One simple way to account for this wall thinning is to assume that the wall cross sectional area remains constant. If this assumption is made, than a simple relationship for the cylinder outside velocity results

$$r_{out}^2 = r_{in}^2 + r_{out_0}^2 - r_{in_0}^2$$

$$v_{out} = \frac{r_{in}}{r_{out}} v_{in}$$

A comparison of finite element prediction of cylinder inside and outside wall velocity versus cylinder wall radius with the products linear radial velocity distribution model results using this simple assumption is shown in figure 21. The analytic results agree very well with finite element predictions.

Slab Geometry. Due to the success of the analytic cylinder expansion modeling, a similar approach was adopted for the modeling of asymmetric high explosive sandwiches in slab geometry. As in the first analytic cylinder test model, a linear radial velocity gas distribution is assumed along cross sectional planes of the detonation products. In addition, based on the work of Chanteret (ref 30) it is assumed that there exists a single axial plane in the detonation products that remains stationary during the entire explosive event. A diagram of the slab geometry model is presented in figure 22. The position r_0 of the stationary detonation products axial plane is defined by considering momentum in the r direction as the material initially accelerates

$$0 = m_1 v_{r1} D + m_2 v_2 D + \frac{1}{2}(v_{r2} + v_{r1})(r_2 - r_1)\rho U$$

$$\Rightarrow \frac{v_{r1}}{v_{r2}} = -\frac{m_2 \frac{C}{2}}{m_1 \frac{C}{2}}$$

$$v_{r0} = 0 = (v_{r2} - v_{r1})\frac{r_0 - r_1}{r_2 - r_1} + v_{r1}$$

$$\Rightarrow r_o = \frac{\left(m_1 + \frac{C}{2}\right) r_1 + \left(m_2 + \frac{C}{2}\right) r_2}{m_1 + m_2 + C}$$

The stationary detonation products axial plane assumption allows the separate solution of the two sandwich sides using a stationary boundary condition at the stationary axial plane location. Using the linear radial velocity gas distribution assumption along with stationary boundary condition for one of the sandwich sides results in the following model formulation

Mass: $$\rho_{cj} U_{cj} (r_{2o} - r_o) = \rho((r_2 - r_o) \quad (78)$$

Axial momentum: $$P_{cj} (r_{2o} - r_o) - P (r_2 - r_o) = m_2 D^2 \cos\Theta_2 - m_2 D^2$$

$$+ \rho U^2 (r_2 - r_o) - \rho_{cj} U_{cj}^2 (r_{2o} - r_o) \quad (79)$$

Energy: $$\rho_{cj} U_{cj} (r_{2o} - r_o)\left(\frac{U_{cj}^2}{2} + e_{cj}\right) + P_{cj} U_{cj} (r_{2o} - r_o)$$

$$= \rho U (r_2 - r_o)\left(\frac{U^2}{2} + \frac{v_{r2}^2}{6} + e\right) + PU(r_2 - r_o) \quad (80)$$

Principle isentrope: $$P = \sum_i A_i e^{-R_i \rho_o/\rho} + C (\rho_o/\rho)^{-(\omega + 1)}$$

$$de = -Pd\left(\frac{1}{\rho}\right) \quad (81)$$

Taylor angle: $$v_2 = 2D\sin\frac{\Theta_2}{2} \quad (82)$$

Tangency: $$\frac{v_{r2}}{U} = \tan\Theta_2 \quad (83)$$

To achieve an easier computational form, the following reduction is made

$$(82)\Rightarrow \cos\Theta_2 = 1 - \frac{(v_2/D)^2}{2},$$

$$\sin\Theta_2 = \left[(v_2/D)^2 - \frac{(v_2/D)^4}{4}\right]^{\frac{1}{2}} \tag{84}$$

$$(78)\Rightarrow U = \frac{\rho_{cj} U_{cj}}{\rho \frac{(r_2 - r_o)}{r_{2o} - r_o}} \tag{85}$$

$$(79),(84)\Rightarrow P_{cj}(r_{2o} - r_o) - P(r_2 - r_o)$$

$$= -m_2 D^2 \frac{(v_2/D)^2}{2} - \rho_{cj} U_{cj}^2 (r_{2o} - r_o) + \rho U^2 (r_2 - r_o)$$

$$\Rightarrow \frac{v_2^2}{2} = \left[P \frac{(r_2 - r_o)}{(r_{2o} - r_o)} - P_{cj} + \rho \frac{(r_2 - r_o)}{(r_{2o} - r_o)} U^2 - \rho_{cj} U_{cj}^2\right] \frac{C_2}{m_2 \rho_o} \tag{86}$$

$$(80)\Rightarrow \frac{U_{cj}^2}{2} + e_{cj} + \frac{P_{cj}}{\rho_{cj}} = \frac{U^2}{2} + \frac{v_{r2}^2}{6} + e + \frac{P}{\rho} \tag{87}$$

$$(87)\Rightarrow \rho = \frac{P}{\frac{U_{cj}^2}{2} + e_{cj} + \frac{P_{cj}}{\rho_{cj}} - \frac{U^2}{2} - \frac{v_{r2}^2}{6} - e} \tag{88}$$

$$(83),(84)\Rightarrow v_{r2} = U\frac{\sin\Theta_2}{\cos\Theta_2} = U\frac{\left[(v_2/D)^2 - \frac{(v_2/D)^4}{4}\right]^{\frac{1}{2}}}{1 - \frac{(v_2/D)^2}{2}} \tag{89}$$

The final form is as follows

$$(81)\Rightarrow P = \sum_i A_i e^{-R_i \rho_o/\rho} + C(\rho_o/\rho)^{-(\omega+1)} \tag{90}$$

$$(81) \Rightarrow e_{cj} - e = \sum_i \frac{A_i}{\rho_o R_i}\left(e^{-R_i\rho_o/\rho_{cj}} - e^{-R_i\rho_o/\rho}\right) + \frac{C_\omega}{\omega\rho_o}\left[(\rho_o/\rho_{cj})^{-\omega} - (\rho_o/\rho)^{\omega}\right] \quad (91)$$

$$(85) \Rightarrow U = -\frac{\rho_{cj}U_{cj}}{\rho\dfrac{(r_2 - r_o)}{(r_{2o} - r_o)}} \quad (92)$$

$$(86) \Rightarrow \frac{v_2^2}{2} = \left[P\frac{(r_2 - r_o)}{(r_{2o} - r_o)} - P_{cj} + \rho\frac{(r_2 - r_o)}{(r_{2o} - r_o)}U^2 - \rho_{cj}U_{cj}^2\right]\frac{C_2}{m_2\rho_o} \quad (93)$$

$$(89) \Rightarrow v_{r2} = U\frac{\left[(v_2/D)^2 - \dfrac{(v_2/D)^4}{4}\right]^{\frac{1}{2}}}{1 - \dfrac{(v_2/D)^2}{2}} \quad (94)$$

$$(88) \Rightarrow \rho = \frac{P}{\dfrac{U_{cj}^2}{2} + e_{cj} + \dfrac{P_{cj}}{\rho_{cj}} - \dfrac{U^2}{2} - \dfrac{v_{r2}^2}{6} - e} \quad (95)$$

Identical formulation may be used for the opposing sandwich side by replacing the sandwich side index. The formulation was solved using the same solution method as used for the three analytical cylinder test models. Again, the solution is compared to dynamic finite element calculations using the JWLB detonation products equation of state and identical octol 70/30 parameters. The explosive sandwich consisted 1/8 in. of copper, 3/4 in. of explosive, and 1/16 in. of copper. A comparison of the dynamic finite element predicted sandwich wall velocities versus wall displacement with the analytic model prediction is presented in figure 23. The agreement is very good with the obvious exception of the dynamic finite element predicted shock phenomenon.

Imploding Cylinder. Due to the success of the slab geometry asymmetric sandwich expansion modeling, a similar approach was adopted for the modeling of imploding cylinder geometry. As in the slab geometry model, a linear radial velocity gas distribution is assumed along cross sectional planes of the detonation products, as well as an assumed single axial cylindrical surface in the detonation products that

remains stationary during the entire explosive event. A diagram of the imploding cylinder geometry is presented in figure 24. The flow velocities are relative to the detonation velocity, D.

The position r_o of the stationary detonation products axial cylindrical surface is again defined by considering momentum in the r direction as the material initially accelerates

$$0 = m_1 v_{r1} D + m_2 v_{r2} D + \frac{1}{3}\frac{\rho U}{r_2 - r_1}\left[v_{r2}\left(2r_2^3 - 3r_1 r_2^2 + r_1^3\right) + v_{r1}\left(r_2^3 - 3r_1^2 r_2 + 2r_1^3\right)\right]$$

$$\Rightarrow \frac{v_{r1}}{v_{r2}} = -\frac{m_2 + \frac{C}{3}\frac{2r_2^3 - 3r_1 r_2^2 + r_1^3}{(r_2^2 - r_1^2)(r_2 - r_1)}}{m_1 + \frac{C}{3}\frac{r_2^3 - 3r_1^2 r_2 + 2r_1^3}{(r_2^2 - r_1^2)(r_2 - r_1)}}$$

$$v_{r0} = 0 = (v_{r2} - v_{r1})\frac{r_0 - r_1}{r_2 - r_1} + v_{r1}$$

$$\Rightarrow r_o = \frac{\left[m_1 + \frac{C}{3}\frac{r_2^3 - 3r_1^2 r_2 + 2r_1^3}{(r_2^2 - r_1^2)(r_2 - r_1)}\right] r_1 + \left[m_2 + \frac{C}{3}\frac{2r_2^3 - 3r_1 r_2^2 + r_1^3}{(r_2^2 - r_1^2)(r_2 - r_1)}\right] r_2}{m_1 + m_2 + C}$$

The stationary detonation products axial cylindrical surface assumption allows the separate solution of the exploding outside and imploding inside using a stationary boundary condition at the stationary axial cylindrical surface location. Using the linear radial velocity gas distribution assumption along with stationary boundary condition for the inside imploding cylinder results in the following model formulation

Mass: $$\rho_{cj} U_{cj}\left(r_{2o}^2 - r_0^2\right) = \rho U\left(r_2^2 - r_0^2\right) \tag{96}$$

Axial momentum $$P_{cj}\left(r_{2o}^2 - r_0^2\right) - P\left(r_2^2 - r_0^2\right) = m_2 D^2 \cos\Theta_2 - m_2 D^2 + \rho U^2\left(r_2^2 - r_0^2\right) - \rho_{cj} U_{cj}^2\left(r_{2o}^2 - r_0^2\right) \tag{97}$$

Energy

$$\rho_{cj}U_{cj}\left(r_{2o}^2 - r_\delta^2\right)\left(\frac{U_{cj}^2}{2} + e_{cj}\right) + P_{cj}U_{cj}\left(r_{2o}^2 - r_\delta^2\right)$$

$$= \rho U\left(r_2^2 - r_\delta^2\right)\left[\frac{U^2}{2} + \frac{v_{r2}^2}{12}\frac{\left(3r_2^2 - 2r_2r_o - r_o^2\right)}{\left(r_2^2 - r_\delta^2\right)} + e\right]$$

$$+ PU\left(r_2^2 - r_\delta^2\right) \tag{98}$$

Principle isentrope

$$P = \sum_i A_i e^{-R_i\rho_o/\rho} + C\left(\rho_o/\rho\right)^{-(\omega+1)}$$

$$de = -Pd\left(\frac{1}{\rho}\right) \tag{99}$$

Taylor angle

$$v_2 = 2D\sin\frac{\Theta_2}{2} \tag{100}$$

Tangency

$$\frac{v_{r2}}{U} = \tan\Theta_2 \tag{101}$$

To achieve an easier computational form, the following reduction is made

$$(100)\Rightarrow\cos\Theta_2 = 1 - \frac{(v_2/D)^2}{2},$$

$$\sin\Theta_2 = \left[(v_2/D)^2 - \frac{(v_2/D)^4}{4}\right]^{\frac{1}{2}} \tag{102}$$

$$(96)\Rightarrow U = \frac{\rho_{cj}U_{cj}}{\rho\dfrac{r_2^2 - r_\delta^2}{\left(r_{2o}^2 - r_\delta^2\right)}} \tag{103}$$

$$(97),(102)\Rightarrow P_{cj}\left(r_{2o}^2 - r_\delta^2\right) - P\left(r_2^2 - r_\delta^2\right)$$

$$= -m_2 D^2 \frac{(v_2/D)^2}{2} - \rho_{cj} U_{cj}^2 \left(r_{2o}^2 - r_\delta^2\right) + \rho U^2 \left(r_2^2 - r_\delta^2\right)$$

$$\Rightarrow \frac{v_2^2}{2} = \left[P\frac{\left(r_2^2 - r_\delta^2\right)}{\left(r_{2o}^2 - r_\delta^2\right)} - P_{cj} + \rho\frac{\left(r_2^2 - r_\delta^2\right)}{\left(r_{2o}^2 - r_\delta^2\right)} U^2 - \rho_{cj} U_{cj}^2 \right] \frac{C_2}{m_2 \rho_o} \tag{104}$$

$$(98)\Rightarrow \frac{U_{cj}^2}{2} + e_{cj} + \frac{P_{cj}}{\rho_{cj}} = \frac{U^2}{2} + \frac{v_{r2}^2}{12}\frac{\left(3r_2^2 - 2r_2 r_o - r_\delta^2\right)}{\left(r_2^2 - r_\delta^2\right)} + e + \frac{P}{\rho} \tag{105}$$

$$(105)\Rightarrow \rho = \frac{P}{\frac{U_{cj}^2}{2} + e_{cj} + \frac{P_{cj}}{\rho_{cj}} - \frac{U^2}{2} - \frac{v_{r2}^2}{12}\frac{\left(3r_2^2 - 2r_2 r_o - r_\delta^2\right)}{\left(r_2^2 - r_\delta^2\right)} - e} \tag{106}$$

$$(101),(102)\Rightarrow v_{r2} = U\frac{\sin\Theta_2}{\cos\Theta_2} = U\frac{\left[(v_2/D)^2 - \frac{(v_2/D)^4}{4}\right]^{\frac{1}{2}}}{1 - \frac{(v_2/D)^2}{2}} \tag{107}$$

The final form is as follows

$$(99)\Rightarrow P = \sum_i A_i e^{-R_i \rho_o/\rho} + C\left(\rho_o/\rho\right)^{-(\omega+1)} \tag{108}$$

$$(99)\Rightarrow e_{cj} - e = \sum_i \frac{A_i}{\rho_i R_i}\left(e^{-R_i\rho_o/\rho_{cj}} - e^{-R_i\rho_o/\rho}\right)$$

$$+ \frac{C}{\omega\rho_o}\left[\left(\rho_o/\rho_{cj}\right)^{-\omega} - \left(\rho_o/\rho\right)^{-\omega}\right] \tag{109}$$

$$(103)\Rightarrow U = \frac{\rho_{cj} U_{cj}}{\rho\frac{\left(r_2^2 - r_\delta^2\right)}{\left(r_{2o}^2 - r_\delta^2\right)}} \tag{110}$$

$$(104)\Rightarrow \frac{v_2^2}{2} = \left[P\frac{(r_2^2 - r_\delta^2)}{(r_{2o}^2 - r_\delta^2)} - P_{cj} + \rho\frac{(r_2^2 - r_\delta^2)}{r_{2o}^2 - r_\delta^2} U^2 - \rho_{cj}U_{cj}^2 \right] \frac{C_2}{m_2\rho_o} \qquad (111)$$

$$(107)\Rightarrow v_{r2} = U \frac{\left[(v_2/D)^2 - \frac{(v_2/D)^4}{4} \right]^{\frac{1}{2}}}{1 - \frac{(v_2/D)^2}{2}} \qquad (112)$$

$$(106)\Rightarrow \rho = \frac{P}{\frac{U_{cj}^2}{2} + e_{cj} + \frac{P_{cj}}{\rho_{cj}} - \frac{U^2}{2} - \frac{v_{r2}^2}{12}\frac{(3r_2^2 - 2r_2r_o - r_\delta^2)}{(r_2^2 - r_\delta^2)} - e} \qquad (113)$$

The formulation was solved using the same solution method as used for the previous acceleration models. Again, the solution is compared to dynamic finite element calculations using the JWLB detonation products equation of state and identical octol 70/30 parameters. The imploding geometry consisted of a 1.8 in. thick, 1 in. outer diameter copper cylinder surrounded by 1 3/4 in. layer of explosive, and then 1/16 in. thick outside copper cylinder. A comparison of the dynamic finite element predicted wall velocities versus wall displacement with the analytic model prediction is shown in figure 25. The predicted imploding velocity falls between the finite element predicted outside and inside surface velocities of the imploding cylinder. The constant wall thickness approximation is not used for velocity calculation of the imploding cylinder wall, as this leads to a predicted infinite velocity for the inside surface. However, the constant wall thickness is used to determine when the imploding cylinder reaches the axis. The agreement is remarkably good with the obvious exception of the dynamic finite element predicted shock phenomenon.

Liner Angular Projection

Liner angular projection is typically based around the Taylor formulation (refs 28, 31, and 34). Another approach is to directly assume that the liner is accelerated in a direction perpendicular to the inside liner surface on which the detonation products act. PASCC1 3.0 was implemented with both methods available. Currently, the Taylor formulation approach is considerably faster.

Jetting Formulation

The jetting formulation implemented in PASCC1 is based on the standard P-E-R jetting theory formulation. The one small difference is that collapse point velocity is calculated from the times and positions that the liner elements reach the

axis. The liner collapse angle β, is than back calculated from the collapse point velocity and the element collapse velocities. This computation method was found to be slightly simpler and faster than the traditional formulation.

PARAMETRIC OPTIMIZATION

Technical Background

Within the last two decades there was a dramatic increase in the efficiency and reliability of optimization methods because of the rigorous application of optimization theory, as well as an increased use of numerically stable linear algebra (ref 10). Discrete parameter optimization problems may be stated in the general form

Minimize: $G(\cdot) \equiv G(\underline{x})$

Subject to: $\underline{g}(\cdot) \equiv \underline{g}(\underline{x}) = \underline{0}$

$\underline{h}(\cdot) \equiv \underline{h}(\underline{x}) \geq \underline{0}$

Almost all modern nonlinear parametric optimization methods attempt to satisfy the Kuhn-Tucker first order necessary conditions (refs 54 and 55)

$$\left.\frac{\partial L}{\partial \underline{x}}\right|_{\underline{x}^*} = \underline{0}$$

$$\underline{g}(\underline{x}^*) = \underline{0}$$

$$\underline{h}(\underline{x}^*) \geq \underline{0}$$

$$\underline{\mu}^T \underline{h}(\underline{x}^*) = \underline{0}$$

$$\underline{\mu}(\underline{x}^*) \geq \underline{0}$$

where

$$L(\underline{x},\lambda,\underline{\mu}) \equiv G(\underline{x}) - \underline{\lambda}^T \underline{g}(\underline{x}) - \underline{\mu}^T \underline{h}(\underline{x})$$

In particular, the very successful method of variable metric sequential quadratic programming satisfies these conditions by minimizing a quadratic subproblem with linearized constraints. Subsequently, the solution vector $\underline{p}$ of the quadratic subproblem is used as a search direction in which a sufficient decrease of a merit function W is found. At this point a new quadratic subproblem is formulated, and the process begins anew. Both the quadratic subproblem and the merit function are based on the Lagrangian function L. The quadratic subproblem cost matrix H, known as the variable metric matrix, is updated for each quadratic subproblem. The first of these "quasi-Newton" algorithms was suggested by Davidon (ref 56), who called it a variable metric method. The name arises from the interpretation of the direction defined by the quadratic subproblem solution vector $\underline{p}$. The length, or metric of $\underline{p}$ is defined by the matrix H. The matrix H changes at every iteration, so the metric of $\underline{p}$ is variable. The entire method is summarized as follows

1. Initialize H, $\underline{x}_o, \left.\frac{\partial G}{\partial \underline{x}}\right|_{\underline{x}_o}, \left.\frac{\partial \underline{g}}{\partial \underline{x}}\right|_{\underline{x}_o}, \left.\frac{\partial \underline{h}}{\partial \underline{x}}\right|_{\underline{x}_o}$

2. Solve for $\underline{p}, \underline{\lambda}, \underline{\mu}$ from the quadratic subproblem

3. Find α to provide a sufficient decrease of $W(\underline{x} + \alpha\underline{p}, \underline{\lambda}, \underline{\mu})$

4. Calculate, $x_{i+1} = \underline{x}_i + \alpha\underline{p}, \left.\frac{\partial G}{\partial \underline{x}}\right|_{\underline{x}_{i+1}}, \left.\frac{\partial \underline{g}}{\partial \underline{x}}\right|_{\underline{x}_{i+1}}, \left.\frac{\partial \underline{h}}{\partial \underline{x}}\right|_{\underline{x}_{i+1}}$

5. Update $H_i \Rightarrow H_{i+1}$

6. Iteration $j = i + 1$, go to 2

Quadratic Subproblem

Normally, it is desired that the subproblem be a positive definite quadratic model of the nonlinear optimization problem with linearized constraints. From a practical point of view, a subproblem model of this form is desirable due to the existence of a unique subproblem solution. From a theoretical point of view, a subproblem of this form is desirable because it has some consistency with the second

order Kuhn-Tucker (ref 54) necessary condition of a positive semi-definite projection of the Hessian onto the active constraint set at the solution (ref 55). Typically, the quadratic subproblem is defined as

$$\text{Minimize:} \quad \frac{1}{2}\underline{p}^T \underline{H}_j \underline{p} + \left.\frac{\partial G}{\partial \underline{x}}\right|_{\underline{x}_i} \underline{p}$$

$$\text{Subject to:} \quad \left.\frac{\partial \underline{g}}{\partial \underline{x}}\right|_{\underline{x}_j} \underline{p} + \underline{g}(\underline{x}_j) = \underline{0}$$

$$\left.\frac{\partial \underline{h}}{\partial \underline{x}}\right|_{\underline{x}_j} \underline{p} + \underline{h}(\underline{x}_j) \geq \underline{0}$$

Solution methods for problems of this type are well established. Stable, reliable methods for solving positive definite quadratic programming problems are discussed by Gill et al. (refs 9 and 10).

Merit Function

The quadratic subproblem is only a local model of the nonlinear optimization problem. The subproblem solution does not guarantee progress toward the nonlinear optimization solution. Therefore, the subproblem solution $\underline{p}$ is used only as a search direction, and a merit function W is introduced to enforce steady progress to the nonlinear solution. The search vector length $||\underline{p}||$ is a convenient initial estimate of the merit function minimum in the direction of $\underline{p}$. The merit function must satisfy a balance between the usually conflicting aims of reducing the cost function and satisfying the problem constraints. Because of the first order necessary conditions, most modern merit functions are based on the Lagrangian function. Probably the most common merit function is a quadratic penalty augmented Lagrangian function (ref 10).

$$W(\underline{x},\underline{\lambda},\underline{\mu}) = G(\underline{x}) - \underline{\lambda}^T \underline{g}(\underline{x}) - \underline{\mu}^T \underline{h}(\underline{x}) + \frac{k}{2}\underline{g}^T(\underline{x})\underline{g}(\underline{x}) + \frac{k}{2}\hat{\underline{h}}^T(\underline{x})\hat{\underline{h}}(\underline{x})$$

where $\hat{\underline{h}}$ is the current set of inequality constraints estimated to be active (as equalities) at the problem solution. This set is called the "working set" and is normally taken as the active set of the quadratic subproblem. Similarly, the Lagrange multipliers obtained from the quadratic subproblem are normally used as current estimates of the nonlinear problem Lagrange multipliers. The penalty parameter k can be any sufficiently large positive constant. However, the parameter k is more often defined in

terms of an increasing series. Difficulties with the penalty parameter choice and slow convergence rates have prompted development of other merit functions. Based on work by Han (ref 57), Powell (ref 12) suggests a merit function of the form

$$\underline{W}(\underline{x},\underline{\lambda},\underline{\mu}) = G(\underline{x}) + |\underline{\lambda}^T \underline{g}(\underline{x})| + |\underline{\mu}^T \underline{h}(\underline{x})|$$

where the Lagrange multipliers obtained from the quadratic subproblem are used and the sufficient decrease search solution must be bounded by the length of the search direction vector $\underline{p}$ obtained from the quadratic subproblem.

Variable Metric Matrix Update

To define the quadratic problem, an update rule is required for the variable metric matrix H. Currently, the most widely accepted variable metric matrix update is the BFGS update (refs 10 and 12). This update is part of a larger family of symmetric rank two updates (ref 9) that approximate the Hessian of unconstrained optimization problems. Several modifications of the update were developed for constrained optimization problems (refs 10 and 12) to prevent the loss of positive definiteness because of the Lagrangian function behavior. To prevent the loss of positive definiteness due to numerical rounding errors, Gill and Murray (ref 58) suggest the use of the Cholesky decomposition R of the variable matrix matrix H($H = R^T R$). The BFGS rank two update of the variable metric matrix H may be expressed as a rank one update of the Cholesky decomposition R.

The simplest BFGS update for constrained optimization may be expressed in the Cholesky decomposition form as

$$\underline{s} = \underline{x}_{i+1} - \underline{x}_i, \quad \underline{u} = R_i^T R_i \underline{s}$$

$$\underline{y}_L = \left.\frac{\partial G^T}{\partial \underline{x}}\right|_{\underline{x}_{i+1}} - \left.\frac{\partial G^T}{\partial \underline{x}}\right|_{\underline{x}_i} - \left.\frac{\partial \underline{g}^T}{\partial \underline{x}}\right|_{\underline{x}_{i+1}} \underline{\lambda} + \left.\frac{\partial \underline{g}^T}{\partial \underline{x}}\right|_{\underline{x}_i} \underline{\lambda} - \left.\frac{\partial \underline{h}^T}{\partial \underline{x}}\right|_{\underline{x}_{i+1}} \underline{\mu} + \left.\frac{\partial \underline{h}^T}{\partial \underline{x}}\right|_{\underline{x}_i} \underline{\mu}$$

$$\underline{y} = \begin{cases} \underline{y}_L & \text{if } \underline{y}_L^T \underline{s} > 0 \\ \underline{u} & \text{if } \underline{y}_L^T \underline{s} \le 0 \end{cases}$$

$$\beta = (\underline{u}^T \underline{s})^{\frac{1}{2}}, \quad \gamma = (\underline{y}^T \underline{s})^{\frac{1}{2}}$$

$$\underline{v} = \frac{1}{\beta} R_i \underline{s}, \quad \underline{w} = \frac{1}{\gamma} \underline{y} - \frac{1}{\beta} \underline{u}$$

$$\bar{R} = R_i + \underline{v}\underline{w}^T$$

$$R_{i+1} = P\bar{R}, \quad P^T P = I$$

where $\bar{R}$ is the nontriangular update and P is an orthogonal factorization that restores R_{i+1} to a triangular matrix (ref 59). This update is equivalent to replacing the new update R_{i+1} with the old update R_i if positive definiteness must be maintained.

Many individuals contend that the practice of maintaining positive definiteness by replacing the new update with the old update reduces optimization efficiency as no gain of curvature information is achieved from these updates. An example of an update form that attempts to overcome this possible problem is Powell's version (ref 12) of the BFGS update for constrained optimization. The Powell BFGS update may be expressed in the Cholesky decomposition form as

$$\underline{s} = \underline{x}_{i+1} - \underline{x}_i, \quad \underline{u} = R_i^T R_i \underline{s}$$

$$\underline{y}_L = \left.\frac{\partial G^T}{\partial \underline{x}}\right|_{\underline{x}_{i+1}} - \left.\frac{\partial G^T}{\partial \underline{x}}\right|_{\underline{x}_i} - \left.\frac{\partial \underline{g}^T}{\partial \underline{x}}\right|_{\underline{x}_{i+1}} \underline{\lambda} + \left.\frac{\partial \underline{g}^T}{\partial \underline{x}}\right|_{\underline{x}_i} \underline{\lambda} - \left.\frac{\partial \underline{h}^T}{\partial \underline{x}}\right|_{\underline{x}_{i+1}} \underline{\mu} + \left.\frac{\partial \underline{h}^T}{\partial \underline{x}}\right|_{\underline{x}_i} \underline{\mu}$$

$$\underline{y} = \begin{cases} \underline{y}_L & \text{if } \underline{y}_L^T \underline{s} \geq 0.2 \underline{u}^T \underline{s} \\ 0.2\underline{u} & \text{if } \underline{y}_L^T \underline{s} \leq 0.2 \underline{u}^T \underline{s} \end{cases}$$

$$\beta = (\underline{u}^T \underline{s})^{\frac{1}{2}}, \quad \gamma = (\underline{y}^T \underline{s})^{\frac{1}{2}}$$

$$\underline{v} = \frac{1}{\beta} R_i \underline{s}, \quad \underline{w} = \frac{1}{\gamma} \underline{y} - \frac{1}{\beta} \underline{u}$$

$$\bar{R} = R_i + \underline{v}\underline{w}^T$$

$$R_{i+1} = P\bar{R}, \quad P^T P = I$$

where $\bar{R}$ is the nontriangular update and P is an orthogonal factorization that restores R_{i+1} to a triangular matrix (ref 57).

Research

A nonlinear optimization program, NLQPEB was developed using a BFGS variable metric sequential quadratic programming methodology. Several different merit functions and variable metric matrix updates were investigated. A subset of the problems defined by Hock (ref 59) and Schittkowski (ref 60) were used to investigate the different merit functions and variable metric matrix updates. The required number of cost function evaluations was used as a measure of numerical optimization performance. A merit function and variable metric matrix update were chosen for final implementation based on the numerical optimization performance. The required number of cost function evaluations for the new nonlinear optimization program NLQPEB were then compared to the results obtained by Schittkowski. Schittkowski has previously compared his nonlinear programming computer program (NLPQL) performance to a large variety of different nonlinear optimization programs. NLPQL was previously demonstrated to perform extremely well, providing an excellent and current database for nonlinear optimization code performance measure.

Quadratic Subproblem

To prevent the loss of positive definiteness because of numerical rounding errors, the Cholesky decomposition R of the variable metric matrix H ($H = R^T R$) was incorporated in NLQPEB. The quadratic subproblem is defined as

Minimize: $$G_l(\underline{p}) \equiv \frac{1}{2}\underline{p}^T R^T R \underline{p} + \underline{f}^T \underline{p}$$

Subject to: $$\underline{g}_l(\underline{p}) \equiv A\underline{p} + \underline{c} = \underline{0}$$

$$\underline{h}_l(\underline{p}) \equiv B\underline{p} + \underline{d} \geq \underline{0}$$

where

$$\underline{f}^T \equiv \left.\frac{\partial G}{\partial \underline{x}}\right|_{\underline{x}_j}$$

$$A \equiv \left.\frac{\partial \underline{g}}{\partial \underline{x}}\right|_{\underline{x}_j}$$

$$\underline{c} \equiv \underline{g}(\underline{x}_j)$$

$$B \equiv \left.\frac{\partial \underline{h}}{\partial \underline{x}}\right|_{\underline{x}_j}$$

$$\underline{d} \equiv \underline{h}(\underline{x}_j)$$

The solution of the quadratic subproblem is achieved by using an active strategy and successive solution of equality constrained quadratic problems.

Active Set Strategy. The active set strategy is the method used to determine the active inequality constraint set that satisfies the Kuhn-Tucker (ref 54) necessary conditions. In the case of positive definite quadratic programming, then necessary conditions are also sufficiency conditions. The Kuhn-Tucker necessary conditions for the quadratic inequality constrained subproblem are

$$\left.\frac{\partial L_l}{\partial \underline{p}}\right|_{\underline{p}^*} = \underline{0}$$

$$\underline{g}_l(\underline{p}^*) = \underline{0}$$

$$\underline{h}_l(\underline{p}^*) \geq \underline{0}$$

$$\underline{\mu}^T \underline{h}_l(\underline{p}^*) = \underline{0}$$

$$\underline{\mu}(\underline{p}^*) \geq \underline{0}$$

where

$$L_l(\underline{p},\underline{\lambda},\underline{\mu}) \equiv G_l(\underline{p}) - \underline{\lambda}^T \underline{g}_l(\underline{p}) - \underline{\mu}^T \underline{h}_l(\underline{p})$$

The active set strategy determines the active inequality constraints by successive solution of equality constrained quadratic subproblems. The active set strategy estimates the active inequality constraints, and an equality constrained quadratic problem is solved using the estimated active constraints. This process is successively repeated until the Lagrange multipliers of the estimated active inequality constraint set are all found to be positive. The active set strategy implemented is as follows

1. Determine feasible constraint working set $\hat{A}, \hat{\underline{c}}$.

   Determine associated nonactive inequality set $\bar{B}, \bar{d}$

2. Solve $\underline{p}, \hat{\underline{\lambda}}$, min. $\frac{1}{2}\underline{p}^T R^T R \underline{p} + \underline{f}^T \underline{p}$, $\hat{A}\underline{p} + \hat{\underline{c}} = 0$

3. If $\hat{\underline{\lambda}} \geq 0$, done

4. Determine most negative $\hat{\lambda}_i$ constraint

   Remove from constraint set $\hat{A}, \hat{\underline{c}}$

   Add to $\bar{B}, \bar{\underline{d}}$

5. Solve $\underline{s}, \hat{\underline{\lambda}}$, min. $\frac{1}{2}\underline{s}^T R^T R \underline{s} + \underline{f}^T \underline{s}$, $\hat{A}\underline{s} + \hat{\underline{c}} = \underline{0}$

6. $\underline{p}_o = \underline{p}$, Solve $\underline{p} = \underline{p}_o + \alpha(\underline{s} - \underline{p}_o)$

   $$\alpha = \min \left\{ 1, -\frac{\bar{\underline{b}}_i^T \underline{p}_o + \bar{d}_i}{\bar{\underline{b}}_i^T (\underline{s} - \underline{p}_o)} \forall_i \middle| \bar{\underline{b}}_i^T \underline{p}_o + \bar{d}_i < 0 \right\}$$

7. If $\alpha \neq 1$, add associated $\bar{\underline{b}}_i, \bar{d}_i$ constraint to $\hat{A}, \hat{\underline{c}}$

   Go to 4

   If $\alpha = 1$, go to 3.

This active set strategy works within a feasible space. A feasible space is defined as any optimization variable state space in which all inequalities and equalities are met. An initial feasible working set is required. To speed computation, the active inequality constraint set is assumed to be the same as the previous quadratic subproblem solution. If this "warm start" set of inequality constraints is not feasible, than a separate initial feasible point procedure is used.

Initial Feasible Point Procedure. The feasible point procedure may be viewed as an additional minimization problem. The linear cost function is defined as the summation of the infeasibility. The constraints are the same constraints as the quadratic subproblem. The main difference between this linear programming problem and a standard linear programming problem is that the cost function changes at every

iteration. The active set strategy for the initial feasible point procedure is essentially identical to the previously described active set strategy. The initial feasible point procedure implemented is as follows:

1. Choose an initial constraint working set $\hat{A}, \hat{\underline{c}}$

   The number of constraints must equal the number of optimization variables.

2. Solve $\underline{p}$, $\hat{A}\underline{p} + \hat{\underline{c}} = \underline{0}$

3. If $\underline{b}_i^T\underline{p} + d_i > 0$, put $\underline{b}_i$, d_i into satisfied set $\bar{B}, \bar{d}$

   Remove from constraint set $\hat{A}, \hat{\underline{c}}$

4. Determine $G_F(\underline{p}) \equiv -\underline{1}^T\left[\hat{B}\underline{p} + \hat{\underline{d}}\right] \Big| \hat{B}\underline{p} + \hat{\underline{d}} < 0$

   If no $\hat{B}\underline{p} + \hat{\underline{d}} < 0$, done

5. Determine $\hat{\underline{\lambda}}$, $\hat{A}^T\hat{\underline{\lambda}} = \hat{B}^T\underline{1}$

6. Determine most negative $\hat{\lambda}_i$ constraint

   Remove from working set $\hat{A}, \hat{\underline{c}}$

7. Add most negative $\left[\hat{B}\underline{p} + \hat{\underline{d}}\right]$ inequality k to working set $\hat{A}, \hat{\underline{c}}$

8. Solve $\underline{s}$, $\hat{A}\underline{s} + \hat{\underline{c}} = \underline{0}$

9. $\underline{p}_o = \underline{p}$, Solve $\underline{p} = \underline{p}_o + \alpha(\underline{s} - \underline{p}_o)$

$$\alpha = \min\left\{1, -\frac{\bar{\underline{b}}_i^T\underline{p}_o + \bar{d}_i}{\bar{\underline{b}}_i^T(\underline{s} - \underline{p}_o)} \; \forall_i \Big| \bar{\underline{b}}_i^T\underline{p}_o + \bar{d}_i < 0\right\}$$

10. If $\alpha \neq 1$, remove k inequality (7.) and add associated $\bar{\underline{b}}_i$, $\bar{d}_i$

    constraint to $\hat{A}, \hat{\underline{c}}$

11. Go to 3.

This procedure is traditionally called "Phase I" of the simplex method for linear programming problems.

Equality Constrained Solution. The inequality constrained quadratic subproblem active set strategy requires the successive solution of an equality constrained quadratic subproblem. The equality constrained quadratic subproblem is defined as:

$$\text{Minimize:} \qquad G_E(\underline{p}) \equiv \frac{1}{2}\underline{p}^T R^T R \underline{p} + \underline{f}^T \underline{p}$$

$$\text{Subject to:} \qquad \underline{g}_E(\underline{p}) \equiv \hat{A}\underline{p} + \hat{\underline{c}} = \underline{0}$$

The Kuhn-Tucker (ref 54) necessary conditions give

$$L_E(\underline{p}, \underline{\lambda}, \underline{\mu}) \equiv G_E(\underline{p}) - \underline{\lambda}^T \underline{g}_E(\underline{p})$$

$$\left.\frac{\partial L_E}{\partial \underline{p}}\right|_{\underline{p}^*} = \underline{p} R^T R^T + \underline{f}^T - \underline{\lambda}^T \hat{A} = \underline{0}$$

$$\underline{g}_E(\underline{p}^*) = \hat{A}\underline{p} + \hat{\underline{c}} = \underline{0}$$

The problem reduces to the solution of

$$\begin{bmatrix} R^T R & \hat{A}^T \\ \hat{A} & 0 \end{bmatrix} \begin{pmatrix} \underline{p} \\ -\underline{\lambda} \end{pmatrix} + \underline{f}^T \hat{\underline{c}} = \underline{0}$$

One method for the solution of this problem is to use an orthogonal factorization

$$AQ = [£0], \; Q^T Q = I$$

$$Q = [Y \; Z]$$

Where A is the original nxm matrix, Q is a mxm matrix, £ is a mxm lower triangular matrix, Y is a mxn submatrix of Q, and Z is a (n-m)xn submatrix of Q. Using the factorization

$$S \equiv \begin{bmatrix} Q & 0 \\ 0 & I \end{bmatrix} = \begin{bmatrix} Y & Z & 0 \\ 0 & 0 & I \end{bmatrix}$$

$$S^T \begin{bmatrix} R^T R^T \hat{A}^T \\ \hat{A} \quad 0 \end{bmatrix} S \begin{Bmatrix} \underline{p} \\ -\underline{\lambda} \end{Bmatrix} = - S^T \begin{Bmatrix} f \\ \hat{\underline{c}} \end{Bmatrix}$$

$$\begin{Bmatrix} \underline{p} \\ -\underline{\lambda} \end{Bmatrix} = S \begin{Bmatrix} \bar{\underline{p}} \\ -\underline{\lambda} \end{Bmatrix}$$

$$\bar{\underline{p}} \equiv \begin{Bmatrix} \underline{p}_Y \\ \underline{p}_Z \end{Bmatrix}, \underline{p} = Y\underline{p}_Y + Z\underline{p}_Z$$

$$\begin{bmatrix} Y^T R^T R Y & Y^T R^T R Z & \mathcal{E}^T \\ Z^T R^T R Y & Z^T R^T R Z & 0 \\ \mathcal{E} & 0 & 0 \end{bmatrix} \begin{Bmatrix} \underline{p}_Y \\ \underline{p}_Z \\ -\underline{\lambda} \end{Bmatrix} = - \begin{Bmatrix} Y^T \underline{f} \\ Z^T \underline{f} \\ \underline{c} \end{Bmatrix}$$

The previous two relations may be expressed in the final form

$$\mathcal{E}\underline{p}_Y = -\underline{c} \Rightarrow \underline{p}_Y$$

$$Z^T R^T R Z \underline{p}_Z = -Z^T f - Z^T R^T R Y \underline{p}_Y \Rightarrow \underline{p}_Z$$

$$\underline{p} = Y\underline{p}_Y + Z\underline{p}_Z \Rightarrow \underline{p}$$

$$\mathcal{E}^T \underline{\lambda} = Y^T (\underline{f} + R^T R \underline{p}) \Rightarrow \underline{\lambda}$$

The solution for this problem is particularly fast because of the triangular form of the Cholesky decomposition update, R. It is interesting to note that the vector components $Y\underline{p}_Y$ and $Z\underline{p}_Z$ may be interpreted as the range space and null space components of $\underline{p}$. The range space component represents the closest step onto the constraints. The null space component represents the step along the constraint functions.

Merit Function

Three different merit functions were investigated. The first merit function investigated was suggested by Powell (ref 12).

$$W(\underline{x}, \underline{\lambda}, \underline{\mu}) = G(\underline{x}) + |\underline{\lambda}^T \underline{g}(\underline{x})| + |\underline{\mu}^T \underline{h}(\underline{x})|$$

This merit function is based on the premise that deviation from constraints should always be penalized, but the penalty should have some consistency with the Lagrange function behavior. One possible disadvantage of this type of merit function is the discontinuous behavior at $\underline{g}(\underline{x}) = \underline{0}$.

The second merit function investigated is a quadratic penalty augmented Lagrangian function

$$W(\underline{x},\underline{\lambda},\underline{\mu}) = G(\underline{x}) - \underline{\lambda}^T\underline{g}(\underline{x}) - \underline{\mu}^T\underline{h}(\underline{x}) + \frac{k}{2}\underline{g}^T(\underline{x})\underline{g}(\underline{x}) + \frac{k}{2}\hat{\underline{h}}^T(\underline{x})\hat{\underline{h}}(\underline{x})$$

This type of merit function is probably the most common merit function used in current nonlinear optimization programs (ref 10). For this merit function, $\hat{\underline{h}}$ is the current set of inequality constraints taken to be active from the quadratic subproblem solution. This type of merit function has the advantage of directly incorporating the local Lagrange function estimate. The penalty parameter k can be any sufficiently large positive constant. However, the parameter k is more often defined in terms of a increasing series. In this way, very small or no initial penalty may be used. If the solution does not meet the constraints within some preset tolerance, the penalty parameter is increased and the optimization is restarted from the local state. The penalty update rule chosen for the merit function is

$$k_{i+1} = a(k_i + b)$$

where a and b are predefined positive constants, and the initial k_0 is set equal to zero. In this way, a nearly pure Lagrangian function may be used.

The third merit function investigated is a quadratic penalty augmented cost function

$$W(\underline{x},\underline{\lambda},\underline{\mu}) = G(\underline{x}) + \frac{k}{2}\underline{g}^T(\underline{x})\underline{g}(\underline{x}) + \frac{k}{2}\hat{\underline{h}}^T(\underline{x})\hat{\underline{h}}(\underline{x})$$

This type of merit function contains no Lagrange function information. Again, $\hat{\underline{h}}$ is the current set of inequality constraints taken to be active from the quadratic subproblem solution. The penalty parameter k was defined as the same increasing series as in the second merit function. In this way, the effect of incorporating a local estimate of the Lagrange multipliers may be assessed by comparing the optimization performance of the second and third merit functions.

Variable Metric Matrix Update

In the case of unconstrained optimization, the variable metric matrix represents an approximation to the cost function Hessian. For constrained optimization the variable metric matrix update represents an approximation to the Hessian of the Lagrangian function of the optimization problem. For this reason, the problem of maintaining a positive definite variable metric matrix is complicated by the constraint function behavior and local approximations to the Lagrange multipliers. Researchers have suggested several different forms of the BFGS variable metric matrix updates for constrained nonlinear programming algorithms. The differences in the update forms reflect different methods of maintaining a positive definite variable metric matrix ($\underline{y}^T\underline{s} > 0$).

Designated as Update 1, Gill's version (ref 10) of the BFGS update for constrained optimization may be generalized in he Cholesky decomposition form as

$$\underline{s} = \underline{x}_{i+1} - \underline{x}_i, \quad \underline{u} = R_i^T R_i \underline{s}$$

$$\underline{y}_L = \left.\frac{\partial G^T}{\partial \underline{x}}\right|_{\underline{x}_{i+1}} - \left.\frac{\partial G^T}{\partial \underline{x}}\right|_{\underline{x}_i} - \left.\frac{\partial \underline{g}^T}{\partial \underline{x}}\right|_{\underline{x}_{i+1}} \underline{\lambda} + \left.\frac{\partial \underline{g}^T}{\partial \underline{x}}\right|_{\underline{x}_i} \underline{\lambda} - \left.\frac{\partial h^T}{\partial \underline{x}}\right|_{\underline{x}_{i+1}} \underline{\mu} + \left.\frac{\partial \underline{h}^T}{\partial \underline{x}}\right|_{\underline{x}_i} \underline{\mu}$$

$$\underline{y}_g = \left(\left.\frac{\partial \underline{g}^T}{\partial \underline{x}}\underline{g}\right|_{\underline{x}_{i+1}} - \left.\frac{\partial \underline{g}^T}{\partial \underline{x}}\underline{g}\right|_{\underline{x}_i}\right) + \left(\left.\frac{\partial \hat{\underline{h}}^T}{\partial \underline{x}}\hat{\underline{h}}\right|_{\underline{x}_{i+1}} - \left.\frac{\partial \hat{\underline{h}}^T}{\partial \underline{x}}\hat{\underline{h}}\right|_{\underline{x}_i}\right)$$

$$\tau_1 = \underline{y}_L^T\underline{s}, \quad \tau_2 = \underline{y}_g^T\underline{s}$$

$$\underline{y} = \begin{cases} \underline{y}_L & \text{if } \tau_1 \geq 0 \\ \underline{y}_L - (1 + k_1)\dfrac{\tau_1}{\tau_2}\underline{y}_g & \text{if } \tau_1 \leq 0,\ \tau_2 \geq 0 \\ \underline{\mu} & \text{if } \tau_1 \leq 0,\ \tau_2 \leq 0 \end{cases} \quad 0 < k_1 < 1$$

$$\beta = (\underline{u}^T\underline{s})^{\frac{1}{2}}, \quad \gamma = (\underline{y}^T\underline{s})^{\frac{1}{2}}$$

$$\underline{v} = \frac{1}{\beta}R_i\underline{s}, \quad \underline{w} = \frac{1}{\gamma}\underline{y} - \frac{1}{\beta}\underline{u}$$

$$\bar{R} = R_i + \underline{v}\underline{w}^T$$

$$R_{i+1} = P\bar{R},\ P^TP = I$$

where $\bar{R}$ is the nontriangular update and P is an orthogonal factorization that restores R_{i+1} to a triangular matrix (ref 58). In this update form, positive definiteness is maintained by incorporating curvature information of the constraint functions in the direction of travel to increase the curvature in directions away from the constants $\left(\underline{y} = \underline{y}_L - k_1\frac{\tau_1}{\tau_2}\underline{y}_g\right)$.

Designated as Update 2, Powell's version (ref 12) of the BFGS update for constrained optimization may be generalized in the Cholesky decomposition form as

$$\underline{s} = \underline{x}_{i+1} - \underline{x}_i,\ \underline{u} = R_i^TR_i\underline{s}$$

$$\underline{y}_L = \left.\frac{\partial G^T}{\partial \underline{x}}\right|_{\underline{x}_{i+1}} - \left.\frac{\partial G^T}{\partial \underline{x}}\right|_{\underline{x}_i} - \left.\frac{\partial \underline{g}^T}{\partial \underline{x}}\right|_{\underline{x}_{i+1}}\underline{\lambda} + \left.\frac{\partial \underline{g}^T}{\partial \underline{x}}\right|_{\underline{x}_i}\underline{\lambda} - \left.\frac{\partial \underline{h}^T}{\partial \underline{x}}\right|_{\underline{x}_{i+1}}\underline{\mu} + \left.\frac{\partial \underline{h}^T}{\partial \underline{x}}\right|_{\underline{x}_i}\underline{\mu}$$

$$\underline{y} = \begin{cases} \underline{y}_L & \text{if } \underline{y}_L^T\underline{s} \geq k_1\underline{u}^T\underline{s} \\ k_1\underline{u} & \text{if } \underline{y}_L^T\underline{s} \leq k_1\underline{u}^T\underline{s} \end{cases} 0 < k_1 < 1$$

$$\beta = (\underline{u}^T\underline{s})^{\frac{1}{2}},\ \lambda = (y^Ts)^{\frac{1}{2}}$$

$$\underline{v} = \frac{1}{\beta}R_i\underline{s},\ \underline{w} = \frac{1}{\lambda}\underline{y} - \frac{1}{\beta}\underline{u}$$

$$\bar{R} = R_i + \underline{v}\,\underline{w}^T$$

$$R_{i+1} = P\bar{R},\ P^TP = I$$

where $\bar{R}$ is the nontriangular update and P is an orthogonal factorization that restores R_{i+1} to a triangular matrix (ref 59). In this update form, positive definiteness is maintained by limiting the reduction of curvature in the direction of travel ($\underline{y} = k_1\underline{u}$).

Two new update forms were developed. Both new updates are based on the notion that separate constraint curvature, Lagrange multiplier approximation, or cost function behavior problems leading to changes required to obtain positive definite

updates should be separately corrected. Designated as Update 3, the first of the two new BFGS updates for constrained optimization that was investigated, may be expressed in the Cholesky decomposition form as

$$\underline{s} = \underline{x}_{i+1} - \underline{x}_i, \; \underline{u} = R_i^T R_i \underline{s}i$$

$$\underline{y}_1 = \left.\frac{\partial G^T}{\partial \underline{x}}\right|_{\underline{x}_{i+1}} - \left.\frac{\partial G^T}{\partial \underline{x}}\right|_{\underline{x}_i}$$

$$\underline{y}_2 = -\left.\frac{\partial \underline{g}^T}{\partial \underline{x}}\right|_{\underline{x}_{i+1}} \underline{\lambda} + \left.\frac{\partial \underline{g}^T}{\partial \underline{x}}\right|_{\underline{x}_i} \underline{\lambda} - \left.\frac{\partial \underline{h}^T}{\partial \underline{x}}\right|_{\underline{x}_{i+1}} \underline{\mu} + \left.\frac{\partial \underline{h}^T}{\partial \underline{x}}\right|_{\underline{x}_i} \underline{\mu}$$

$$\tau_1 = \underline{y}_1^T \underline{s}, \; \tau_2 = \underline{y}_2^T \underline{s}, \; \tau_3 = \tau_1 + \tau_2$$

$$\underline{y} = \left\{ \begin{array}{ll} \underline{y}_1 + \underline{y}_2 & \text{if } \tau_3 > 0 \\ -k_1 \underline{y}_1 + \underline{y}_2 & \text{if } \tau_3 \le 0, \; \tau_1 \le 0, \; \tau_2 > 0 \\ \underline{y}_1 - k_1 \underline{y}_2 & \text{if } \tau_3 \le 0, \; \tau_1 > 0, \; \tau_2 \le 0 \\ -k_1 (\underline{y}_1 + \underline{y}_2) & \text{if } \tau_3 \le 0, \; \tau_1 \le 0, \; \tau_2 \le 0 \end{array} \right| \quad 0 < k_1 < 1$$

$$\beta = (\underline{u}^T \underline{s})^{\frac{1}{2}}, \; \gamma = (\underline{y}^T \underline{s})^{\frac{1}{2}}$$

$$\underline{v} = \frac{1}{\beta} R_i \underline{s}, \; \underline{w} = \frac{1}{\gamma} \underline{y} - \frac{1}{\beta} \underline{u}$$

$$\overline{R} = R_i + \underline{v}\, \underline{w}^T$$

$$R_{i+1} = P\overline{R}, \; P^T P = I$$

where $\overline{R}$ is the nontriangular update and P is an orthogonal factorization that restores R_{i+1} to a triangular matrix (ref 59). Loss of positive definiteness because of cost function behavior ($\tau_1 \le 0$) is treated separately from loss of positive definiteness due to

constraint or Lagrange multiplier approximation behavior ($\tau_2 \leq 0$). Designated as Update 4, the second of the two new BFGS updates for constrained optimization that was investigated may be expressed in the Cholesky decomposition form as

$$\underline{s} = \underline{x}_{i+1} - \underline{x}_i, \; \underline{u} = R_i^T R_i \underline{s}i$$

$$\underline{y}_1 = \left.\frac{\partial G^T}{\partial \underline{x}}\right|_{\underline{x}_{i+1}} - \left.\frac{\partial G^T}{\partial \underline{x}}\right|_{\underline{x}_i}$$

$$\underline{y}_2 = \left.\frac{\partial \underline{g}^T}{\partial \underline{x}}\underline{\lambda}\right|_{\underline{x}_{i+1}} - \left.\frac{\partial \underline{g}^T}{\partial \underline{x}}\underline{\lambda}\right|_{\underline{x}_i} + \left.\frac{\partial \underline{h}^T}{\partial \underline{x}}\underline{\mu}\right|_{\underline{x}_{i+1}} - \left.\frac{\partial \underline{h}^T}{\partial \underline{x}}\underline{\mu}\right|_{\underline{x}_i}$$

$$\tau_1 = \underline{y}_1^T \underline{s}, \; \tau_2 = \underline{y}_2^T \underline{s}, \quad \tau_3 = \tau_1 + \tau_2$$

$$\underline{y} = \left\{ \begin{array}{ll} \underline{y}_1 + \underline{y}_2 & \text{if } \tau_3 > 0 \\ -k_1 \underline{y}_1 + \underline{y}_2 & \text{if } \tau_3 \leq 0, \; \tau_1 \leq 0, \; \tau_2 > 0 \\ \underline{y}_1 - k_1 \underline{y}_2 & \text{if } \tau_3 \leq 0, \; \tau_1 > 0, \; \tau_2 \leq 0 \\ -k_1(\underline{y}_1 + \underline{y}_2) & \text{if } \tau_3 \leq 0, \; \tau_1 \leq 0, \; \tau_2 \leq 0 \end{array} \right\} \quad 0 < k_1 < 1$$

$$\beta = (\underline{u}^T \underline{s})^{\frac{1}{2}}, \; \gamma = (\underline{y}^T \underline{s})^{\frac{1}{2}}$$

$$\underline{v} = \frac{1}{\beta} R_i \underline{s}, \; \underline{w} = \frac{1}{\gamma}\underline{y} - \frac{1}{\beta}\underline{u}$$

$$\overline{R} = R_i + \underline{v}\,\underline{w}^T$$

$$R_{i+1} = P\overline{R}, \; P^T P = I$$

where $\overline{R}$ is the nontriangular update and P is an orthogonal factorization that restores R_{i+1} to a triangular matrix (ref 59). Loss of positive definiteness because of cost function behavior ($\tau_1 \leq 0$) is treated separately from loss of positive definiteness due to constraint or Lagrange multiplier approximation behavior ($\tau_2 \leq 0$).

Test Problems

The test problems used for the nonlinear programming algorithm investigation included a variety of unconstrained, equality constrained and inequality constrained problems. The test problems used for the numerical investigation are summarized in table 2. FN is the problem number (refs 60 and 61). Z is the cost function value at the global solution. NV is the number of optimization variables. NE is the number of equality constraints. NI is the number of inequality constraints. A full description of the optimization problems may be found in references 60 and 61.

Optimization Performance

The three different merit functions and four different variable metric matrix updates were used for the optimization performance investigation. The different merit functions performance were investigated first. Based on the results of the merit function investigation, the Powell merit function form was chosen for a more complete investigation of the four update forms. The final cost function values and optimization performance of the different update forms were then compared to the extremely good performance achieved by Schittkowski (ref 61) using his nonlinear optimization program NLPQL. Based on the comparison, an extremely reliable and high performance merit function and variable metric matrix update combination were chosen for final implementation.

Merit Function. The three different merit functions were investigated using all four different variable metric matrix updates. The same penalty update with an initial value of zero was used for the quadratic penalty augmented merit functions. Three different values of the variable metric matrix update parameter k_1 were used. The results are presented in tables 3 through 5. The number of cost function calls for all of the problem solutions were summed, and the complete data set from the investigation is included in appendix A. The number of function calls including partial derivative calculations is denoted nfp. The number of function calls excluding partial derivative calculations is denoted nf.

In all cases, the three merit functions achieved the same solution within the solution tolerance settings. The merit function form suggested by Powell (ref 12) has an obvious increase in optimization performance, and no ill effects are noted due to the discontinuous nature of the Powell form. Surprisingly, the quadratic penalty cost

function based merit function outperforms the quadratic penalty Lagrangian based merit function. This indicates poor local estimates of the Lagrange multipliers. Based on these results, it was decided to investigate the effect of the initial penalty value on the quadratic penalty cost function based merit function.

The variable metric matrix update parameter k_1 was fixed to 0.1 for this investigation. The initial penalty constant value was set at 0.1, 1, 10, 100, and 1000. The computational results are presented in tables 6 and 7. At first glance of the number of cost evaluation totals, one would be led to believe that some increase of the initial penalty brings the quadratic penalty based merit function performance closer to the performance achieved by the Powell merit function. Closer inspection reveals that with the higher penalty values, FN 218 and 220 failed to achieve solutions because of math domain errors (very large numerical values). Additionally, with the higher penalty values, the number of cost evaluations was decreasing for FN 216, but the correct global minimum is no longer being achieved. It is clear that the penalty value chosen will affect the optimization performance on a single problem, but that no generalized trends exist. A good example is to compare the number of function evaluations required for FN 6 and 7. The number of function evaluations increased with penalty value for FN 6, but the opposite trend is noted for FN 7. Based on these results, the premise that deviation from constraints should always be penalized, but the penalty should have some consistency with the Lagrange function behavior is justified. The penalty scaling provided by the local estimates of the Lagrange multipliers produces a significant increase in optimization performance for the problems investigated.

Variable Metric Matrix Update

The four different variable metric matrix updates were used with the Powell merit function. To fairly compare the updates, the update parameter k_1 was varied for all the updates. The number of cost function calls for all of the problem solutions were summed and the summed results are presented in table 8. The complete data set from the investigation is included in appendix B. The number of cost function evaluations including partial derivative calculations is denoted nfp. The number of cost function evaluations excluding partial derivative calculations is denoted nf.

All four of the update forms demonstrated very efficient and consistent performance. The final cost functions for the four update forms were nearly identical, with the solutions falling within the optimization tolerances. The only exception is the performance of the Powell (ref 62) update with the update parameter k_1 above a value of 0.6. Close inspection of the Powell results reveal that not only are the number of iterations increased with values of k_1 above 0.6, but that the global solutions are no

longer achieved for many of the problems with the value of k_1 above 0.9. This is consistent with the notion that the practice of maintaining positive definiteness by replacing the new update with the old update reduces optimization efficiency. When the value of the update parameter k_1 equals 1, the Powell update replaces the new update with the old update. It is interesting to note that although the Powell update produced the poorest performance with large k_1, it also produced the best optimization performance of the four updates when the parameter k_1 equaled 0.45. The other update forms show considerably less variation over the range of k_1. The Gill (ref 58) update form and the third update form produce slightly better performance than the fourth update form. The best third update form performance is slightly better than the best Gill update form performance. The Gill update form produced slightly less performance variation than the third and fourth update forms. The best performance for each update was achieved with k_1 values of 0.50, 0.45, 0.15, and 0.75, respectively. The corresponding number of cost function evaluations including gradient calculations were 2368, 2269, 2360, and 2429. The corresponding number of cost function evaluations not including gradient calculations were 891, 844, 891, and 912.

Performance Comparison. The final cost function values and optimization performance of the different update forms were compared to the extremely good performance achieved by Hock (ref 59) and Schittkowski (ref 60). The value of k_1 that produced the best optimization performance for each update form was used for the comparison. The final cost function values comparison is presented in table 9. The number of required cost function evaluations is presented in table 10. Schittkowski did not achieve the global solution for four of the problems (FN 2, FN 210, FN 214, and FN 216). The other updates do not achieve the global solution for FN 210 using the initial conditions specified by Schittkowski. Numerical investigation of FN 210 found that the global solution was achieved by starting the problem at other initial conditions.

Final Implementation. Based on the comparison, an extremely reliable and high performance merit function and variable metric matrix update combination were chosen for final implementation. The Powell merit function was chosen, with a slight modification. The final implemented merit form chosen is

$$W(\underline{x},\underline{\lambda},\underline{\mu}) = G(\underline{x}) + |\underline{\lambda}^T \underline{g}(\underline{x})| + |\underline{\mu}^T \underline{h}(\underline{x})|$$

$$+ \frac{k}{2}\underline{g}^T(\underline{x})\underline{g}(\underline{x}) + \frac{k}{2}\underline{\hat{h}}^T(\underline{x})\underline{\hat{h}}(\underline{x})$$

where the Lagrange multipliers obtained from the quadratic subproblem are used and the sufficient decrease search solution must be bounded by a constant times the length of the search direction vector $\underline{p}$ obtained from the quadratic subproblem. This

form is identical to the form suggested by Powell, with the addition of quadratic penalties. However, the quadratic penalties are initially set to zero. If the optimization solution does not meet the required constraints within a specified tolerance, the penalties are increased and the problem is resolved starting from the current state. The penalties are increased using the following update rule

$$k_{i+1} = a(k_i + b)$$

where a and b are predefined positive constants, and the initial k_0 is set equal to zero. In this way, a nearly pure Lagrangian function may be used, but constraint adherence is obtained. In practice, the quadratic penalties are rarely needed, due to adherence to the Kuhn-Tucker (ref 34) necessary conditions at the solution. Although the Powell (ref 12) update form was found to achieve the lowest number of cost evaluations, the result depends strongly on the value of the update parameter k_1 chosen. The Gill (ref 58) variable metric matrix update form was chosen due to the consistent performance over a range of k_1, and the slightly better performance than update 3 and 4 over the range of k_1.

SHAPED CHARGE OPTIMIZATION

Technical Background

Although shaped charge modeling parametric studies are used for the design and analysis of shaped charge devices, surprisingly little investigation has focused on the formal application of numerical optimization methodology to shaped charge modeling. The inclusion of constraint functions is vital for the practical application of shaped charge optimization to real world shaped charge problems. These constraints include physical system constraints, as well as, phenomenological constraints. Typical physical constraints include dimensional constraints, a maximum weight and a specified center of gravity. Typical phenomenological constraints include no jet overdriving (sonic criterion) and no jet mass accumulation (no positive jet gradients). The process of shaped charge liner collapse and jet formation is represented by distributed parameter nonlinear dynamic models. Optimization of distributed parameter systems, has traditionally been very difficult (ref 8). Nonlinear dynamic system behavior adds more complication to an already difficult optimization problem. The Rayleigh-Ritz method (refs 63 and 64) of solving distributed parametric optimization problems is to successively solve discrete optimization subproblems using an analytic series. The idea being that the distributed solution will be approached as the number of series terms increases. If the solution no longer changes considerably with additional series terms, a solution approximation is achieved. This method has the obvious advantage that discrete optimization methodology may be directly applied

to the solution of distributed parameter problems. Recent advances of numerical methods for discrete parametric optimization provide dramatic increases of efficiency and reliability. The application of these new variable metric sequential quadratic programming algorithms to distributed parameter nonlinear dynamic systems should also yield improved optimization efficiency, and prove to be a significant contribution to the technology base.

Research

A shaped charge model was used to investigate the direct distributed parameter optimization of a nonlinear dynamic system using recent variable metric nonlinear programming techniques. Research has centered on the use of a Cholesky decomposition BFGS variable metric sequential quadratic programming algorithm and the Raleigh-Ritz method. Two types of optimization problems were solved: a distributed parameter optimization problem and a discrete optimization problem. The distributed parameter optimization problem was chosen so that the application of distributed optimization could be investigated on a fairly difficult optimization problem with inequality and equality constraints. A very practical discrete optimization problem was chosen so that continuum modeling and experimentation could be used to verify the optimization results. The first optimization problem consisted of determining the required liner contour and thickness profile required to produce a desired jet profile in the least squares sense. The second optimization problem consisted of maximizing the jet tip velocity using detonation wave shaping on an existing liner design. Both problems included optimization constraints.

Liner Geometry Optimization

In many shaped charge applications, particular shaped charge jet characteristics are desired. One method of obtaining desired jet characteristics is to successively modify the shaped charge liner shape until the produced jet characteristics agree to some extent with the desired jet characteristics. The problem is a distributed parametric optimization problem, as the optimization problem consists of determining the function (liner shape) that minimizes a cost function (deviation from desired jet profile). Therefore, it was decided to parametrically optimize initial shaped charge liner contour and thickness to achieve a desired jet profile in the least squares sense. The optimization cost function was chosen to be the sum of the square differences between the desired jet profiles and the predicted jet profiles. Additionally, one equality constraint and one inequality constraint were used. The inequality constraint was defined to specify that no jet inverse velocity gradient exist. The equality constraint was defined to produce a given jet tip velocity.

Problem Definition. For investigative purposes, a fairly difficult optimization problem was defined that included one equality and one inequality constraint. A constant jet radius of 1.5 mm and a linear jet velocity profile from 3 km/s to 8 km/s over 250 mm at 50 μs were chosen as the desired jet profile. An inequality constraint that no jet inverse velocity gradient be produced, and an equality constraint specifying a jet tip velocity of 8 km/s were imposed. The problem definition was expressed as

Optimization variables: a_n, b_n

Minimize: $G(\cdot)$

Subject to: $\underline{g}(\cdot) = \underline{0}$

$$\underline{h}(\cdot) \geq \underline{0}$$

$$r_{liner} = \sum_n a_n x^n, \; T_{liner} = \sum_n b_n x^n$$

$$G(\cdot) \equiv \sum_i \left[r_{jcalc}(z_i) - r_{jdef}\right]^2 + \sum_i \left[v_{jcalc}(z_i) - v_{jdef}(z_i)\right]^2$$

$$r_{jdef} = k_0, \; k_0 \equiv 1.5 \text{ mm}$$

$$v_{jdef}(z_i) = k_1 (z_1 - z_{last}) + k_2, \; k_1 = \frac{8 - 3}{250} \mu s^{-1}, \; k_2 = 3 \text{ mm}/\mu s$$

$$g_1(\cdot) \equiv v_{tip} = v_{jcalc}(z_1) = k_3, \; k_3 = 8 \text{ mm}/\mu s$$

$$h_1(\cdot) \equiv \sum_i \frac{-Dv_i}{(x_{i+1} - x_i)}$$

$$Dv_i = \begin{cases} \left[v_{jcalc}(x_{i+1}) - v_{jcalc}(x_i)\right] & \text{if } v_{jcalc}(x_{i+1}) > v_{jcalc}(x_i) \\ 0 & \text{if } v_{jcalc}(x_{i+1}) < v_{jcalc}(x_i) \end{cases}$$

Where r_{liner} is the liner inside radial position, T_{liner} is the liner thickness, z_i is the axial jet position of the i^{th} Lagrangian element at 50 μs, r_{jcalc} is the calculated jet radius, r_{jdef} is the defined jet radius, v_{jcalc} is the calculated jet velocity, v_{jdef} is the defined jet velocity, and x_i is the original liner axial position of the i^{th} Lagrangian element. The initial geometry used for the optimization was a truncated BRL 81 mm loaded with

octol. The liner thickness and contour were chosen as the optimization variables. The liner thickness and liner profile were described as polynomials. The optimization problem was subsequently run three times using first, second, and third order polynomials to describe the liner thickness and contour.

Optimization Results. The initial liner profile and the resulting first, second, and third order liner profiles is presented in figure 25. The resulting liner angles are larger than the initial liner angle in all three cases. Additionally, the resulting liner contours thin significantly toward the liner bases. The cubic liner design is considerably thinner near the base than the linear and quadratic designs, with a slightly larger initial liner angle and a smaller liner angle near the base. The jet velocity versus jet axial position is at 50 μs is shown in figure 26. The optimized designs all produce the prescribed jet tip velocity of 8 km/s. Although subtle, the desired linear velocity gradient is more closely achieved by the cubic design than the quadratic or linear design. The jet radius versus jet axial position at 50 μs is shown in figure 27. All three polynomial liner designs produced jet profiles closer to the prescribed 1.5 mm constant radius than the original design. Both the cubic and quadratic design results are much closer to the prescribed 1.5 mm radius than the linear design results. Finally, figure 28 presents jet velocity versus initial liner position at 50 μs. As can be seen from the result, the prescribed inequality constraint that no inverse jet gradient exist for the optimized designs has been maintained.

Wave Shaper Optimization

In the previous optimization problem, PASCC1 was demonstrated to parametrically optimize initial liner geometry to obtain desired jet profiles in the least squares sense. No continuum modeling or experimental verification of the PASCC1 optimization results were done. Because of the success of the optimization procedure, it was decided to demonstrate the PASCC1 optimization capabilities on a problem that would be both computationally verified, using continuum modeling, as well as experimentally verified. To demonstrate the application of the PASCC1 parametric optimization capabilities, a fairly practical optimization problem was chosen. Many current shaped charge applications require the highest possible shaped charge jet tip velocity be obtained from a given shaped charge liner and explosive charge design envelope. Detonation wave shaping is often used with a given shaped charge liner geometry to adjust the jet tip velocity. Traditionally, experimental iterations with varied detonation wave shapers are used to obtain an extreme shaped charge design. The standard BRL 81 mm shaped charge is a conservative copper liner shaped charge design that produces a relatively low jet tip velocity. The PASCC1 optimization capability was used to design a detonation wave shaper that maximizes the jet tip velocity within jet tip stability and geometric constraints. Current theory maintains that a jet cannot be formed if the Mach number of

the collapsing liner is above this critical Mach number. An overdriven jet is characterized by splashing, hollowness, radial displacement, and fine particulation. For copper a critical Mach number of 1.23 based on the static sound speed is often used. The BRL 81 mm shaped charge is considered a conservative design (well below overdriven); whereas, many modern shaped charge designs are extreme (very nearly overdriven).

Problem Definition. The shaped charge jet tip velocity was chosen as the function to be maximized. The detonation wave shaper radius and axial location were chosen as the optimization variables. To assure a coherent jet tip, an inequality constraint that the liner collapse Mach number based on the static speed of sound not exceed 1.23 was imposed. To assure a jet with reasonable mass, an inequality constraint that the jet profile radius at 50 μs be greater than 1/2 mm for the entire jet was imposed. An additional inequality constraint of no jet inverse velocity gradient was also used. To assure proper detonation transfer around the wave shaper, a geometric inequality constraint was imposed on the wave shaper radius to be no greater than 34.15 mm (1.4 in. smaller than the charge radius). Finally, geometric inequality constraints that the wave shaper position could not be in front of the liner apex position and that the wave shaper radius could not be negative were imposed. The problem definition was expressed as:

Optimization variables: r_{ws}, x_{ws}

Minimize: $G(\cdot)$

Subject to: $\underline{h}(\cdot) \geq \underline{0}$

$$G(\cdot) \equiv -v_{tip} = -v_{jcalc}(z_1)$$

$$h_1(\cdot) \equiv k_0 - \max[v_{cl}(x_i)]/C_0,\ k_0 = 1.23,\ C_0 = 3.98\ \text{mm/}\mu\text{s}$$

$$h_2(\cdot) \equiv \sum_i Dr_i$$

$$Dr_i = \begin{cases} r_{jcalc}(z_i) - k_1 & \text{if } r_{jcalc}(x_i) < k_1 \\ & k_1 \equiv 0.5\ \text{mm} \\ 0 & \text{if } r_{jcalc}(x_1) > k_1 \end{cases}$$

$$h_3(\cdot) \equiv \sum_i \frac{-Dv_i}{(x_{i+1} - x_i)}$$

$$Dv_i = \begin{cases} [v_{jcalc}(x_{i+1}) - v_{jcalc}(x_i)] & \text{if } v_{jcalc}(x_{i+1}) > v_{jcalc}(x_i) \\ 0 & \text{if } v_{jcalc}(x_{i+1}) < v_{jcalc}(x_i) \end{cases}$$

$$h_4(\cdot) \equiv k_2 - r_{ws},\ k_2 = 34.15 \text{ mm}$$

$$h_5(\cdot) \equiv x_1 - x_{ws}$$

$$h_6(\cdot) \equiv r_{ws}$$

where r_{liner} is the liner inside radial position, T_{liner} is the liner thickness, z_i is the axial jet position of the i^{th} Lagrangian element at 50 μs, r_{jcalc} is the calculated jet radius, r_{jdef} is the defined radius, v_{jcalc} is the calculated jet velocity, v_{jdef} is the defined jet velocity, and x_i is the original liner axial position of the i^{th} Lagrangian element. Octol 70/30 was used for the explosive charge. The optimization problem was subsequently run using the BRL 81 mm with an extremely small wave shaper introduced for the initial geometry. The initial wave shaper was placed at the initiation point of the original design so that the initial conditions reproduce the original design predicted jet characteristics. The original BRL 81 mm shaped charge geometry, as used in the optimization initial conditions is shown in figure 30.

Optimization Results. The optimization problem ran approximately 7 min. on a Silicon Graphics 4D 340 GTX computer work station. A predicted jet tip velocity of 10.1 km/s was achieved for the final optimized design. The final optimized wave shaper geometry is shown in figure 31. The geometric wave shaper maximum radius inequality constraint is clearly active at the solution. The jet velocity versus initial liner axial position for the original and final optimized design is shown in figure 32. The 10.1 km/s jet tip velocity of the optimized design can be clearly seen. The result also shows that the prescribed inequality constraint of no inverse jet gradient for the optimized design was maintained. The produced collapse Mach number versus jet velocity for the original and the final optimized design is shown in figure 33. The result clearly shows that the collapse Mach number inequality constraint is active at the solution. The collapse Mach number associated with the jet tip is at the prescribed 1.23 limit. The optimization problem was rerun using a variety of initial wave shaper geometries. Although the final wave shaper geometry varied to some extent, the final jet tip velocity was always very similar in all cases.

Computational Verification. Continuum modeling was used to verify the optimized design. Both the original and the optimized design were modeled using the arbitrary Lagrange Eulerian program, CALE (ref 4). The copper liner, wave shaper, and aluminum body were modeled using the Stinberg-Guinan rate independent material model (ref 65). The Jones-Wilkens-Lee-Baker product equation of state (ref 53) was used to model the octol 70/30 explosive. The air was modeled using the constant gamma equation of state. Material boundaries, mesh position, and pressure contours at 10 μs intervals for the original and optimized designs are presented in figures 34 and 35. The CALE calculations produced a jet tip velocity of 8.38 km/s for the original design and 9.79 km/s for the optimized design.

Experimentation. Four cast octol 70/30 BRL 81 mm shaped charges were fabricated. The optimized design shaped charges were fabricated by machining out a cylindrical cavity in the explosive charge, placing the copper wave shaper into the cavity and finally replacing the machined explosive cavity with a machined cylinder of explosive. Long standoff (20 CD) x-rays were used to experimentally determine the jet tip velocity. Jet tip region traces from the x-rays at approximately 7 CD standoff are shown in figure 36.

The original design produced a jet tip velocity of 8.4 km/s. The optimized design produced a jet tip velocity of 9.8 km/s. Both the original design and the optimized design produced extremely straight jets, indicating very good shaped charge fabrication and loading. The original design produced jet tip is relatively massive. The optimized design produces a relatively thin jet tip, indicating no jet inverse gradient. Close inspection of the x-rays reveals that the optimized design jet tip is hollow, indicating that the jet is very close to being overdriven. Finally, the optimized design was tested for penetration capability into steel at an 8 CD standoff. The optimized design produced a 19% increase of penetration over the original design baseline penetration.

Results Comparison. A comparison of the PASCC1, CALE, and experimental BRL 8 1 mm precision shaped charge jet tip velocity results for the original and optimized designs are shown in table 11. The PASCC1, CALE, and experimental jet tip velocities agree fairly closely for both the original and the optimized shaped charge designs. The predicted and experimental jet tip geometries differ somewhat. The original design produced jet tip is relatively massive, which disagrees with the PASCC1 calculation that predicts no jet inverse gradient. This is not unexpected, as the PASCC1 calculation does not include the liner apex hemispherical cap. The CALE calculation of the original design agrees more closely with the experiment, although there is a small amount of jetting material ahead of the main jet tip that is not predicted in the CALE calculation. The optimized design predicted jet tip characteristics are more consistent with the experimental results. The experimental result

indicates very little jet inverse velocity gradient. The fine details of the CALE predicted jet tip geometry is very similar to the experimental result, with the exception that no jet hollowness is predicted. In all, the PASCC1, CALE, and experimental results agree fairly well.

CONCLUSIONS

Shaped Charge Modeling

To predict shaped charge characteristics over a broader range of materials and geometries, a more fundamental shaped charge model (PASCC1 version 3.0) was developed. Research has focused on the development of improved liner collapse velocity and acceleration models. These more physically based models were incorporated in PASCC1. In addition, an improved detonation products equation of state was researched, developed, and calibrated for a variety of military high explosives. The Jones-Wilkens-Lee-Baker equation of state provides an improved description for the overdriven detonation regime, while maintaining lower pressure behavior. The new equation of state is used for the improved liner collapse modeling, as well as for continuum modeling in the computer programs DYNA2D, DYNA3D, and CALE.

Parametric Optimization

A nonlinear optimization program (NLQPEB), was researched and developed for use on problems with computationally intensive cost function evaluations. NLQPEB uses a Broyden, Fletcher, Goldfarb, and Shanno update (BFGS) variable metric sequential quadratic programming methodology. Several different merit functions and variable metric matrix updates were investigated. A subset of the problems defined by Hock and Schittkowski were used to investigate the different merit functions and variable metric matrix updates. The required number of cost function evaluations was used as a measure of numerical optimization performance. A comparison of the final cost function values was used as a measure of optimization routine robustness. Based on these measures, an extremely reliable and high performance merit function and variable metric matrix update combination were chosen for final implementation. The merit function optimization performance results indicate that deviation from constraints should always be penalized, but the penalty should have some consistency with the Lagrange function behavior. The variable metric matrix update optimization performance results indicate that the practice of maintaining positive definiteness by replacing the new update with the old update greatly reduces optimization efficiency. Additionally, reduced sensitivity to update constants may be achieved by separately treating constraint curvature, Lagrange multiplier approximation, or cost function behavior problems to obtain positive definite updates.

Comparison with the optimization performance obtained by Schittkowski using his nonlinear programming computer program (NLPQL) performance verifies that NLQPEB is extremely efficient.

Shaped Charge Optimization

A variable metric nonlinear programming algorithm was successfully applied to the analytical shaped charge model, PASCC1. The resulting program was demonstrated to parametrically optimize initial shaped charge geometry to achieve desired shaped charge jet properties. Two types of optimization problems were solved: a distributed parameter optimization problem was chosen to investigate the direct distributed parameter optimization of a nonlinear dynamic system using a variable metric nonlinear programming technique. The problem was to optimize the liner contour and thickness to obtain desired jet profiles in the least squares sense. The problem included a jet tip velocity equality constraint and an inequality constraint to prevent the occurrence of an inverse jet velocity gradient. The problem was successfully solved, demonstrating the use of a Cholesky decomposition BFGS variable metric sequential quadratic programming algorithm and the Raleigh-Ritz method. The ability to address system equality and inequality constraints was also demonstrated. The optimization results indicate that by increasing the order of a polynomial description of the liner profile, improved agreement with the prescribed jet profile is achieved. Unfortunately, by increasing the polynomial order, the number of optimization variables increases, resulting in larger computational requirements. The increased computational requirements are due primarily to the numerical calculation of partial derivatives. Reduced computational times can be achieved through the use of parallel computer architecture. The partial derivatives can be calculated in parallel instead of sequentially. The partial derivative routine is being rewritten to take advantage of parallel architecture. Also, higher order polynomials are increasingly numerically sensitive. This results in large changes during the initial steps of the optimization routine while curvature information is being accrued. These initial steps necessitate a very robust mathematical model. The choice of a different analytic series is being considered for the solution of distributed parameter optimization. A very practical discrete optimization problem was chosen so that continuum modeling and experimentation could be used to verify the optimization results. The jet tip velocity of an existing liner geometry was maximized by optimizing the detonation wave shaping. The resulting extreme design was both computationally verified using continuum modeling, as well as experimentally verified using flash radiography. The predicted and experimental jet tip velocities agree extremely well. Some differences in the predicted and experimental jet tip geometries are noted. Improved analytical modeling will focus on liner apex hemispherical cap modeling. Improved continuum modeling using material failure criteria will be investigated. Although the optimized

wave shaped design produced extremely good penetration, it should be clearly noted that the penetration was not directly optimized. The application of variable metric sequential quadratic programming to shaped charge analytic modeling is an extraordinary contribution to shaped charge technology, and constitutes an entirely new method for the analysis and design of shaped charge devices. This new technology is resulting in improved shaped charge designs and greatly reduced analysis and designs times. Finally the application of direct distributed parameter optimization of nonlinear dynamic systems using variable metric nonlinear programming techniques has proven to be a significant contribution to the technology base.

Table 1. JWLB parameters calibrated using the LLNL revised BKW parameters (BKWR) along with ARDEC cylinder test results

	PAX2	PAX2A	OCTOL75/25	OCTOL70/30
ρo,g/cc	1.7370	1.770	1.821	1.803
Eo,Mbar	.086116	.090798	.096034	.093757
D,cm/μs	.83460	.85173	.85381	.84120
Pcj,Mbar	.30502	.32416	.33755	.32528
A_1,Mbar	909.13	909.14	909.17	549.98
A_2,Mbar	10.513	10.195	8.9469	5.8075
A_3,Mbar	.92253	.76191	.81495	.041638
R_1	16.661	16.266	15.941	15.323
R_2	5.9113	5.6415	5.4178	4.0477
R_3	2.3618	2.1540	2.1956	.62665
C,Mbar	.011724	.011325	.0104772	.0058269
ω	.35956	.36989	.30731	.27665
$A_{\lambda 1}$	46.898	69.018	65.093	1.5621
$A_{\lambda 2}$	-215.40	-176.03	-179.81	-
$A_{\lambda 3}$	270.22	163.48	156.04	-
$A_{\lambda 4}$	.88536	.76214	.78487	-
$B_{\lambda 1}$	-	-	-	-.27665
$R_{\lambda 1}$	4.3128	4.0339	3.6906	1.0841
$R_{\lambda 2}$	5.7197	4.8830	4.52693	-
$R_{\lambda 3}$	7.3188	6.5455	5.8014	-
$R_{\lambda 4}$	1.0892	1.0394	.95864	-

Table 2. Summary of nonlinear programming test problems

FN	Z	NV	NE	NI
1	0.	2	0	1
2	5.043E-02	2	0	1
3	0.	2	0	1
4	2.667E+00	2	0	2
5	-1.913E+00	2	0	4
6	0.	2	1	0
7	-1.732E+00	2	1	0
8	-1.000E+00	2	2	0
9	-5.000E-01	2	1	0
10	-1.000E+00	2	0	1
201	0.	2	0	0
202	0.	2	0	0
203	0.	2	0	0
204	1.836E-01	2	0	0
205	0.	2	0	0
206	0.	2	0	0
207	0.	2	0	0
208	0.	2	0	0
209	0.	2	0	0
210	0.	2	0	0
211	0.	2	0	0
212	0.	2	0	0
213	0.	2	0	0
214	0.	2	0	0
215	0.	2	0	2
216	1.	2	1	0
217	-8.000E-01	2	1	2
218	0.	2	0	2
219	-1.000E+00	4	2	0
220	1.000E+00	2	1	1
221	-1.000E+00	2	0	3
222	-1.500E+00	2	0	3
223	-8.340E-01	2	0	6
224	-3.040E+02	2	0	8
225	2.000E+00	2	0	5
226	-5.000E-01	2	0	4
227	1.000E+00	2	0	2

Table 3. Powell merit function performance

	Update 1		Update 2		Update 3		Update 4	
k_1	nfp	nf	nfp	nf	nfp	nf	nfp	nf
.05	2459	942	2409	914	2400	913	2451	930
.10	2378	899	2422	919	2384	899	2442	921
.15	2390	907	2437	932	2360	891	2426	915

Table 4. Quadratic penalty Lagrangian merit function performance

	Update 1		Update 2		Update 3		Update 4	
k_1	nfp	nf	nfp	nf	nfp	nf	nfp	nf
.05	10457	7174	10438	7165	11741	8178	11813	8206
.10	10445	7170	10450	7171	9730	6607	9825	6656
.15	10461	7178	10458	7179	9701	6596	9811	6650

Table 5. Quadratic penalty cost merit function performance

	Update 1		Update 2		Update 3		Update 4	
k_1	nfp	nf	nfp	nf	nfp	nf	nfp	nf
.05	8899	4372	8222	3867	7735	3564	9019	4614
.10	7864	3745	8433	4094	7873	3640	7905	3676
.15	7853	3624	8545	3976	8240	3891	7783	3606

Table 6. Comparison of final cost function values for different initial penalty constant values

FN	.1	1.	10.	100.	1000.
1	3.846E-14	3.846E-14	3.846E-14	3.846E-14	3.846E-14
2	5.043E-02	5.043E-02	5.043E-02	5.043E-02	5.043E-02
3	2.500E-28	2.500E-28	2.500E-28	2.500E-28	2.500E-28
4	2.667E+00	2.667E+00	2.667E+00	2.667E+00	2.667E+00
5	-1.913E+00	-1.913E+00	-1.913E+00	-1.913E+00	-1.913E+00
6	4.843E-21	2.516E-23	2.500E-23	3.426E-13	4.174E-13
7	-1.732E+00	-1.732E+00	-1.732E+00	-1.732E+00	-1.732E+00
8	-1.000E+00	-1.000E+00	-1.000E+00	-1.000E+00	-1.000E+00
9	-5.000E-01	-5.000E-01	-5.000E-01	-5.000E-01	-5.000E-01
10	-1.000E+00	-1.000E+00	-1.000E+00	-1.000E+00	-1.000E+00
201	1.229E-22	1.229E-22	1.229E-22	1.229E-22	1.229E-22
202	4.898E+01	4.898E+01	4.8984E+0	4.898E+01	4.898E+01
203	3.197E-14	3.197E-14	3.197E-14	3.197E-14	3.197E-14
204	1.836E-01	1.836E-01	1.836E-01	1.836E-01	1.836E-01
205	5.621E-14	5.621E-14	5.621E-14	5.621E-14	5.621E-14
206	3.334E-15	3.334E-15	3.334E-15	3.334E-15	3.334E-15
207	1.491E-17	1.491E-17	1.491E-17	1.491E-17	1.491E-17
208	1.922E-16	1.922E-16	1.922E-16	1.922E-16	1.922E-16
209	7.030E-13	7.030E-13	7.030E-13	7.030E-13	7.030E-13
210	2.460E+00	2.460E+00	2.460E+00	2.460E+00	2.460E+00
211	6.479E-14	6.479E-14	6.479E-14	6.479E-14	6.479E-14
212	8.223E-16	8.223E-16	8.223E-16	8.223E-16	8.223E-16
213	3.199E-19	3.199E-19	3.199E-19	3.199E-19	3.199E-19
214	3.286E-03	3.286E-03	3.286E-03	3.286E-03	3.286E-03
215	-8.739E-05	-8.739E-05	-8.888E-05	-8.727E-05	-3.704E-08
216	9.994E-01	9.994E-01	4.897E+01	4.897E+01	4.897E+01
217	-8.000E-01	-8.000E-01	-8.000E-01	-8.000E-01	-8.000E-01
218	-3.761E-20	4.544E-27	-.-------	-.-------	-.-------
219	-1.038E+00	-1.000E+00	-1.000E+00	-1.000E+00	-1.000E+00
220	1.000E+00	3.024E+01	-.-------	-.-------	-.-------
221	-1.000E+00	-1.000E+00	-1.000E+00	-1.000E+00	-1.000E+00
222	-1.500E+00	-1.500E+00	-1.500E+00	-1.500E+00	-1.500E+00
223	-8.340E-01	-8.340E-01	-8.340E-01	-8.340E-01	-8.340E-01
224	-3.040E+02	-3.040E+02	-3.040E+02	-3.040E+02	-3.040E+02
225	2.000E+00	2.000E+00	2.000E+00	2.000E+00	2.000E+00
226	-5.000E-01	-5.000E-01	-5.000E-01	-5.000E-01	-5.000E-01
227	9.998E-01	9.999E-01	9.998E-01	9.998E-01	9.999E-01

Table 7. Comparison of the number of cost function evaluations for different initial penalty constant values

	.1		1.		10.		100.		1000.	
FN	nfp	nf	nfp	nf	nfp	nf	nfp	nf	nfp	nf
1	64	26	64	26	64	26	64	26	64	26
2	50	22	50	22	50	22	50	22	50	22
3	19	7	19	7	19	7	19	7	19	7
4	7	3	7	3	7	3	7	3	7	3
5	27	11	27	11	27	11	27	11	27	11
6	84	56	85	41	191	105	608	358	1391	813
7	676	338	230	114	206	102	191	101	48	24
8	16	6	17	7	17	7	17	7	17	7
9	29	17	29	17	29	17	29	17	29	17
10	548	294	326	160	258	126	143	67	34	13
201	15	7	15	7	15	7	15	7	15	7
202	44	22	44	22	44	22	44	22	44	22
203	36	14	36	14	36	14	36	14	36	14
204	22	10	22	10	22	10	22	10	22	10
205	42	16	42	16	42	16	42	16	42	16
206	25	11	25	11	25	11	25	11	25	11
207	39	15	39	15	39	15	39	15	39	15
208	119	49	119	49	119	49	119	49	119	49
209	457	187	457	187	457	187	457	187	457	187
210	35	19	35	19	35	19	35	19	35	19
211	77	33	77	33	77	33	77	33	77	33
212	41	17	41	17	41	17	41	17	41	17
213	326	114	326	114	326	114	326	114	326	114
214	107	55	107	55	107	55	107	55	107	55
215	323	161	323	161	259	129	236	118	83	41
216	253	167	155	79	336	172	39	15	35	13
217	544	272	251	123	102	48	102	48	26	10
218	239	111	131	47	----	----	----	----	----	----
219	2295	1095	641	217	441	141	368	116	211	63
220	191	65	2567	1967	----	----	----	----	----	----
221	79	27	79	27	79	27	79	27	79	27
222	304	152	304	152	284	142	192	96	111	55
223	211	103	100	48	77	37	157	85	457	265
224	13	5	13	5	13	5	13	5	13	5
225	19	7	19	7	19	7	19	7	19	7
226	117	65	117	65	162	80	131	65	71	35
227	347	209	232	116	243	121	119	59	39	19
Total	7840	3788	7181	3991	4268	1904	3995	1829	4215	2052

Table 8. Comparison of different variable metric matrix update optimization performance

	Update 1		Update 2		Update 3		Update4	
k_1	nfp	nf	nfp	nf	nfp	nf	nfp	nf
.05	2459	942	2409	914	2400	913	2451	930
.10	2378	899	2422	919	2384	899	2442	921
.15	2390	907	2437	932	2360	891	2426	915
.20	2376	897	2409	924	2389	906	2439	920
.25	2377	898	2326	879	2390	905	2446	921
.30	2384	901	2436	927	2394	905	2452	923
.35	2387	906	2271	856	2395	902	2458	921
.40	2377	898	2279	860	2380	901	2467	932
.45	2385	900	2269	844	2400	909	2513	950
.50	2368	891	2296	847	2382	899	2460	929
.55	2372	893	2398	889	2410	911	2476	935
.60	2386	901	2547	934	2378	899	2460	931
.65	2381	898	2677	984	2364	891	2431	914
.70	2390	905	2845	1030	2382	897	2447	918
.75	2383	898	3170	1139	2368	893	2429	912
.80	2384	899	3438	1219	2428	921	2483	938
.85	2382	899	4209	1474	2392	901	2442	915
.90	2383	898	4844	1689	2379	894	2441	914
.95	2384	899	6194	2127	2391	904	2451	922
1.00	2379	896	9430	3191	2375	894	2485	932

Table 9. Comparison of final cost function value

FN	Schittkowski	Update 1	Update 2	Update 3	Update4
1	.2584E-07	.5163E-12	.1577E-15	.5163E-12	.5163E-12
2	.2844E+02	.5043E-01	.5043E-01	.5043E-01	.5043E-01
3	.1792E-22	.2500E-27	.2500E-27	.2500E-27	.2500E-27
4	.2667E+01	.2667E+01	.2667E+01	.2667E+01	.2667E+01
5	-.1913E+01	-.1913E+01	-.1913E+01	-.1913E+01	-.1913E+01
6	.1913E-12	.2975E-20	.1758E-17	.9420E-19	.1013E-14
7	-.1732E+01	-.1732E+01	-.1732E+01	-.1732E+01	-.1732E+01
8	.1000E+01	.1000E+01	-.1000E+01	-.1000E+01	-.1000E+01
9	-.5000E+00	-.5000E+00	-.5000E+00	-.5000E+00	-.5000E+00
10	-.1000E+01	-.1000E+01	-.1000E+01	-.1000E+01	-.1000E+01
201	.0000E+00	.1229E-21	.1229E-21	.1229E-21	.1229E-21
202	.4898E+02	.4898E+02	.4898E+02	.4898E+02	.4898E+02
203	.7808E-08	.3197E-13	.3197E-13	.3197E-13	.3197E-13
204	.1836E+00	.1836E+00	.1836E+00	.1836E+00	.1836E+00
205	.1562E-07	.5621E-13	.1062E-15	.5621E-13	.5621E-13
206	.2192E-10	.3334E-14	.3334E-14	.3334E-14	.3334E-14
207	.2703E-07	.1491E-16	.1078E-17	.1491E-16	.1491E-16
208	.1122E-07	.1922E-15	.1123E-16	.1922E-15	.1922E-15
209	.6137E-05	.7030E-12	.1209E-12	.7030E-12	.7030E-12
210	.2485E+00	.2460E+01	.2460E+01	.2460E+01	.2460E+01
211	.4781E-08	.6503E-13	.3722E-16	.6503E-13	.6503E-13
212	.1651E-09	.8223E-15	.8343E-17	.2276E-15	.1776E-12
213	.7429E-07	.3199E-18	.2124E-20	.1644E-23	.1644E-23
214	.7346E+00	.3286E-02	.6899E-02	.4847E-02	.4007E-02
215	-.2659E-08	-.2804E-17	-.1384E-11	-.2804E-17	-.6468E-14
216	.4897E+02	.9994E+00	.9994E+00	.9994E+00	.9994E+00
217	-.8000E+00	-.8000E+00	-.8000E+00	-.8000E+00	-.8000E+00
218	.0000E+00	-.6536E-25	.2088E-25	.5364E-25	.5364E-25
219	-.1000E+01	-.1000E+01	-.1000E+01	-.1000E+01	-.1000E+01
220	.1000E+01	.1000E+01	.1000E+01	.1000E+01	.1000E+01
221	-.1000E+01	-.1000E+01	-.1000E+01	-.1000E+01	-.1000E+01
222	-.1500E+01	-.1500E+01	-.1500E+01	-.1500E+01	-.1500E+01
223	-.8340E+00	-.8340E+00	-.8340E+00	-.8340E+00	-.8340E+00
224	-.3040E+03	-.3040E+03	-.3040E+03	-.3040E+03	-.3040E+03
225	.2000E+01	.2000E+01	.2000E+01	.2000E+01	.2000E+01
226	-.5000E+00	-.5000E+00	-.5000E+00	-.5000E+00	-.5000E+00
227	.1000E+01	.1000E+01	.1000E+01	.1000E+01	.1000E+01

Table 10. Comparison of required number of cost function evaluations

	Schittkowski		Update 1		Update 2		Update 3		Update4	
FN	nfp	nf	nfp	nf	nfp	nf	nfp	nf	nfp	nf
1		24	57	22	67	26	57	22	57	22
2		16	50	21	54	21	59	24	48	21
3		10	19	6	55	18	19	6	19	6
4		2	7	2	7	2	7	2	7	2
5		8	24	9	24	9	24	9	24	9
6		10	26	9	29	10	25	8	25	8
7		12	32	11	30	11	31	12	29	10
8		5	17	6	17	6	17	6	17	6
9		6	32	17	37	16	32	17	29	16
10		12	35	12	35	12	35	12	35	12
201		5	15	6	15	6	15	6	15	6
202		17	44	21	44	21	44	21	44	21
203		12	36	13	36	13	36	13	36	13
204		7	22	9	22	9	22	9	22	9
205		14	42	15	39	14	42	15	42	15
206		10	25	10	25	10	25	10	25	10
207		14	39	14	42	15	39	14	39	14
208		47	119	48	119	46	119	48	119	48
209		179	457	186	414	163	457	186	457	186
210		263	35	18	35	18	35	18	35	18
211		26	77	32	83	32	77	32	77	32
212		22	41	16	38	15	36	15	39	16
213		52	326	113	242	85	401	138	401	138
214		169	107	54	72	41	82	45	98	51
215		7	22	7	22	7	22	7	22	7
216		12	41	18	61	30	51	22	40	17
217		9	25	8	25	8	25	8	25	8
218		14	118	39	76	25	64	21	64	21
219		18	87	18	87	18	87	18	114	25
220		63	187	62	229	76	175	58	218	73
221		29	79	26	79	26	79	26	79	26
222		7	19	6	19	6	19	6	19	6
223		9	30	11	22	7	30	11	33	14
224		4	13	4	13	4	13	4	13	4
225		7	19	6	19	6	19	6	19	6
226		7	27	10	19	6	27	10	27	10
227		6	17	6	17	6	17	6	17	6
Total		1134	2368	891	2369	844	2360	891	2429	912

Table 11. Jet tip velocity results for the original and optimized designs

	PASCC1	CALE	Experiment
Original	8.26	8.38	8.4
Optimized	10.1	9.79	9.8

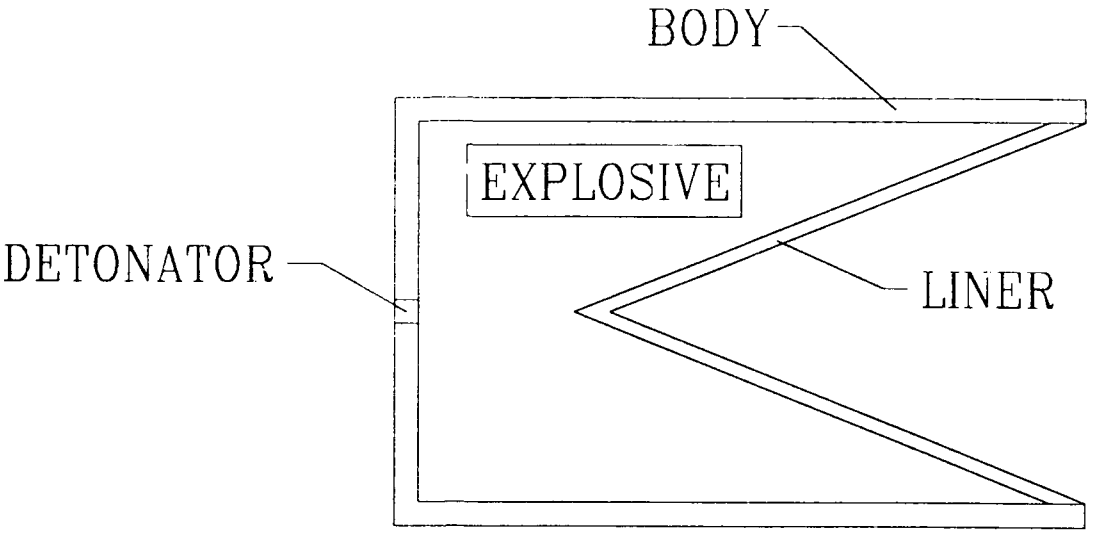

Figure 1. Initial shaped charge configuration

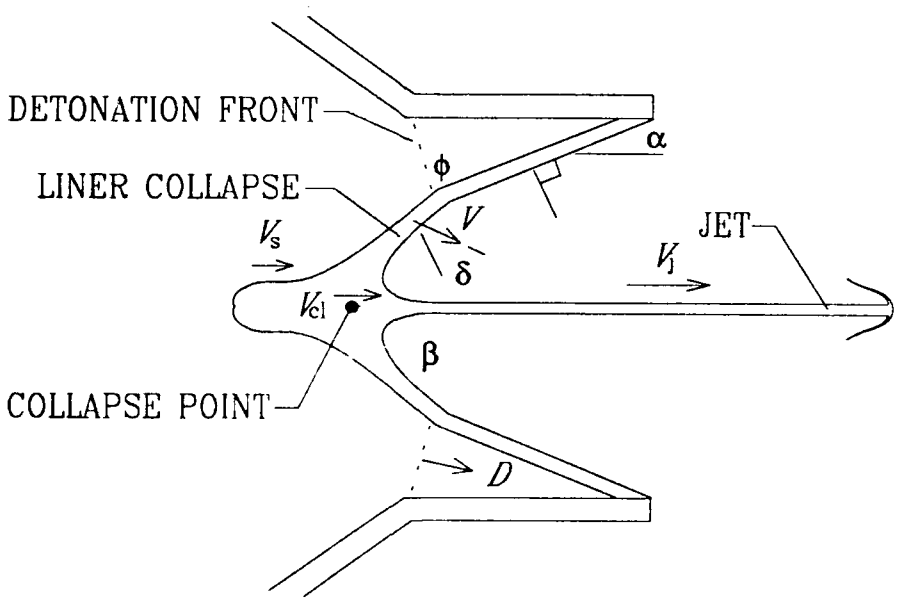

Figure 2. Linear collapse and jet formation

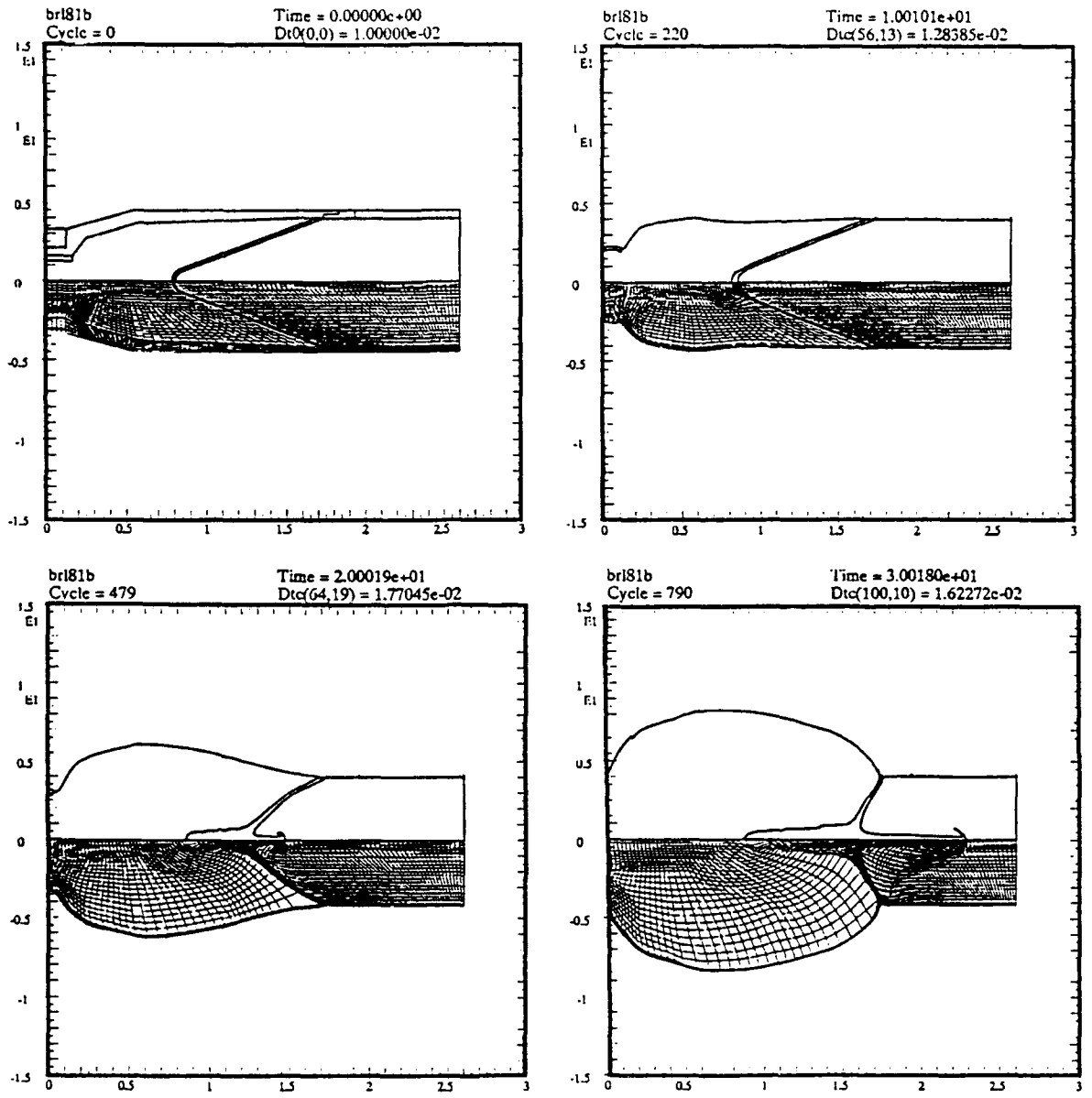

Note: Mesh position and material interfaces at 10 μs intervals.

Figure 3. Continuum solution of linear collapse and jet formation of the BRL 81 mm precision shaped charge using the arbitrary Lagrange Eulerian program CALE

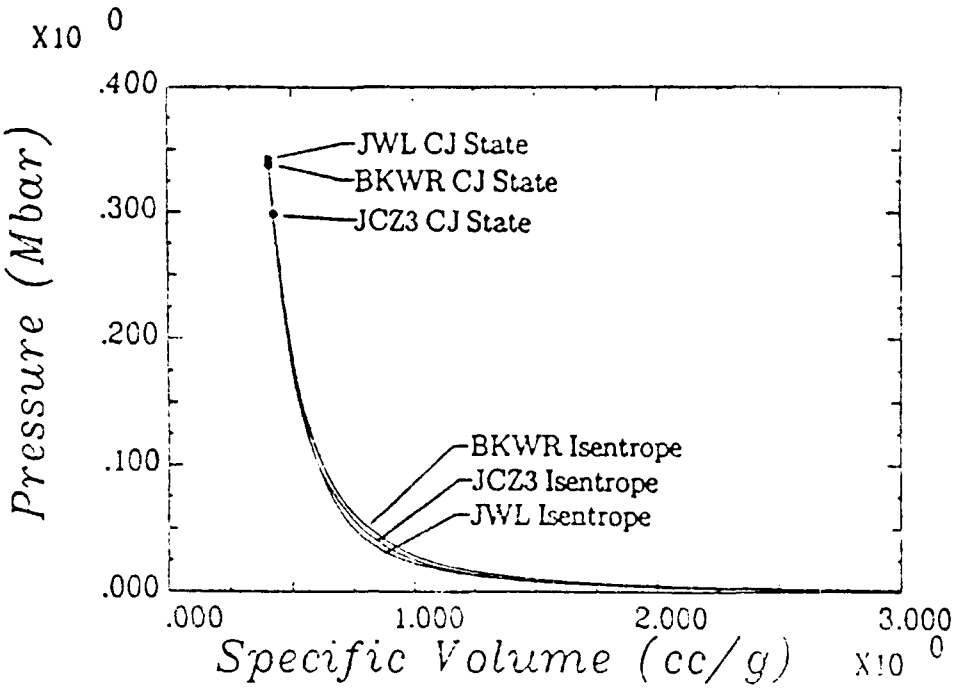

Note: Thermochemical calculations (BKWR) and JCZ3) agree fairly well with the standard JWL.

Figure 4. Pressure versus specific volume for the principle isentrope of octol 75/25 below the Chapman-Jouguet state

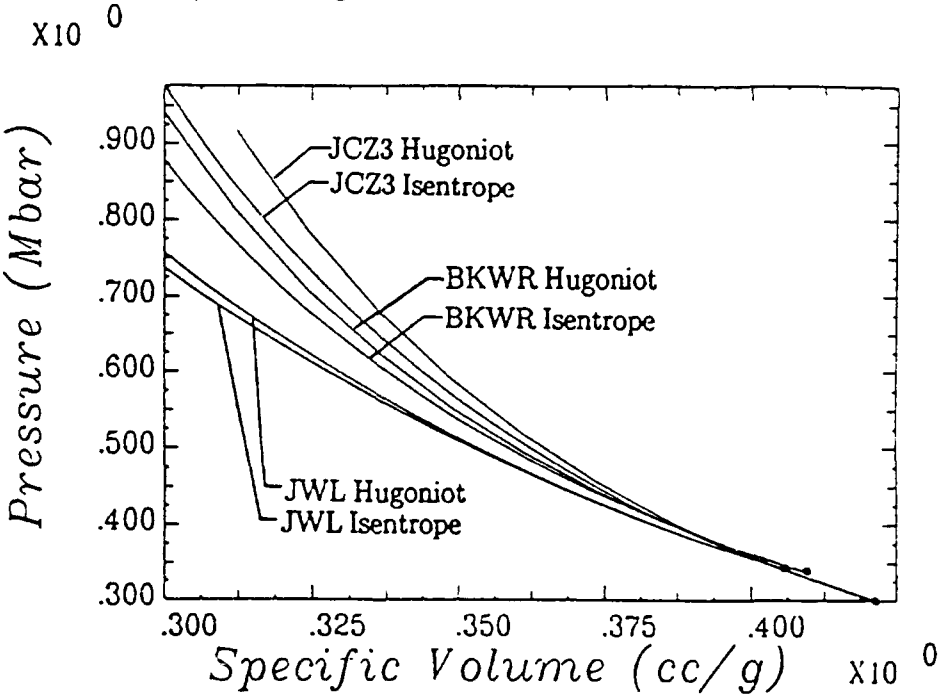

Note: The standard JWL underpredicts the high pressure region

Figure 5. Pressure versus volume for the principle isentrope and reactive Hugoniot of octol 75/25 above the Chapman-Jouguet state

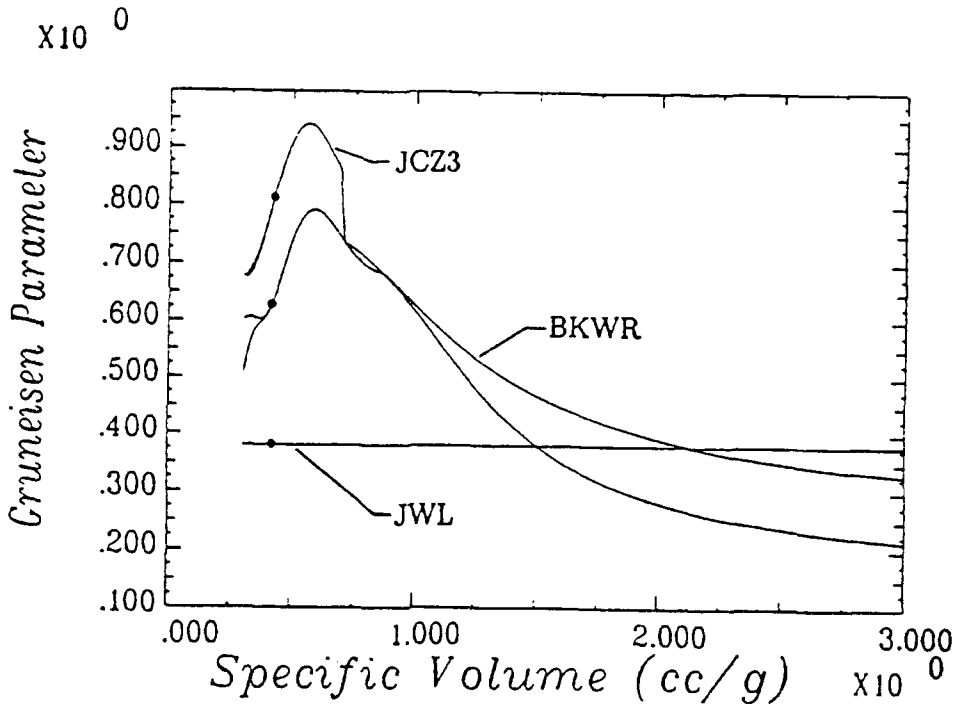

Figure 6. The Gruneisen parameter versus specific volume for the principle isentrope and reactive Hugoniot

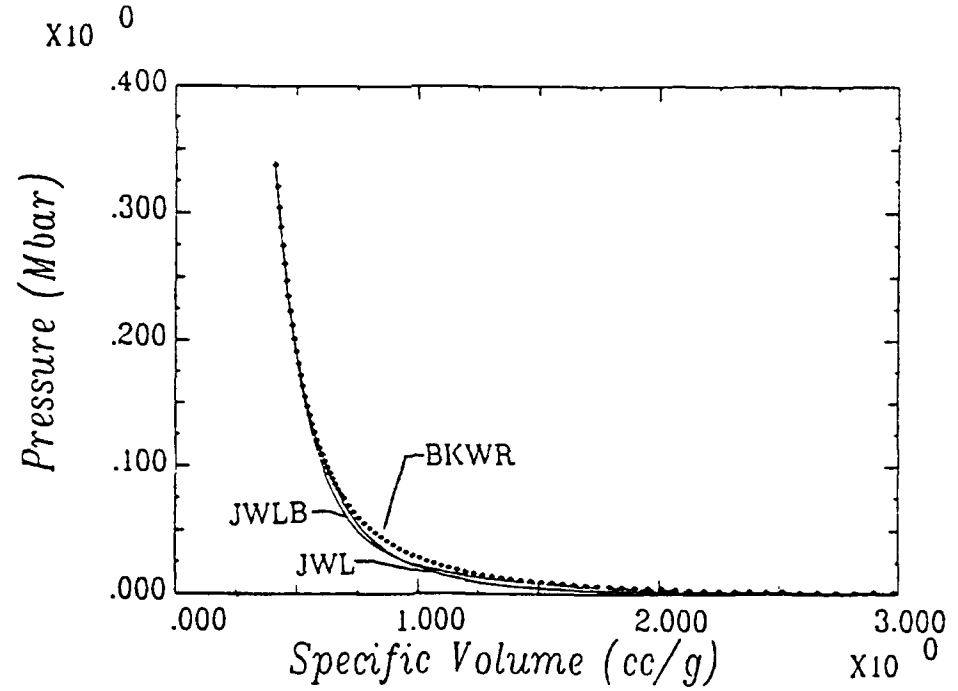

Note: The BKWR and JWLB calculations agree fairly well.

Figure 7. Pressure versus specific volume for the principle isentrope of octol 75/25 below the Chapman-Jouguet state

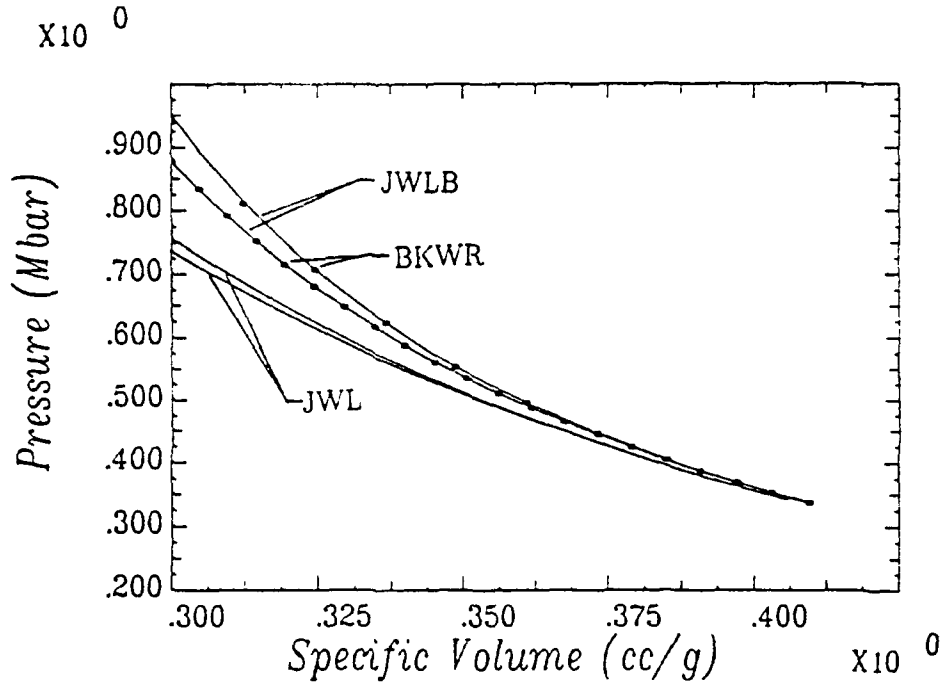

Note: The BLWR and JWLB calculations agree very closely.

Figure 8. Plots of pressure versus specific volume for the principle isentrope and reactive Hugoniot of octol 75/25 above the Chapman-Jouguet state

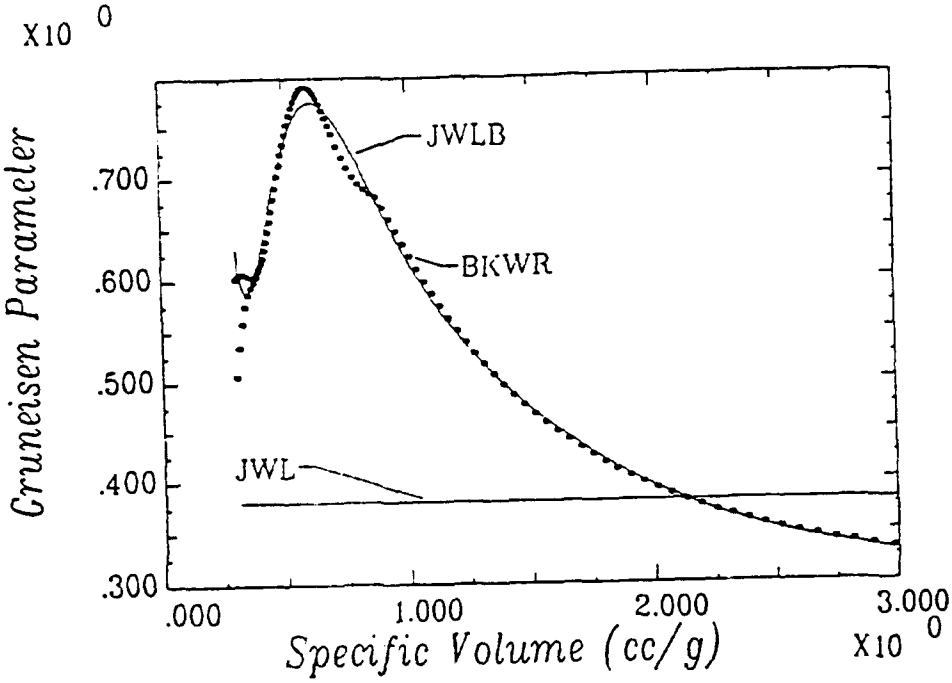

Note: The BKWR and JWLB calculations agree very closely.

Figure 9. Plot of the Gruneisen parameter versus specific volume for the principle isentrope and reactive Hugoniot

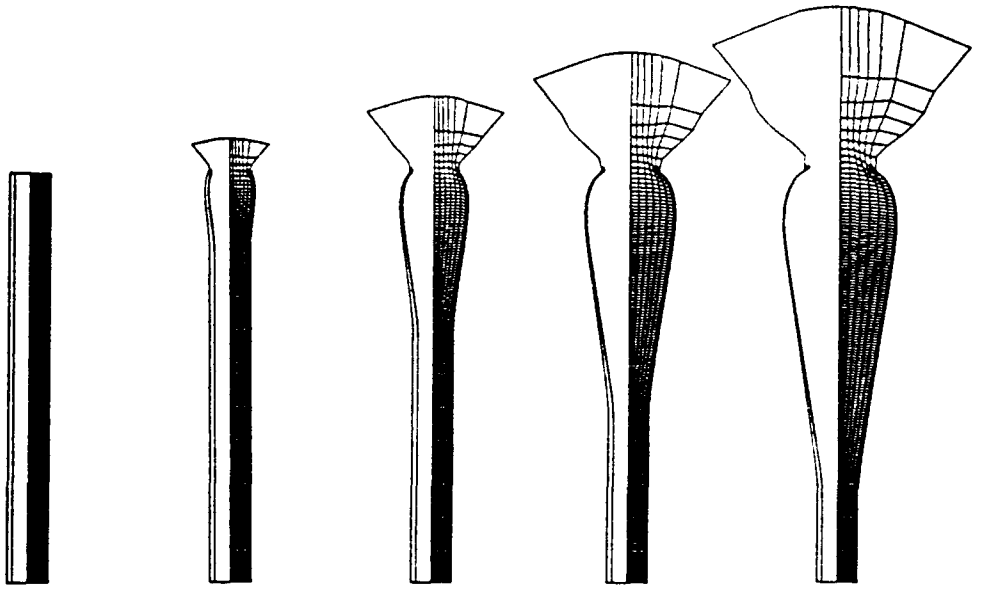

Figure 10. Cylinder expansion test finite element computation at 6 μs intervals

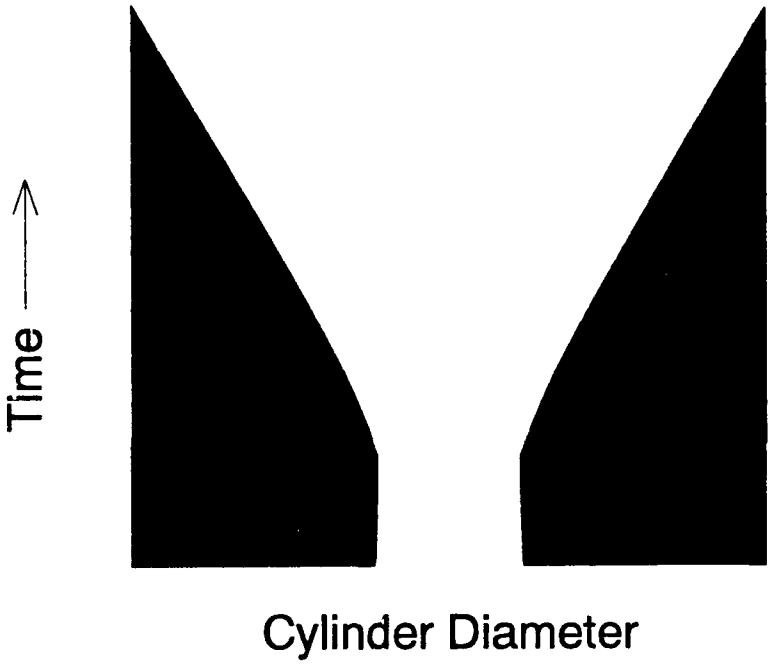

Figure 11. Experimental streak photography result of displacement versus time for the cylinder expansion test

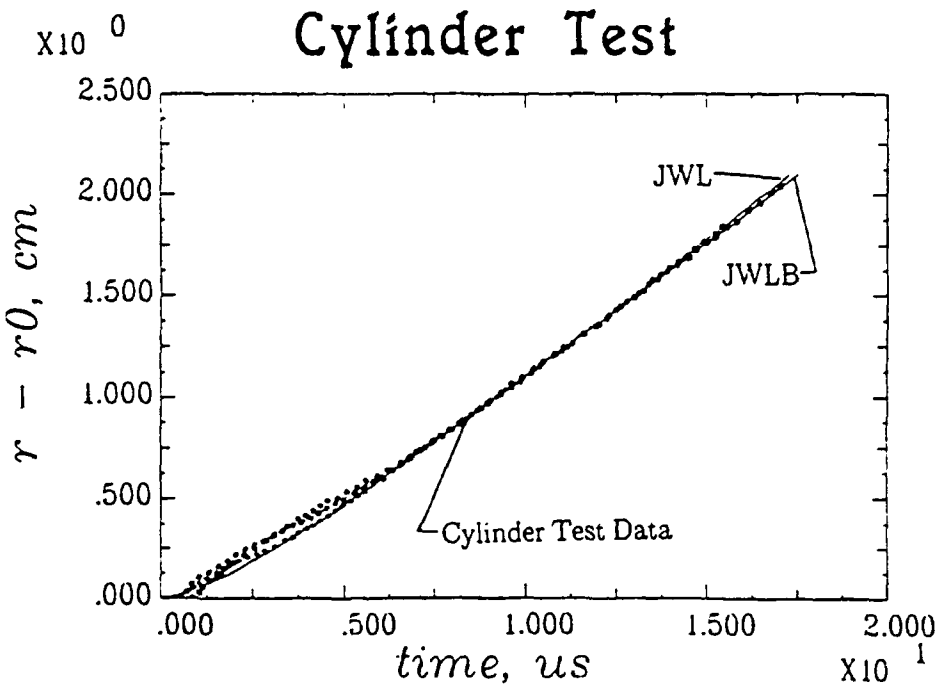

Figure 12. Dynamic finite element and experimental displacement versus time for the cylinder expansion test

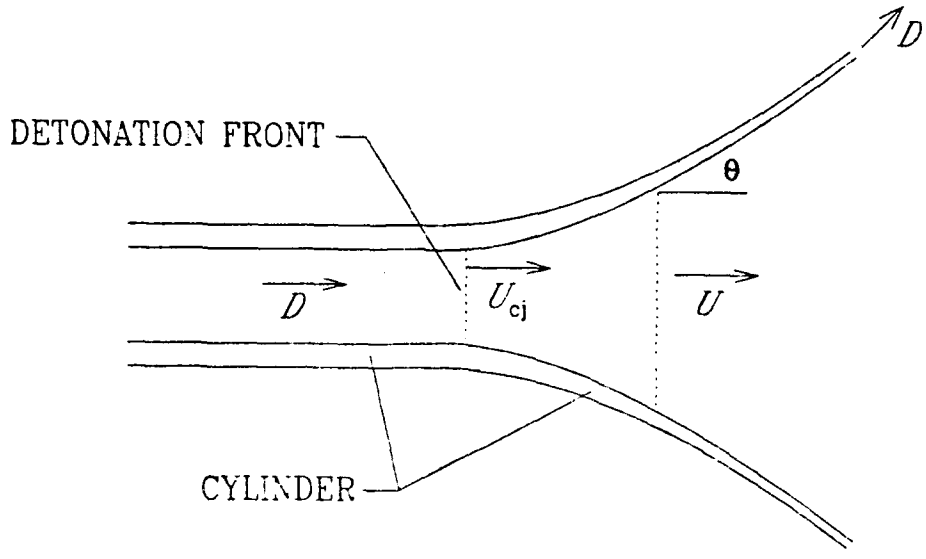

Figure 13. Taylor heavy long cylinder expansion due to high explosive detonation

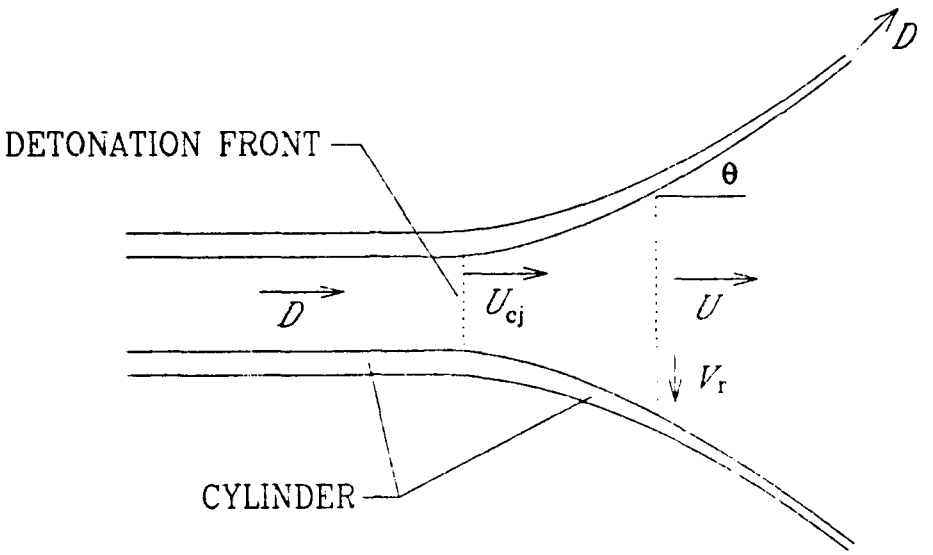

Figure 14. Products linear radial velocity distribution cylinder expansion due to high explosive detonation

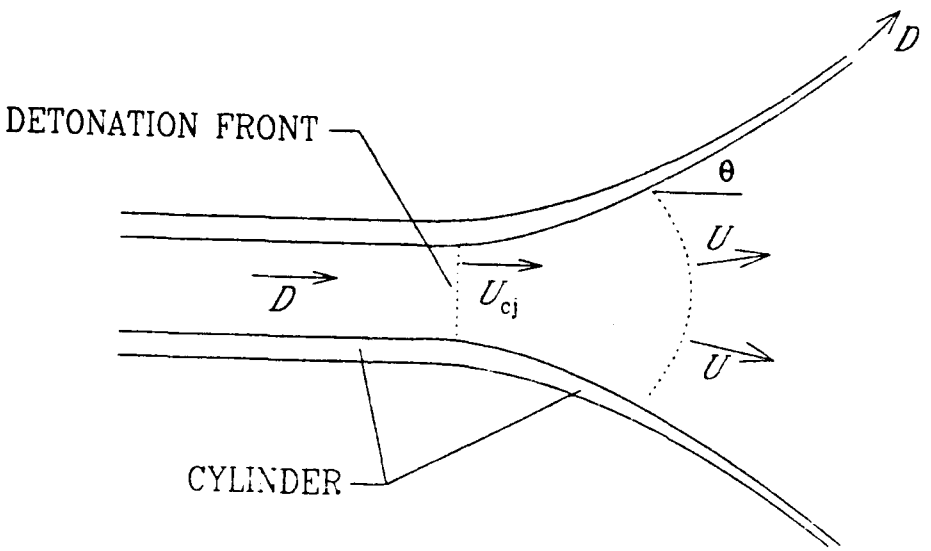

Figure 15. Products constant spherical surfaces distribution cylinder expansion due to high explosive detonation

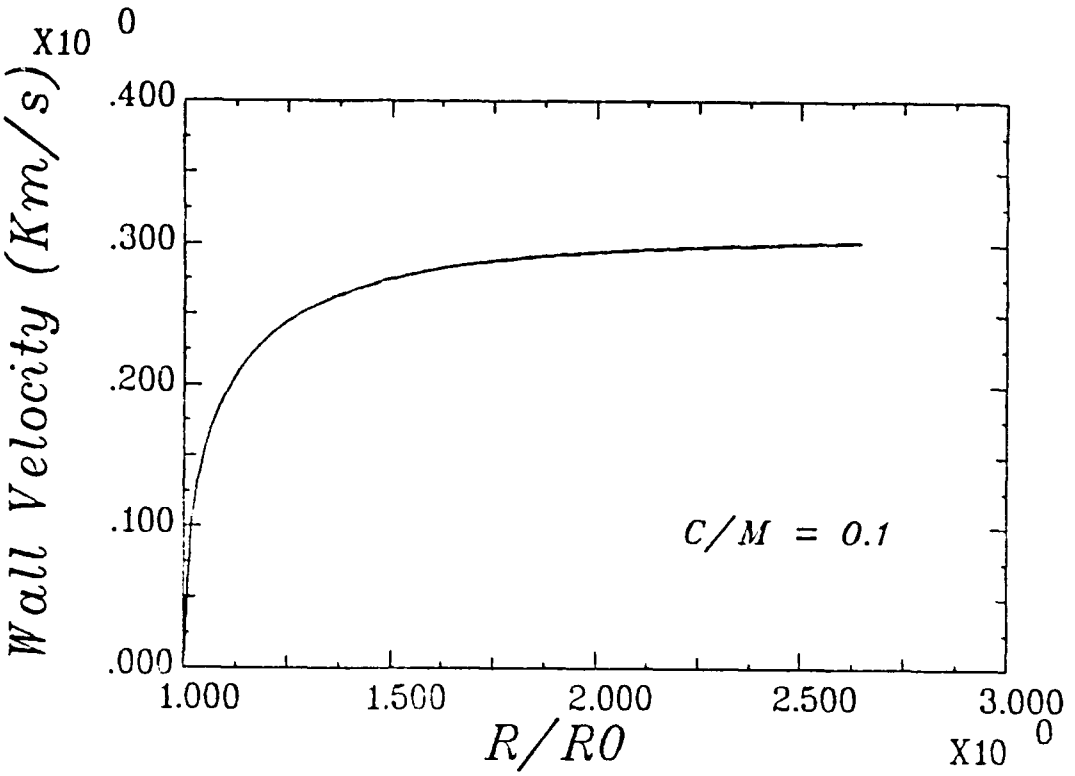

Figure 16. Predicted cylinder wall velocity versus cylinder radius for a 0.1 charge to mass ratio

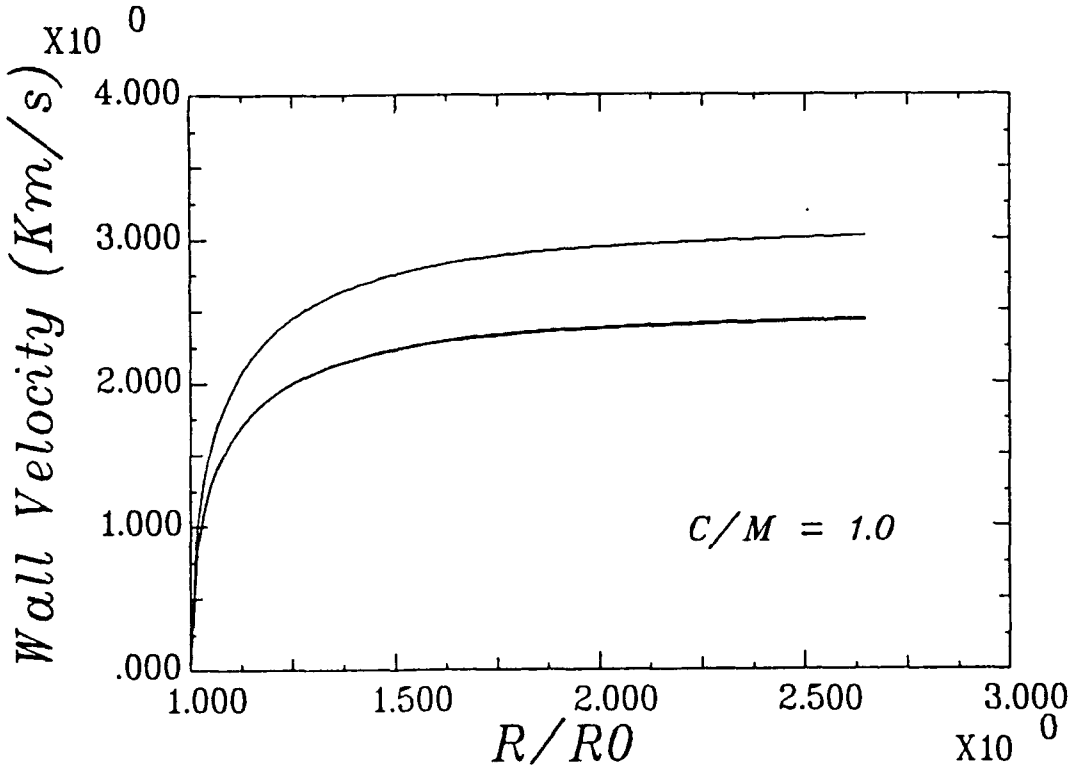

Figure 17. Predicted cylinder wall velocity versus cylinder radius for a 1 charge to mass ratio

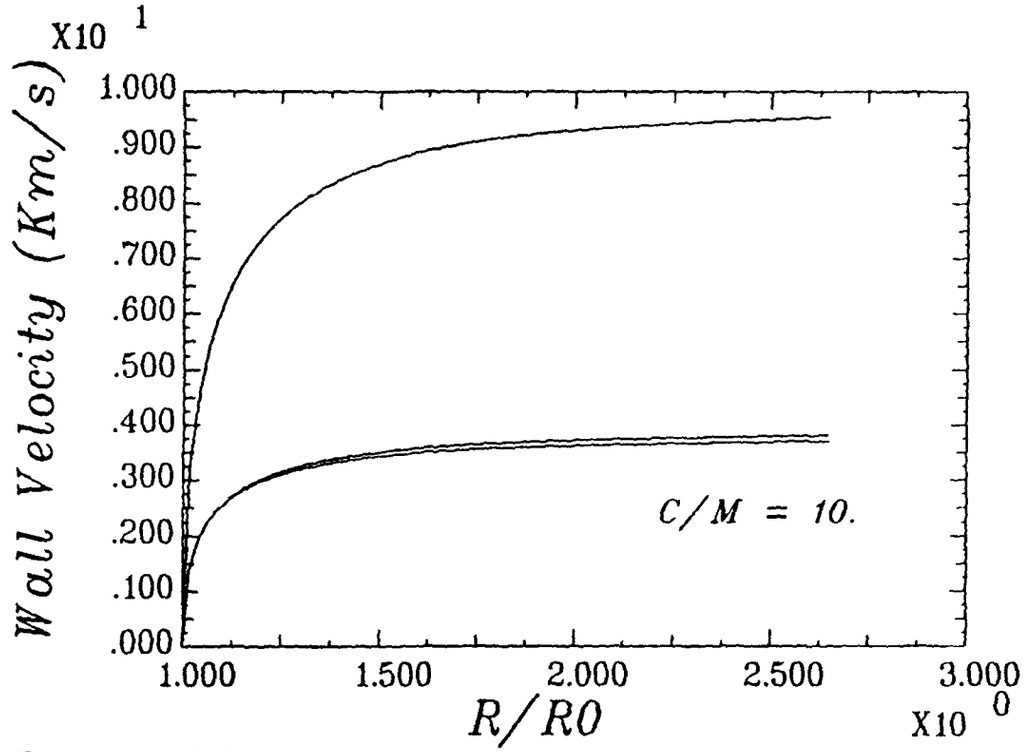

Figure 18. Predicted cylinder wall velocity versus cylinder radius for a 10 charge to mass ratio

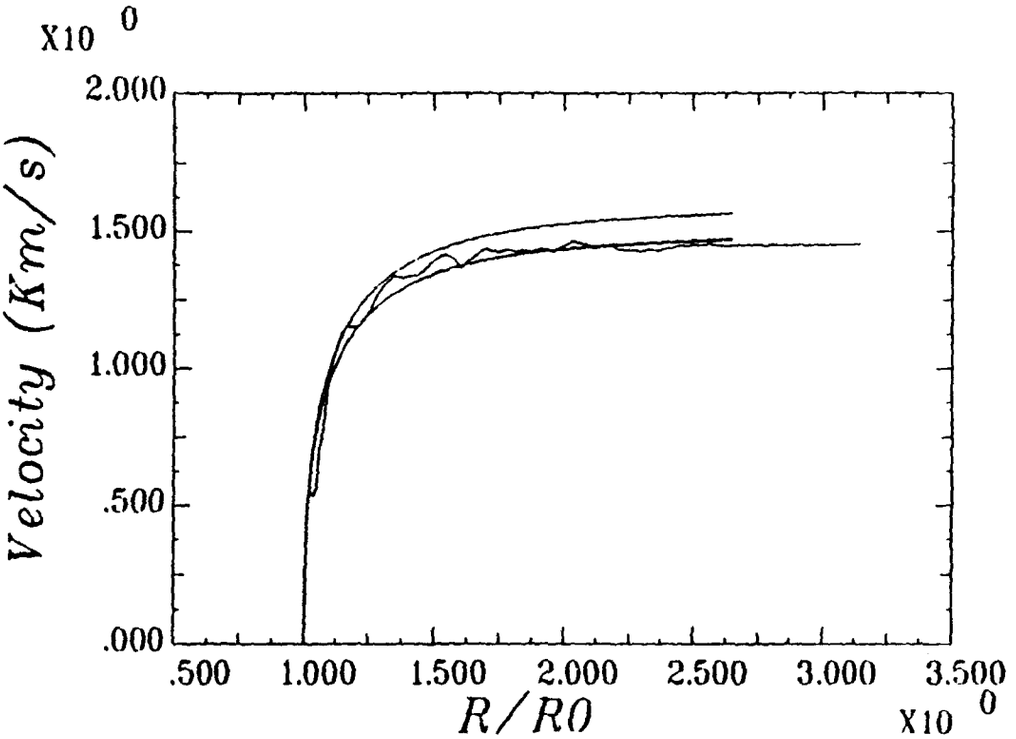

Figure 19. Comparison of finite element and analytic models predicted cylinder wall velocity versus cylinder radius

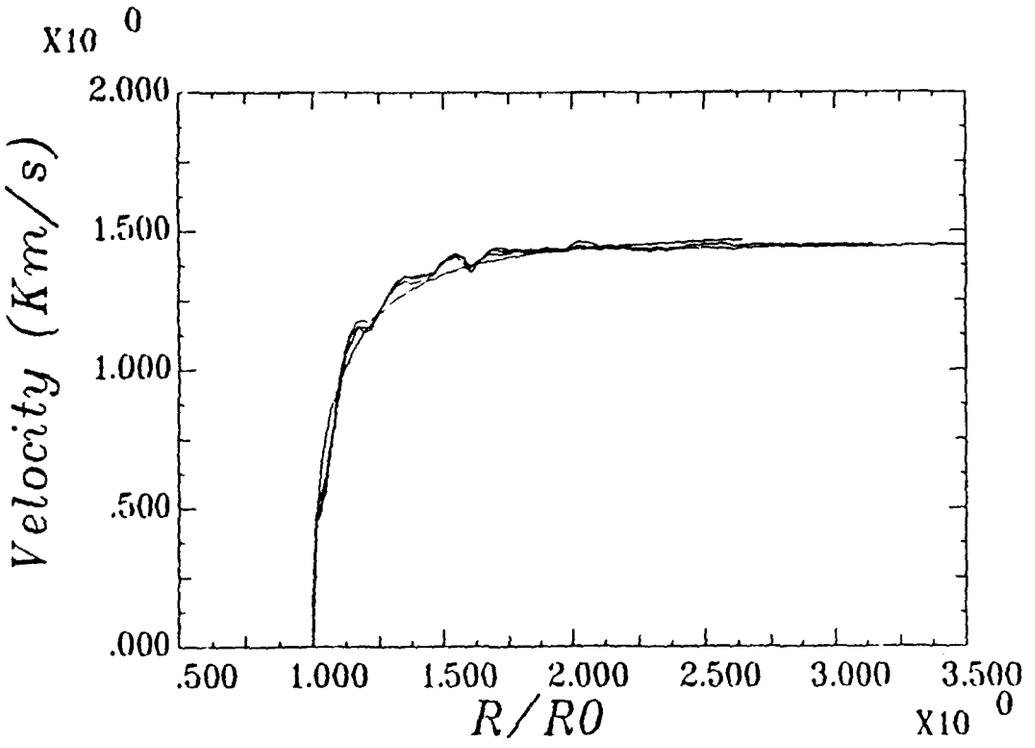

Figure 20. Finite element predicted cylinder wall velocity versus cylinder radius at 2 1/2 in., 5 in., and 7 1/2 in heights

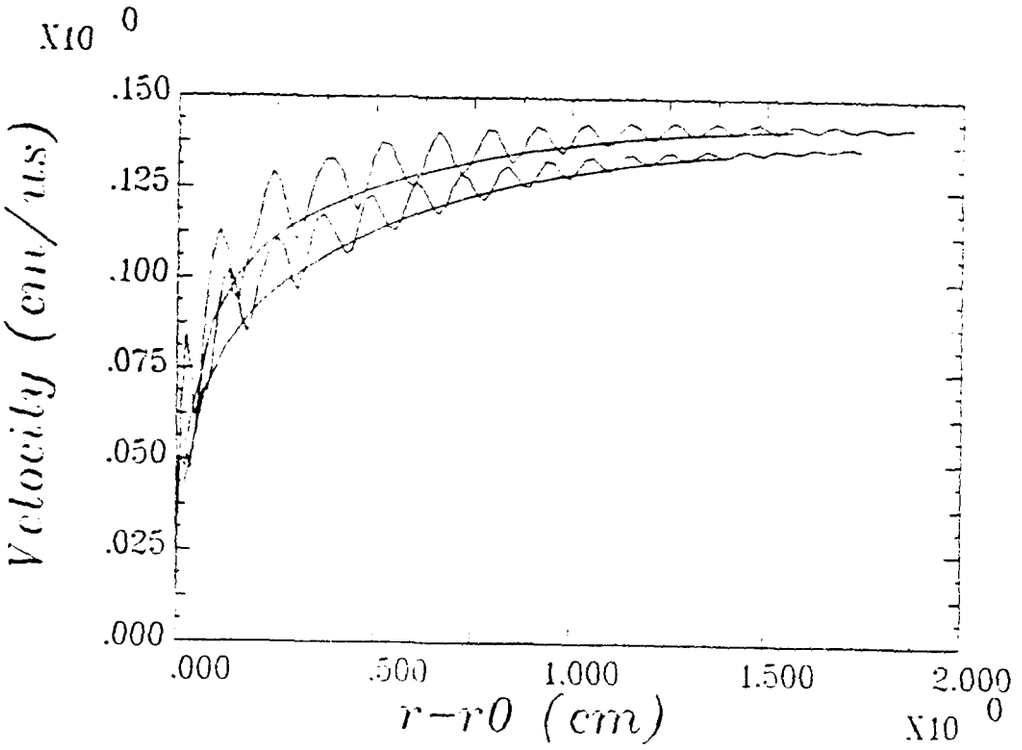

Figure 21. Cylinder inside and outside wall velocity versus cylinder wall radius predicted by finite element and analytic modeling

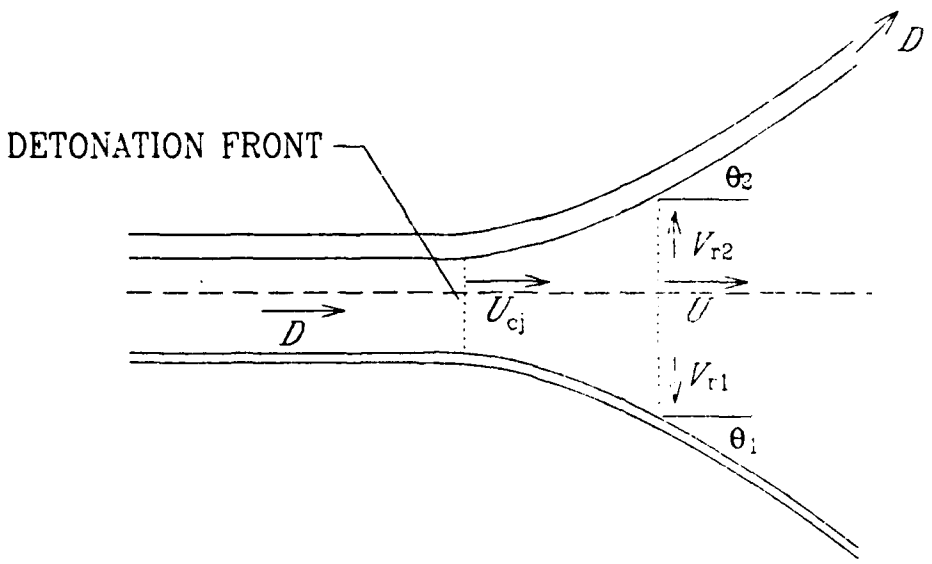

Figure 22. Slab geometry asymmetric high explosive sandwich acceleration

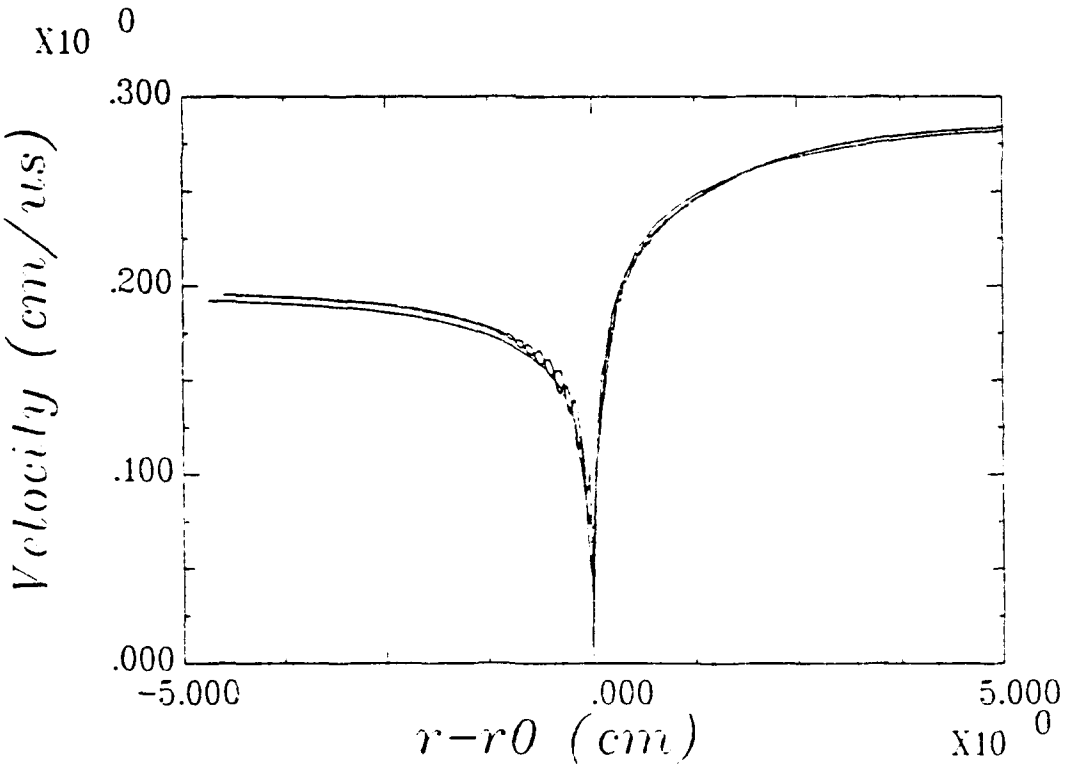

Figure 23. Sandwich wall velocity versus wall displacement

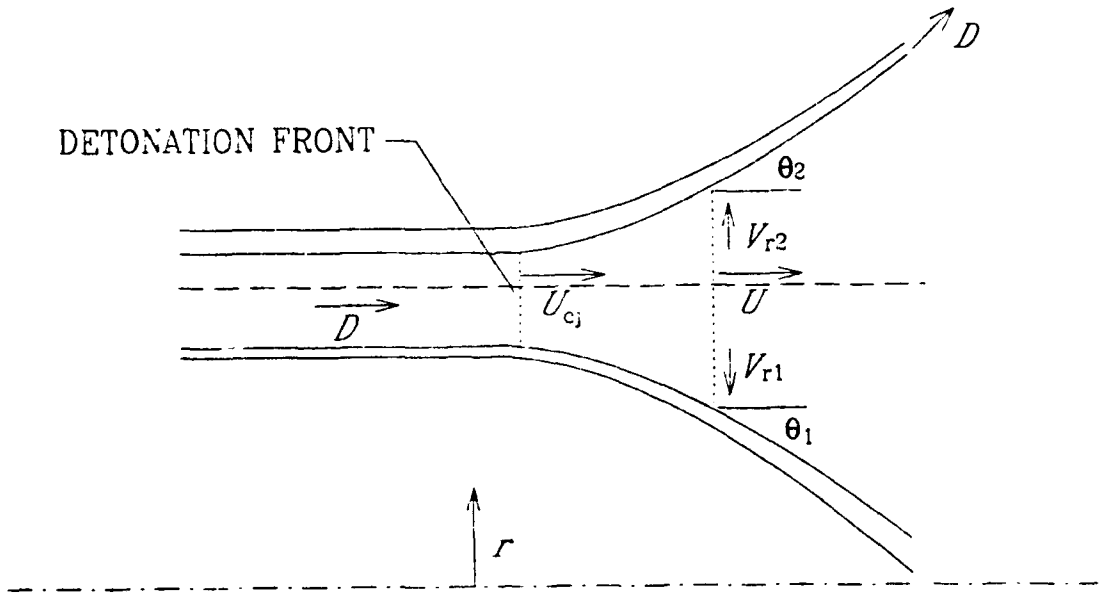

Figure 24. High explosive imploding cylinder acceleration

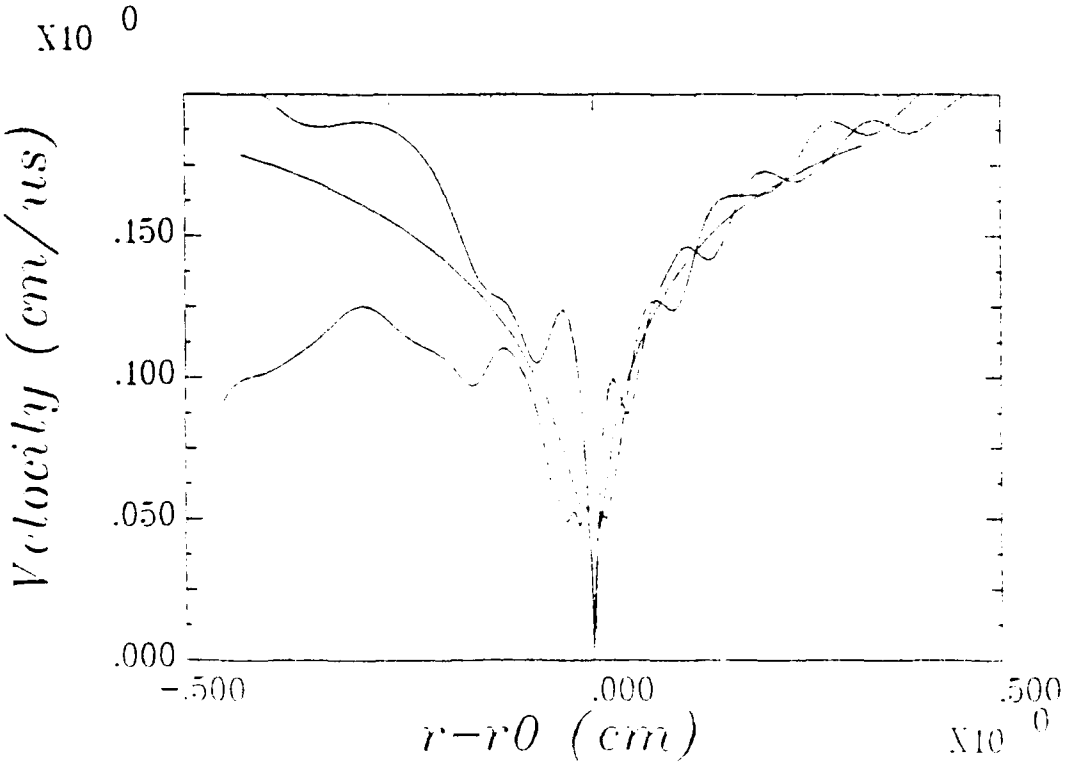

Figure 25. Cylinder wall velcoity versus wall displacement

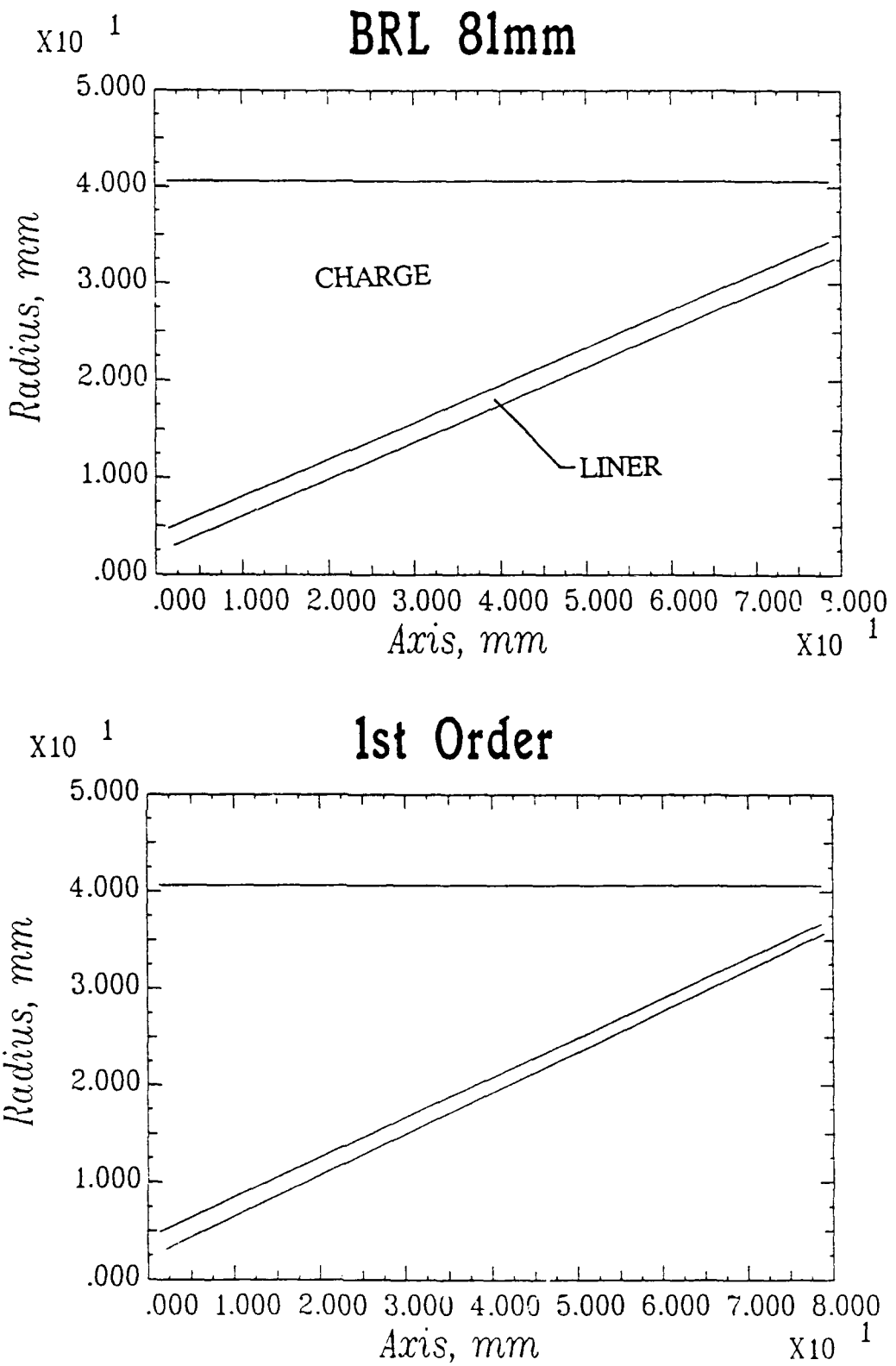

Figure 26. Comparison of liner profiles

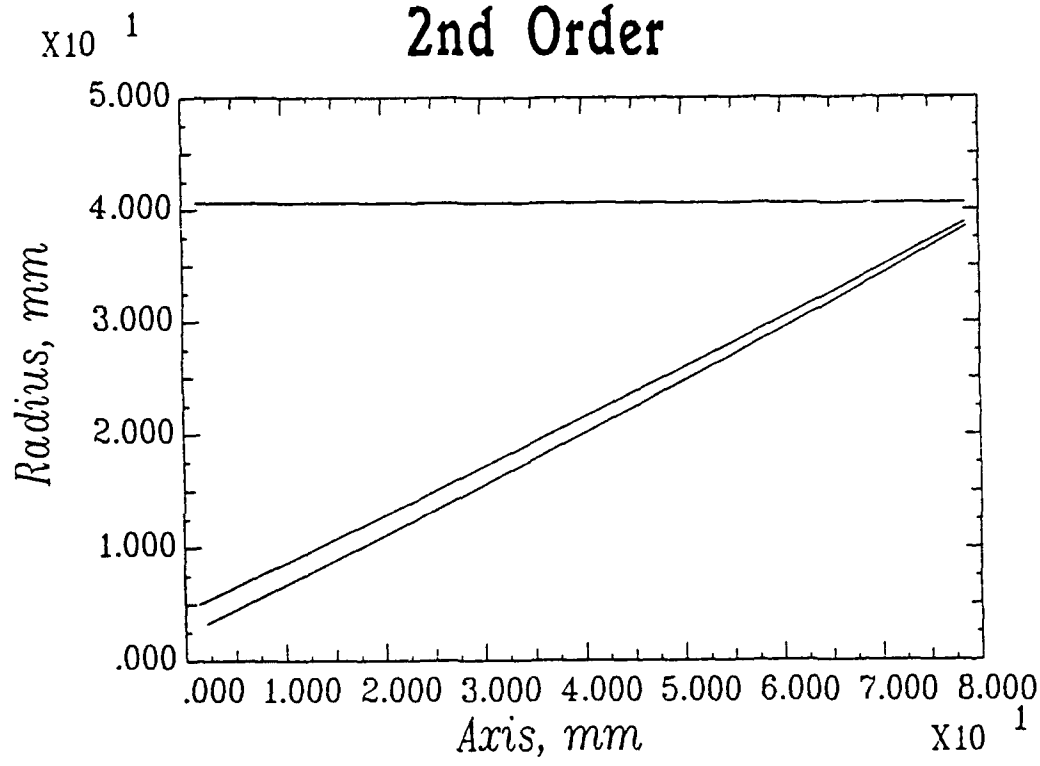

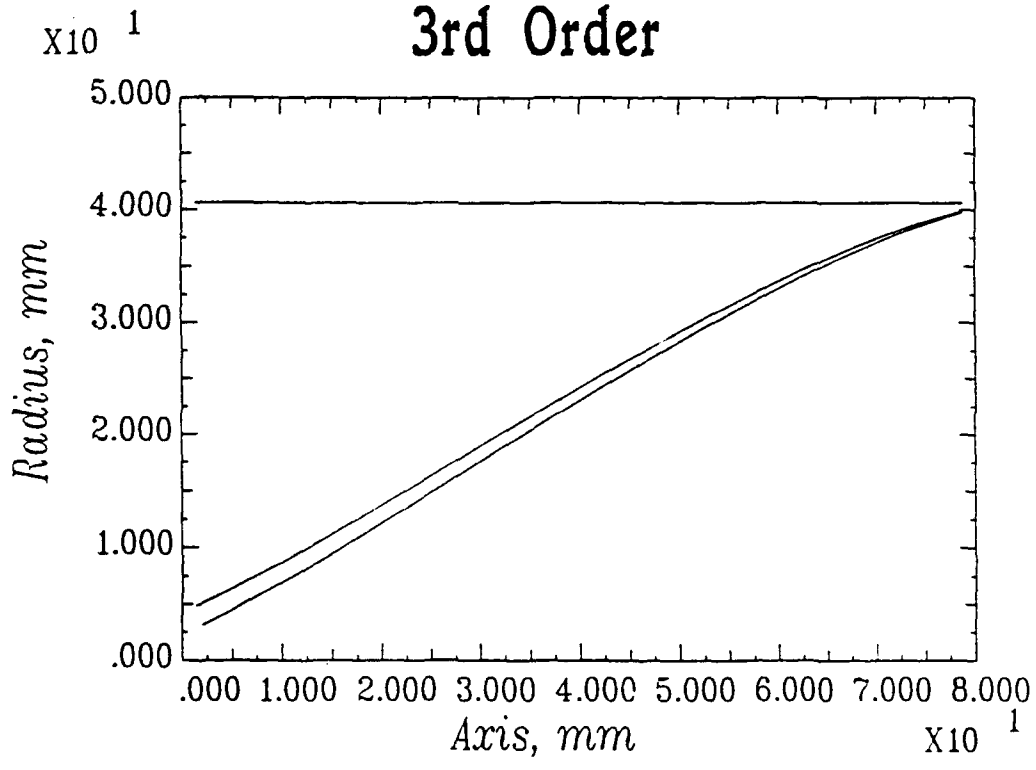

Figure 26. (cont)

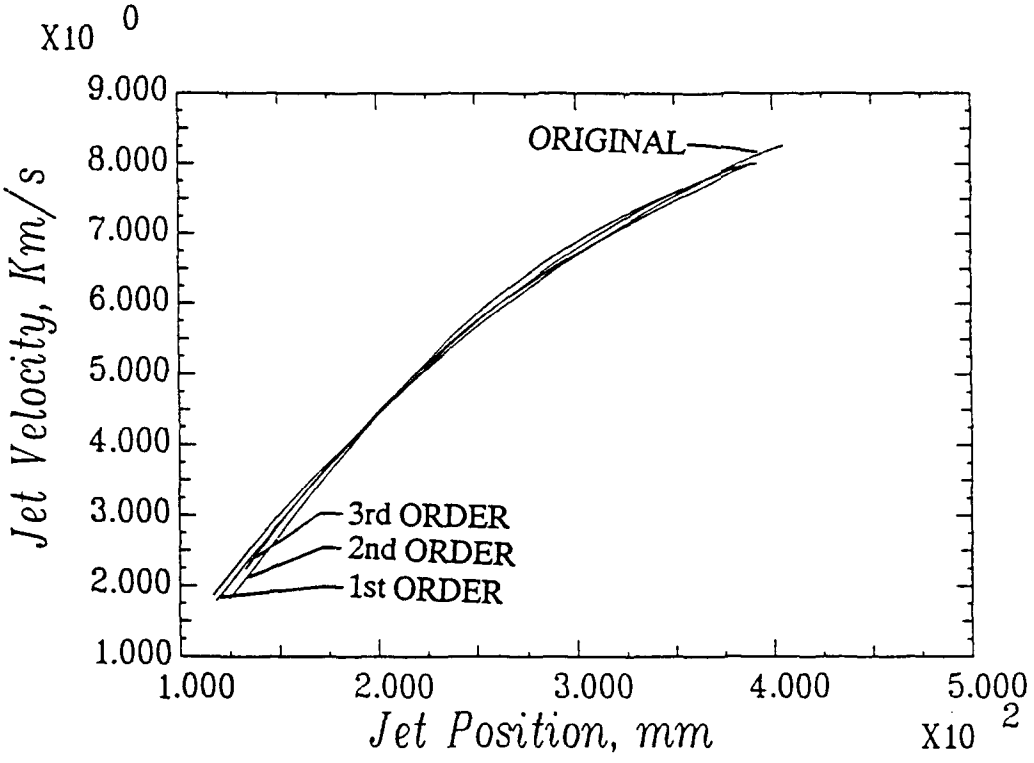

Figure 27. Jet velocity versus jet axial position at 50 μs

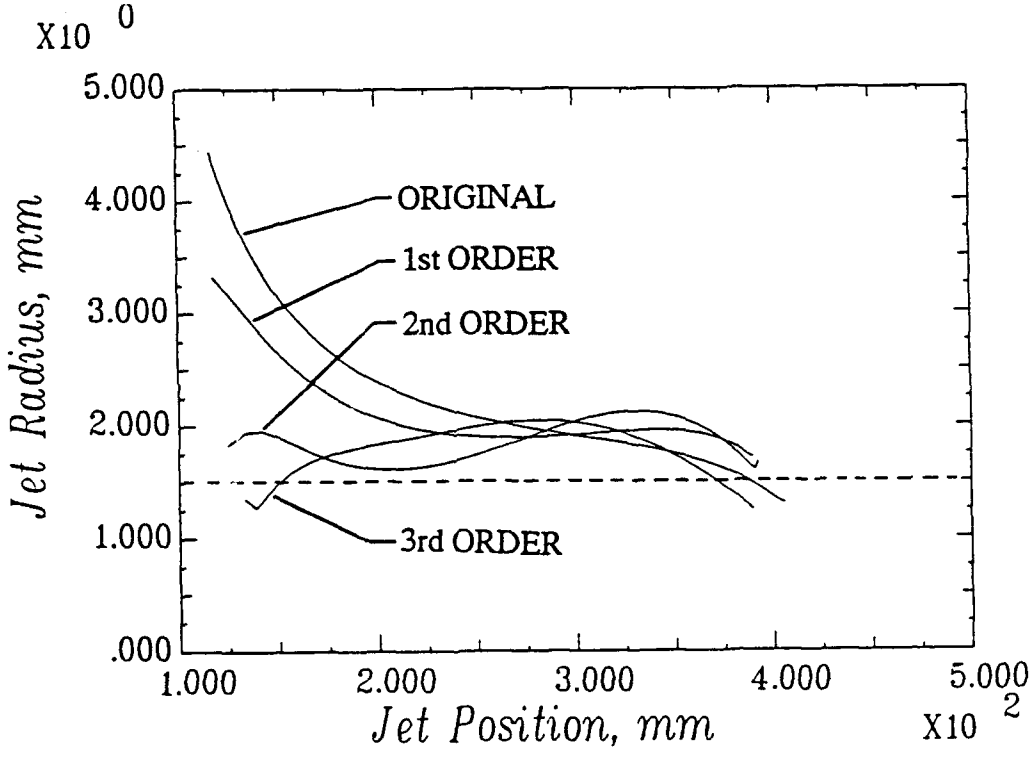

Figure 28. Jet radius versus jet axial position at 50 μs

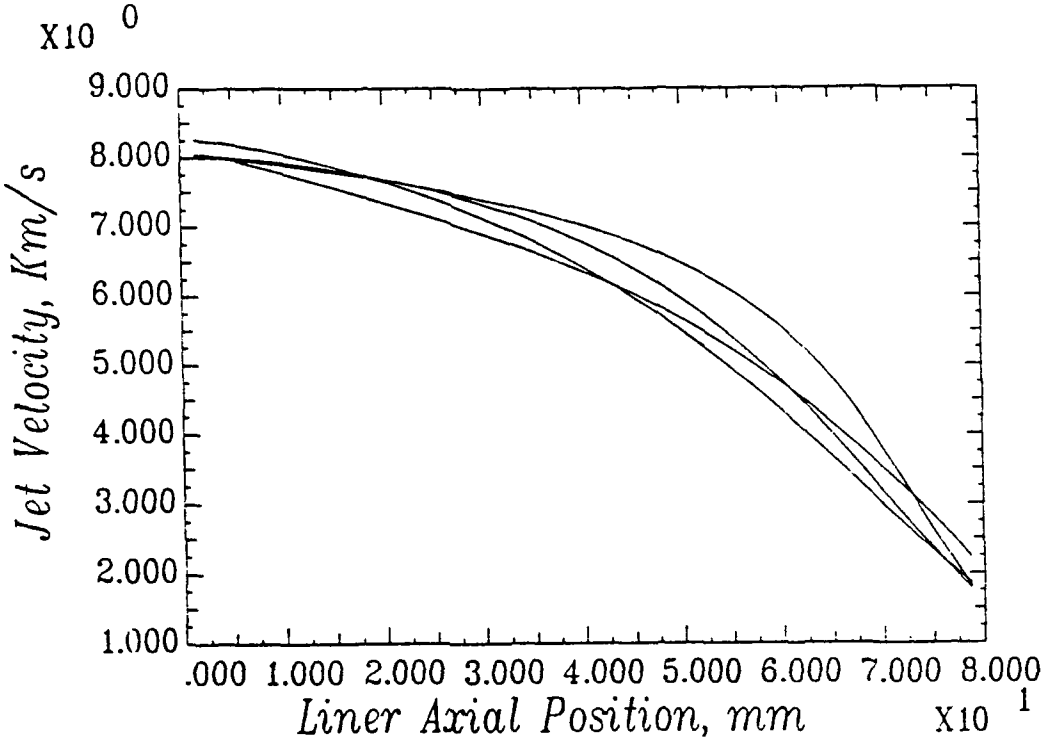

Figure 29. Jet velocity versus initial liner position at 50 μs

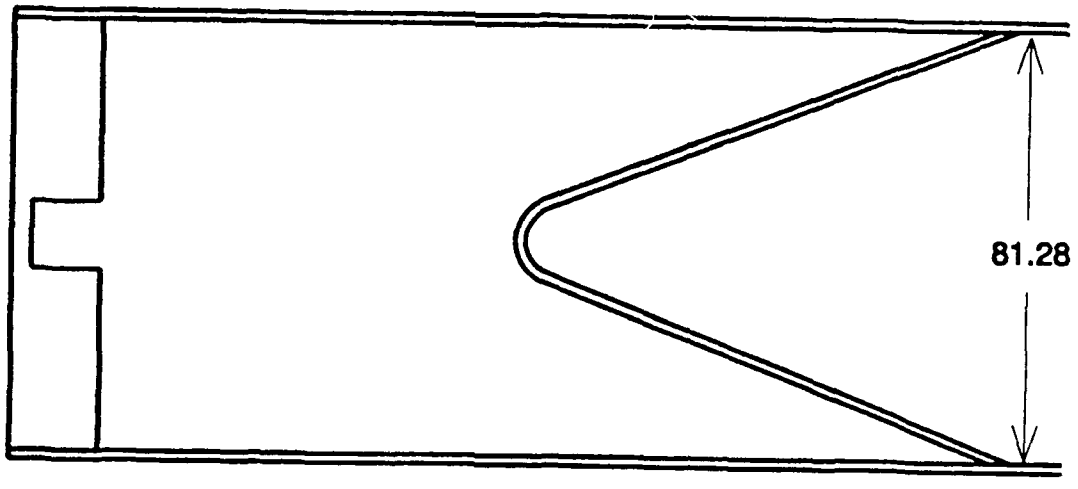

Figure 30. Original ERL 81 mm shaped charge design

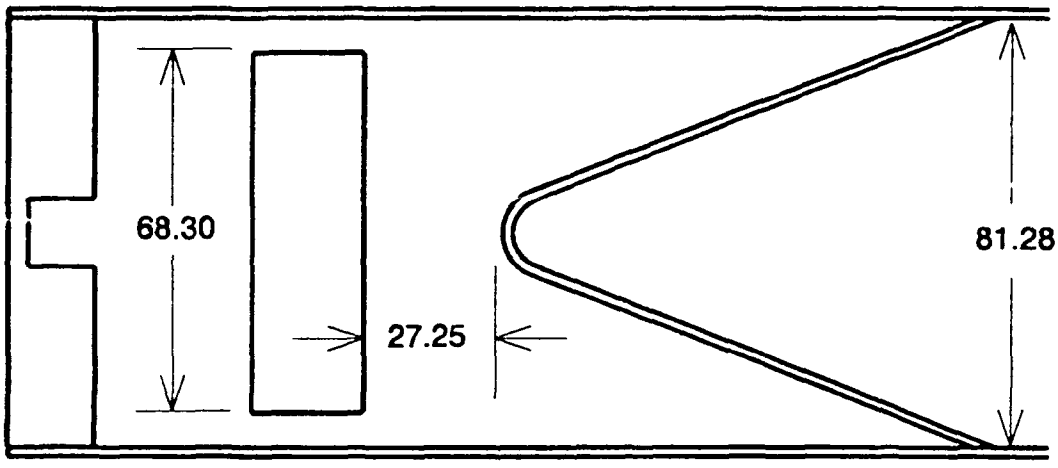

Figure 31. Optimized detonation wave shaping design

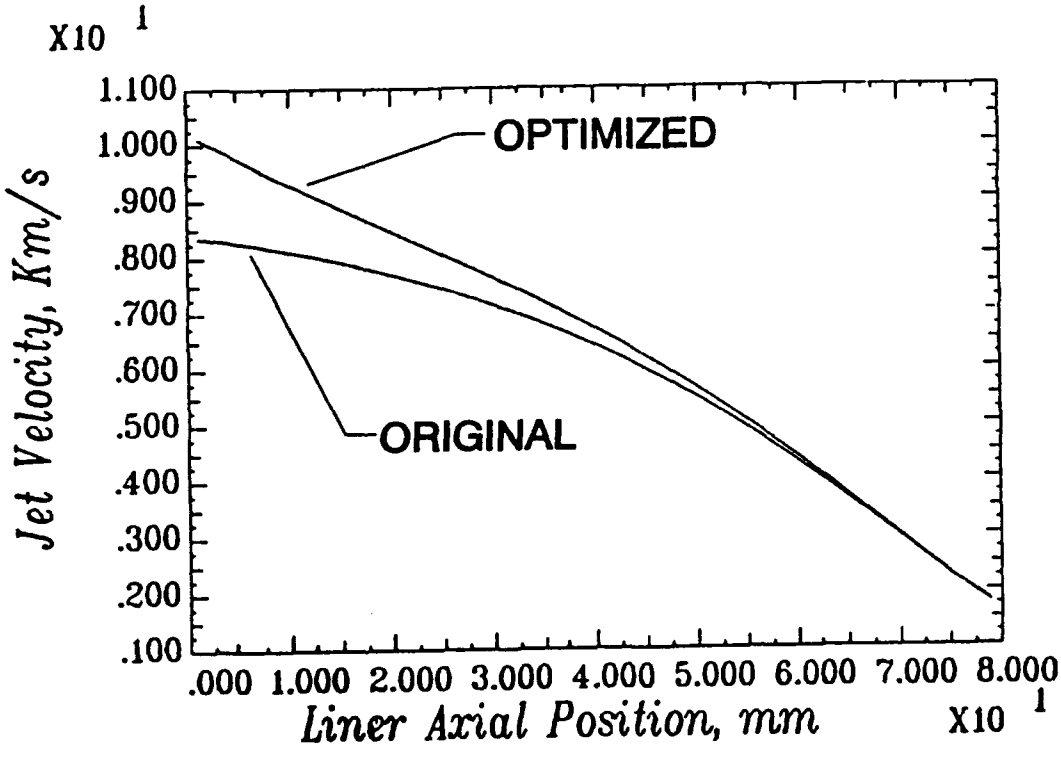

Figure 32. Jet velocity versus initial liner position

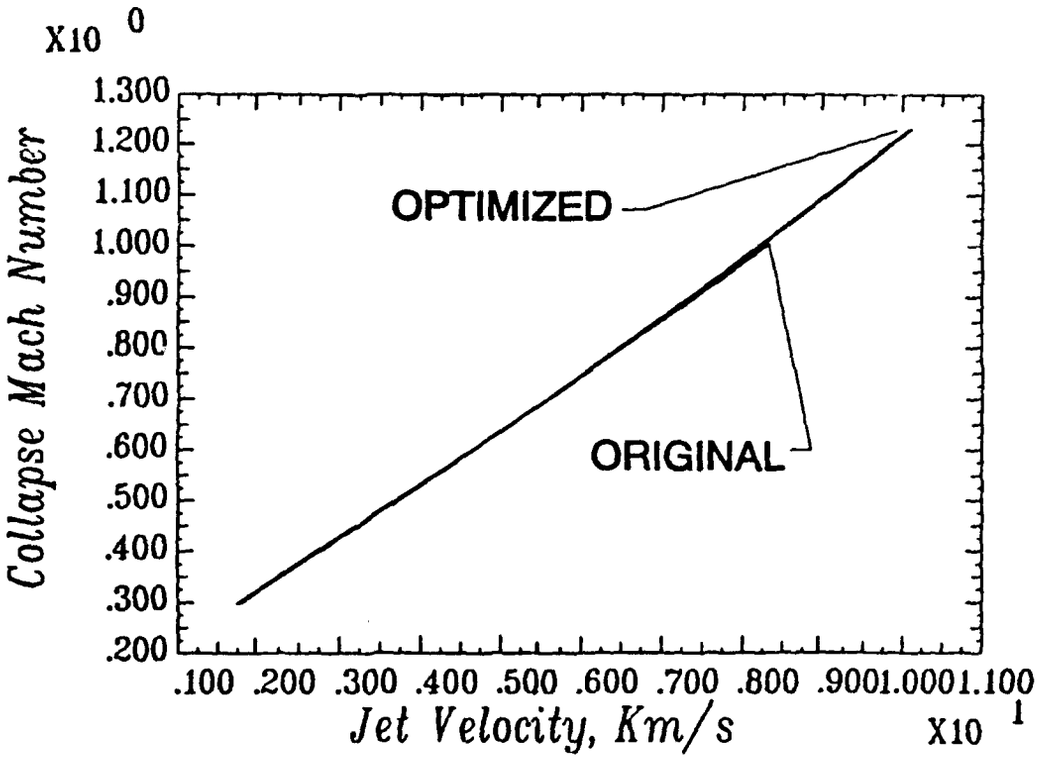

Figure 33. Collapse Mach number versus jet velocity

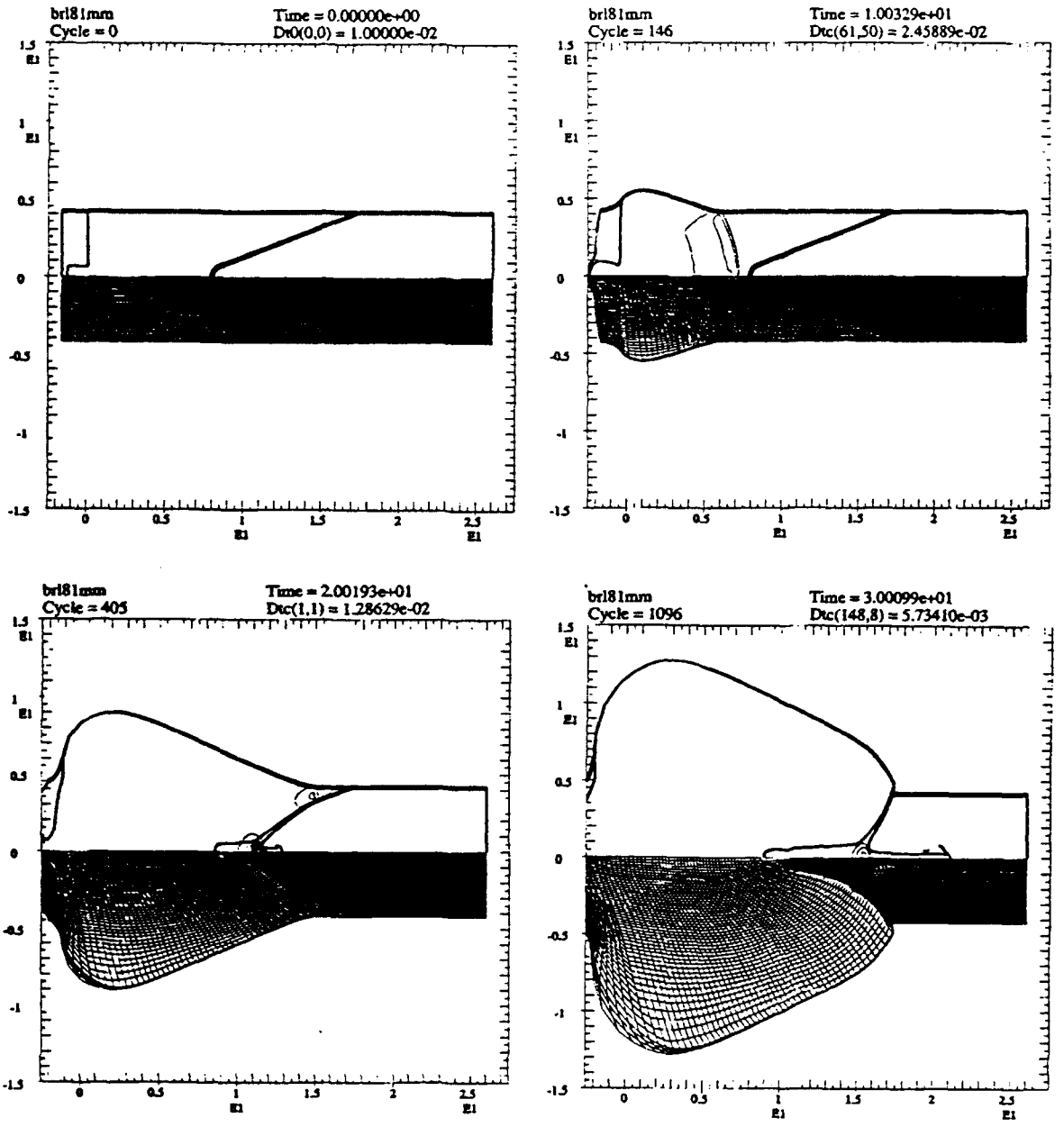

Figure 34. CALE calculated material boundaries, mesh, position, and 100 Kbar pressure contours of the original design at 10 μs intervals

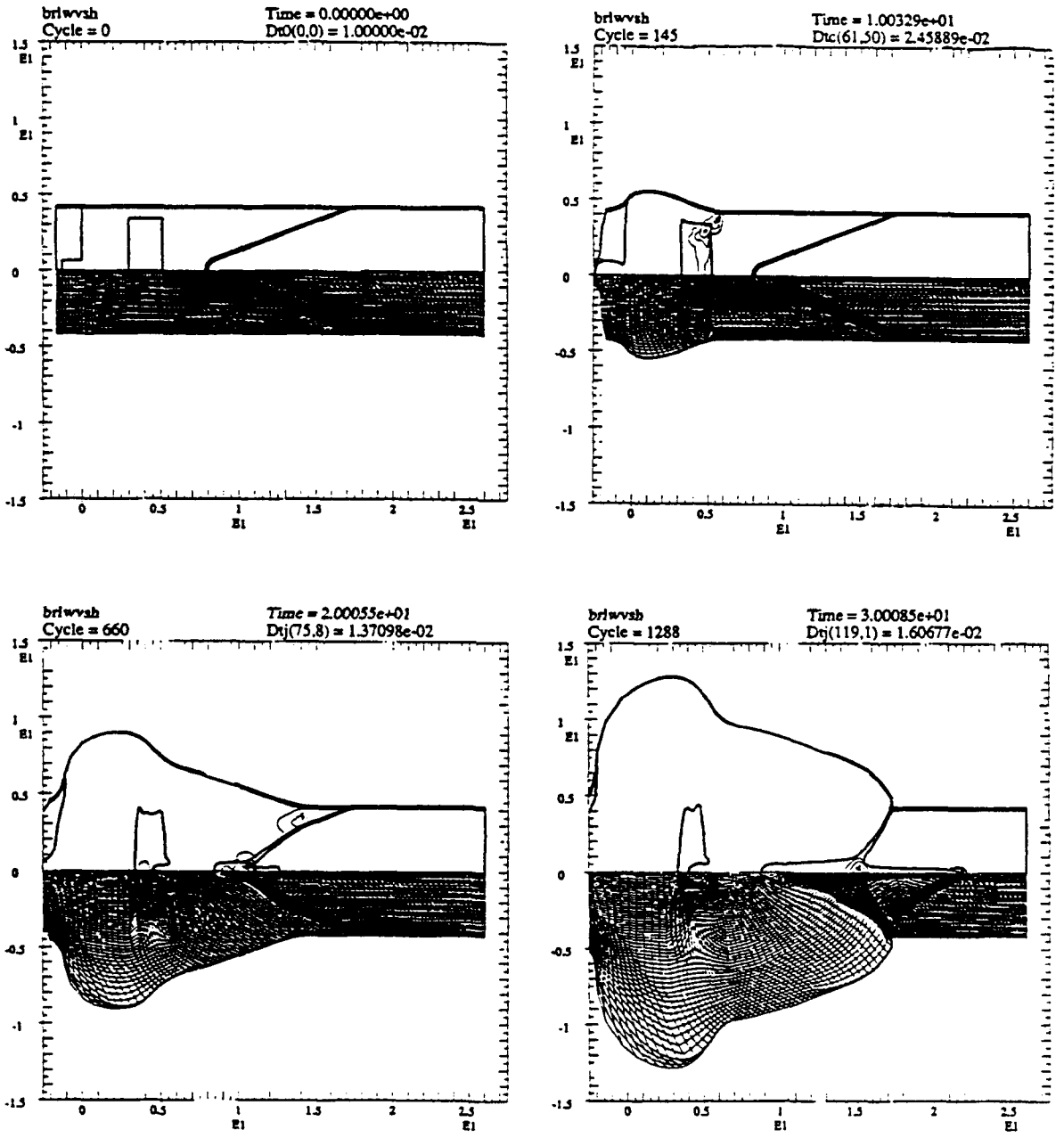

Figure 35. CALE calculated material boundaries, mesh position, and 100 Kbar pressure contours of the optimized design at 10 μs intervals

ORIGINAL

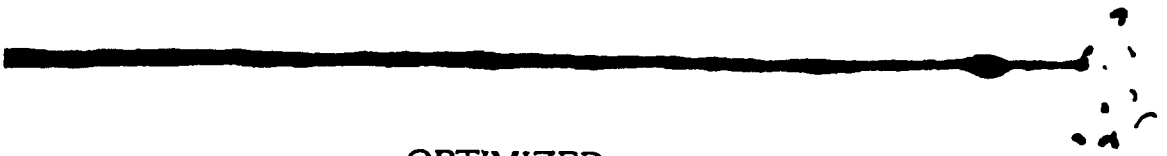

OPTIMIZED

Figure 36. Jet tip region x-rays of the original and optimized shaped charge jets at approximately 7 OD standoff

REFERENCES

1. Sedgwick, R. T., Gittings, M. L.; and Walsh, J. M., "Numerical Techniques for Shaped Charge Design," Behavior and Utilization of Explosives in Engineering Design, Proceedings of the 12th Annual Symposium, New Mexico Section ASME: 243-250, Albuquerque, NM, 1972.

2. DeFrank, P., Industrial Applications of Conical and Linear Shaped Charges, Behavior and Utilization of Explosives in Engineering Design, Proceedings of the 12th Annual Symposium, New Mexico Section ASME: 251-255, Albuquerque, NM, 1972.

3. Austin, C. F., "Lined Cavity Shaped Charges and Their Use in Rock and Earth Materials," Bulletin 69, State Bureau of Mines and Mineral Resources, New Mexico Institute of Mining and Technology, Socorro, NM, 1959.

4. Tipton, R., "CALE Users Manual," Cale Documentation, Lawerence Livermore National Laboratory, Livermore, CA, August 1989.

5. Pugh, E. M.; Eichelberger, R. J.; and Rostoker, N., "Theory of Jet Formation by Charges with Lined Conical Cavities," J. App. Phys. 23, no. 5: 532-536, 1952.

6. Birkhoff, G.; MacDougall, D. P.; Pugh, E. M.; and Taylor, G. I., "Explosives with Lined Cavities," Journal of Applied Physics 19: 563-582m 1948.

7. Chou, P. C. and Flis, W. J, "Recent Developments in Shaped Charge Technology," Propellants, Explosives, and Pyrotechnics 11: 99-114, 1983.

8. Haug, E. J. and Arora, J. S., Applied Optimal Design: Mechanical and Structural Systems, John Wiley and Sons, New York, 1979.

9. Gill, P. E.; Murray, W.; and Wright, M. H., Practical Optimization, Academic Press, London, 1981.

10. Gill, P.E. et al., "Model Building and Practical Aspects of Nonlinear Programming," Computational Programming, NATO ASI Series, Vol F15, Springer-Verlag, Berlin, 1985.

11. Schittkowski, K., Nonlinear Programming Codes, Lecture Notes in Economics and Mathematical Systems 183, Springer-Verlag, 1980.

12. Powell, M. J. D., A Fast Algorithm for Nonlinearly Constrained Optimization Calculations, Proceedings, Biennial Conference, Dundee 1977, Lecture Notes in Mathematics 630, Springer-Verlag, 1978.

13. Carleone, J.; Chou, P. C.; and Tanzio, C. A., "User's Manual for DESC-1, A One-Dimensional Computer Code to Model Shaped Charge Liner Collapse, Jet Formation, and Jet Properties," Technical Report DE-TR-74-4, Dyna East Corporation, 1975.

14. Harrison, J. T., BASC, an Analytical Code for Calculating Shaped Charge Properties, Proc. 6th Int. Symp. on Ballistics: 27-29, Orlando, FL, 1979.

15. Robinson, A. C., "SCAP--A Shaped Charge Analysis Program, User's Manual for SCAP 1.0," Report SAND86-0708, Sandia National Laboratories, 1985.

16. Baker, E. L., "PASCC1: Picatinny Arsenal Shaped Charge Code, One-Dimensional Analysis, Version 2.1," Technical Report ARAED-TR-88019, ARDEC, Picatinny Arsenal, NJ, 1988.

17. Courant, R. and Friedrichs, K. O., "Supersonic Flow and Shock Waves," Interscience Publishers, New York, 1984.

18. Ficket, W. and Davis, W. C., Detonation, University of California Press, Berkeley, CA, 1979.

19. Chapman, D., "On the Rate of Explosion in Gases," Phil. Mag, XLVII: 90-104, 1899.

20. Jouguet, M., J. Math (6), I:347, 1905.

21. Dobratz, B. M., "LLNL Explosives Handbook, Properties of Chemical Explosives and Explosive Simulants," Technical Report UCRL-52997, University of California, CA, 1981.

22. Mader, C. L., "FORTRAN BKW--A Code for Computing the Detonation Properties of Explosives," Technical Report LA-3704, University of California, CA, 1967.

23. Cowperthwaite, M. and Zwisler, W. H., "TIGER Computer Program Documentation," SRI Publication No. Z106, Stanford Research Institute, Menlo Park, CA, 1973.

24. Gurney, R. W., "The Initial Velocities of Fragments from Bombs, Shells, and Grenades," BRL Report 405, U.S. Army Ballistic Research Lab, 1943.

25. Henry, I. G., "The Gurney Formula and Related Approximations for High-Explosive Deployment of Fragments," Hughes Publication - 189, AD 813398, 1967.

26. Jones, E. E., Extension of Gurney Formulas, Document S5B-2, Honeywell Systems and Research Division, 1965.

27. Kennedy, J. E., Explosive Output for Driving Metal, Proc. 12th Annual Symp. on Behavoir and Utilization of Explosives in Engineering Design, N.M., 1972.

28. Chou, P.C. et al, "Improved Formulas for Velocity, Acceleration and Projection Angle of Explosively Driven Liners," Propellants, Explos., Pyrotech. 8(6):175 - 183, 1983.

29. Hennequin, E. M., Analytical Model for the Shaped Charge Liner Collapse, Proc. 7th Int. Symp. on Ballistics, The Haugue, Netherlands, 1983.

30. Chanteret, P.Y., An Analytical Model for Metal Acceleration by Grazing Detonation, Proc. 7th Int. Symp. on Ballistics, The Haugue, Netherlands, 1983.

31. Randers-Pehrson, G., An Improved Equation for Calculating Fragment Projection Angle, Proc. 2nd Symp on Ballistics, Daytona Beach, FL, 1976.

32. Jacobs, S. J., "The Gurney Formula: Variations on a Theme by Lagrange," Technical Report NOLTR74-86, Navel Ordnance Laboratory, 1979.

33. Jones, G. E.; Kennedy, J. E., and Bertholf, L. D., "Ballistics Calculations of R.W. Curney," Am. J. Phys. 48, No. 4:264-269, 1980.

34. Taylor, G. I., Analysis of the Explosion of a Long Cylindrical Bomb Detonated at One End, Scientific Papers of Sir G. I. Taylor, Vol III:2770286, Cambridge University Press (1963), 1941.

35. Defourneaux, M. et Didler, L., "Equations Approches de l'Ecoulement Derrirre une Detonation avec Confinement Lateral," Astronautica Acta 17:615-621, 1972.

36. Kerdraon, A., Etude de la Projection Cylindrique Convergente, ISL Symposium, 1975.

37. Allison, F. E. and R. Vitali, "An Application of the Jet Formation Theory to a 105 mm Shaped Charge," Report 1165, BRL, 1962.

38. Eichelberger, R. J., "Re-Examination of the Nonsteady Theory of Formation by Lined Cavity Charges," J. Appl. Phys. 26 (4):398-402, 1955.

39. DiPersio, R.; Jones, W. H.; Merendino, A. B., and Simon, J., "Characteristics of Jets from Small Caliber Shaped Charges with Copper and Aluminum Liners," Memorandum Report 1866, Ballistics Research Laboratory, 1967.

40. Walsh, J. M.; Shreffler, R. G.; and Willig, F. J., "Limiting Conditions for Jet Formation in High Velocity Collisions," J. Appl. Phys. 24 (3):349-359, 1965.

41. von Neumann, J., "Oblique Reflection of Shocks," Explosives Research Report 12, Navy Department Bureau of Ordnance, Washington, DC, 1943.

42. Chou, P. C.; Carleone, J.; and Karpp, R. R., The Effect of Compressibility on the Formation of Shaped Charge Jets, Proj 1st Int. Symp. on Ballistics, Orlando, FL, 1974.

43. Chou, P. C.; Carleone, J.; and Karpp, R. R., "Criteria for Jet Formulation from Impinging Shell and Plates," J. Appl. Phys. 37:2975 - 2981, 1976.

44. Kiwan, A. R. and Wisniewski, H., "Theory and Computations of Collapse and Jet Velocities of Metallic Shaped Charge Liners," Report 1620, U.S. Army Ballistic Research Laboratories, 1972.

45. Carleone, J; Jameson, R.; and Chou, P. C., "The Tip Origin of a Shaped Charge Jet," Propellants Explos 2: 126-130, 1977.

46. Hallquist, J. O., "DYNA3D User's Manual," Report UCID-19592, Rev 2, Lawrence Livermore National Laboratory, 1986.

47. Baker, E. L., "A Computational Investigation of High Explosive Density and Composition Gradient Effects on Shaped Charge Jet Characteristics," Proceedings of the Ballistics Conference, 1989 SCS Multiconference, Nashville, TN, 1989.

48. Mader, C. L., Numerical Modeling of Detonations, University of California Press, CA, 1979.

49. Wilkens, M. L., "The Equation of State of PBX 9404 and LX04-01," Report UCRL-7797, Lawrence Radiation Laboratory, Livermore, CA, 1964.

50. Lee, E. L.; Horning, H. C.; and Kury, J. W., "Adiabatic Expansion of High Explosive Detonation Products, Report UCRL-50422, University of California, CA, 1968.

51. Green, L. G.; Traver, C. M.; and Erskine, D. J., "Reaction Zone Structure in Supracompressed Detonating Explosives," Report UCRL-101862, University of California, 1989.

52. Baker, E. L. and Orosz, J., "Advanced Warhead Concepts: An Advanced Thermodynamic Equation of State for Overdriven Detonation," Technical Report ARAED-TR-91003, ARDEC, Picatinny Arsenal, NJ, 1991.

53. Baker, E.L., "An Explosives Products Thermodynamic Equation of State Appropriate for Material Acceleration and Overdriven Detonation: Theoretical Backgound and Formulation," Technical Report ARAED-TR-91013, ARDEC, Picatinny Arsenal, NJ, 1991.

54. Kuhn, H. W. and Tucker, A. W., Nonlinear Programming, Proc. Second Berkeley Symposium on Mathematical Statistics and Probability, University of California Press, Berkeley, 1951.

55. Vincent, T. L. and Grantham, W. J., Optimality in Parametric Systems, John Wiley and Sons, NY, 1981.

56. Davidon, W. C., "Variable Metric Methods for Minimization," A.E.C. Res. and Develop. Report ANL-5990, Argonne National Laboratory, Argonne, IL, 1959.

57. Han, S. P., "A Globally Convergent Method for Nonlinear Programming," Report TR 75-257, Computer Science, Cornell University, 1975.

58. Gill, P.E. and Murray, W., "Quasi-Newton Methods for Unconstrained Optimization," J. Inst. Maths. Applics. 9:91 - 108, 1972.

59. Gill, P. E.; Golub, G. H.; Murray, W.; and Saunders, M. A., "Methods for Matrix Factorizations," Math. Comp. 28:505-535, 1974.

60. Hock, W. and Schittkowski, K., Test Examples for Nonlinear Programming Codes, Lecture Notes in Econimics and Mathematical Systems, 187, Springer-Verlag, 1981.

61. Schittkowski, K., More Test Examples for Nonlinear Programming Codes, Lecture Notes in Economics and Mathematical Systems 188, Springer-Verlag, 1987.

62. Powell, M. J. D., "Algorithms for Nonlinear Constraints That Use Lagrangian Functions," Math. Prog. 14:224-248, 1978.

63. Burley, D. M., Studies in Optimization, John Wiley & Sons, NY, pp 78 - 85, 1974.

64. Pierre, D. A., Optimization Theory with Applications, John Wiley & Sons, NY, pp 119-121, 1969.

65. Steinberg, D. J.; Cochran, S. G.; and Guinan, M. W., "A Constitutive Model for Metal Applicable at High-Strain Rate," J. Appl. Phys. 51(3), March 1980.

SYMBOLS

Shaped Charge Modeling Symbols:

P	≡	Pressure
ρ	≡	Density
V	≡	Ratio of specific volume to initial specific volume
E	≡	Specific internal energy divided by initial specific volume
λ	≡	Gruneisen parameter
γ	≡	Adiabatic gamma
c	≡	Sound speed
D	≡	Detonation Velocity
u	≡	Mass velocity
ΔH	≡	Heat of detonation
$A_i, R_i, C, A_{\lambda i},$ $B_{\lambda i}, R_{\lambda i}, \omega$	≡	Equation of state constants
s	≡	Isentropic
cj	≡	Chapman-Jouguet state
o	≡	Initial conditions
U_{det}	≡	Liner sweep velocity
v	≡	liner collapse velocity
v_o	≡	Final liner co llapse velocity

v_{in}	≡	Liner collapse velocity with respect to the collapse point
v_{cl}	≡	Collapse point velocity
v_j	≡	Jet velocity
v_s	≡	Slug velocity
v_{tip}	≡	Jet tip velocity
α	≡	Initial liner angle
δ	≡	Liner collapse velocity vector angle
β	≡	Liner collapse angle
φ	≡	Detonation incidence angle
μ	≡	Charge to mass ratio
C	≡	Charge mass
M	≡	Wall mass
N	≡	Tamping mass
m	≡	Liner mass
E_{gur}	≡	Gurney energy
n	≡	Spatial geometry constant (0 for rectilinear, 1 for cylindrical, and 2 for spherical)
z	≡	Axial position of a Lagrangian jet element

r_j ≡ Jet radius

r_o ≡ Initial liner radial position

r ≡ Liner radial position

U ≡ Mass velocity with respect to D

e ≡ Specific internal energy

Θ ≡ Wall angle

t ≡ time

Parametric Optimization Symbols:

G ≡ Cost function

$\underline{g}$ ≡ Equality constraints

$\underline{h}$ ≡ Inequality constraints

$\underline{x}$ ≡ Optimization variables

$\underline{x}^*$ ≡ Optimal solution

L ≡ Lagrangian function

$\underline{\lambda}$ ≡ Equality Lagrange multipliers

$\underline{\mu}$ ≡ Inequality Lagrange multipliers

W ≡ Merit function

H ≡ Variable metric matrix

$R \equiv$ Upper triangular Cholesky factorization of H ($H = R^T R$)

Shaped Charge Optimization Symbols:

$r_{liner} \equiv$ Liner inside radial position

$T_{liner} \equiv$ Liner thickness

$z_i \equiv$ Axial jet position

$r_{jcalc} \equiv$ Calculated jet radius

$r_{jdef} \equiv$ Defined jet radius

$v_{jcalc} \equiv$ Calculated jet velocity

$v_{jdef} \equiv$ Defined jet velocity

$x_i \equiv$ Original liner axial position

GLOSSARY

ALE	Arbitrary Lagrange Eulerian
BFGS	Broyden, Fletcher, Goldfarb, and Shanno update
BKW	Becker-Kistiakowsky-Wilson
BRL	Ballistic Research Laboratory
CYLTEST	Mathematical cylinder test model
EFP	Explosively formed penetrators
FN	Problem number
Hemi's	Hemispherical shaped charges
JCZ3	Jacobs-Cowperthwaite-Awisler
JWL	Jones-Wilkens-Lee
JWLB	Jones-Wilkens-Lee-Baker equation of state
NLPQL	Nonlinear programming computer program
NLQPEB	Nonlinear optimization program
P-E-R	Pugh, Eichelberger, and Rostoker theory
TIGER	Thermochemical potential calculations

APPENDIX A

MERIT FUNCTION PERFORMANCE

This section presents a computer printout of the merit function performance for the three different merit functions and four different variable metric matrix updates. k1 is the value of the variable metric matrix update parameter. FN is the problem number. Zn is the solution cost for the update n. nfpn is the number of cost function evaluations including cost function evaluations required for partial derivative calculations. nfn is the number of cost function evaluations not including evaluations required for partial derivative calculations.

k1: .05

	Merit Function 1				Merit Function 2				Merit Function 3			
FN	Z1	Z2	Z3	Z4	Z1	Z2	Z3	Z4	Z1	Z2	Z3	Z4
1	.5163E-12	.5163E-12	.5163E-12	.5163E-12	.7575E-14	.7575E-14	.7575E-14	.7575E-14	.3846E-13	.3846E-13	.3846E-13	.3846E-13
2	.5043E-01	.5043E-01	.5043E-01	.5043E-01	.5043E-01	.5043E-01	.5054E-01	.5054E-01	.5043E-01	.5043E-01	.5043E-01	.5043E-01
3	.2500E-27	.2505E-27	.2500E-27	.2500E-27	.1175E-02	.1175E-02	.1175E-02	.1175E-02	.2500E-27	.2505E-27	.2500E-27	.2500E-27
4	.2667E+01	.2667E+01	.2667E+01	.2667E+01	.2670E+01	.2670E+01	.2670E+01	.2670E+01	.2667E+01	.2667E+01	.2667E+01	.2667E+01
5	-.1913E+01	-.1913E+01	-.1913E+01	-.1913E+01	-.1913E+01	-.1913E+01	-.1913E+01	-.1913E+01	-.1913E+01	-.1913E+01	-.1913E+01	-.1913E+01
6	.2486E-22	.2284E-22	.3326E-18	.1013E-14	.2486E-22	.2284E-22	.3326E-18	.1013E-14	.1964E-11	.2362E-22	.3326E-18	.1013E-14
7	-.1732E+01	-.1732E+01	-.1732E+01	-.1732E+01	-.1732E+01	-.1732E+01	-.1732E+01	-.1732E+01	-.1732E+01	-.1732E+01	-.1732E+01	-.1732E+01
8	-.1000E+01	-.1000E+01	-.1000E+01	-.1000E+01	-.1000E+01	-.1000E+01	-.1000E+01	-.1000E+01	-.1000E+01	-.1000E+01	-.1000E+01	-.1000E+01
9	-.5000E+00	-.5000E+00	-.5000E+00	-.5000E+00	-.5000E+00	-.5000E+00	-.5000E+00	-.5000E+00	-.5000E+00	-.5000E+00	-.5000E+00	-.5000E+00
10	-.1000E+01	-.1000E+01	-.1000E+01	-.1000E+01	-.1000E+01	-.1000E+01	-.1000E+01	-.1000E+01	-.1000E+01	-.1000E+01	-.1000E+01	-.1004E+01
201	.1229E-21	.1229E-21	.1229E-21	.1229E-21	.1229E-21	.1229E-21	.1229E-21	.1229E-21	.1229E-21	.1229E-21	.1229E-21	.1229E-21
202	.4898E+02	.4898E+02	.4898E+02	.4898E+02	.4898E+02	.4898E+02	.4898E+02	.4898E+02	.4898E+02	.4898E+02	.4898E+02	.4898E+02
203	.3197E-13	.3197E-13	.3197E-13	.3197E-13	.3197E-13	.3197E-13	.3197E-13	.3197E-13	.3197E-13	.3197E-13	.3197E-13	.3197E-13
204	.1836E+00	.1836E+00	.1836E+00	.1836E+00	.1836E+00	.1836E+00	.1836E+00	.1836E+00	.1836E+00	.1836E+00	.1836E+00	.1836E+00
205	.5621E-13	.5621E-13	.5621E-13	.5621E-13	.5621E-13	.5621E-13	.5621E-13	.5621E-13	.5621E-13	.5621E-13	.5621E-13	.5621E-13
206	.3334E-14	.3334E-14	.3334E-14	.3334E-14	.3334E-14	.3334E-14	.3334E-14	.3334E-14	.3334E-14	.3334E-14	.3334E-14	.3334E-14
207	.1491E-16	.1491E-16	.1491E-16	.1491E-16	.1491E-16	.1491E-16	.1491E-16	.1491E-16	.1491E-16	.1491E-16	.1491E-16	.1491E-16
208	.1922E-15	.1922E-15	.1922E-15	.1922E-15	.1922E-15	.1922E-15	.1922E-15	.1922E-15	.1922E-15	.1922E-15	.1922E-15	.1922E-15
209	.7030E-12	.7030E-12	.7030E-12	.7030E-12	.7030E-12	.7030E-12	.7030E-12	.7030E-12	.7030E-12	.7030E-12	.7030E-12	.7030E-12
210	.2460E+01	.2460E+01	.2460E+01	.2460E+01	.2460E+01	.2460E+01	.2460E+01	.2460E+01	.2460E+01	.2460E+01	.2460E+01	.2460E+01
211	.6503E-13	.2117E-15	.6503E-13	.6503E-13	.6503E-13	.2117E-15	.6503E-13	.6503E-13	.6503E-13	.2117E-15	.6503E-13	.6503E-13
212	.8223E-15	.3959E-14	.1481E-14	.1481E-14	.8223E-15	.3959E-14	.1481E-14	.1481E-14	.8223E-15	.3959E-14	.1481E-14	.1481E-14
213	.3199E-18	.1644E-23	.1644E-23	.1644E-23	.3199E-18	.1644E-23	.1644E-23	.1644E-23	.3199E-18	.1644E-23	.1644E-23	.1644E-23
214	.3286E-02	.4938E-02	.3391E-02	.3391E-02	.3286E-02	.4938E-02	.3391E-02	.3391E-02	.3286E-02	.4938E-02	.3391E-02	.3391E-02
215	-.2804E-17	-.2537E-10	-.2804E-17	-.6468E-14	-.3074E-10	-.3074E-10	-.3074E-10	-.3561E-14	-.8739E-04	-.8739E-04	-.8739E-04	-.8740E-04
216	.9994E+00	.9994E+00	.9994E+00	.9994E+00	.9994E+00	.9994E+00	.9994E+00	.9994E+00	.9994E+00	.9994E+00	.9994E+00	.9994E+00
217	-.8000E+00	-.8000E+00	-.8000E+00	-.8000E+00	-.8000E+00	-.8000E+00	-.8000E+00	-.8000E+00	-.8000E+00	-.8000E+00	-.8000E+00	-.8000E+00
218	-.6536E-25	-.6223E-25	.5364E-25	.5364E-25	-.6536E-25	-.6223E-25	.5364E-25	.5364E-25	-.3761E-19	-.7138E-21	-.1174E-20	-.1405E-21
219	-.1000E+01	-.1000E+01	-.1000E+01	-.1000E+01	-.1000E+01	-.1000E+01	-.1000E+01	-.1000E+01	-.1002E+01	-.1002E+01	-.1000E+01	-.9925E+00
220	.1000E+01	.1000E+01	.1000E+01	.1000E+01	.1000E+01	.1000E+01	.1000E+01	.1000E+01	.1000E+01	.1000E+01	.1000E+01	.1000E+01
221	-.1000E+01	-.1000E+01	-.1000E+01	-.1000E+01	-.1000E+01	-.1000E+01	-.1000E+01	-.1000E+01	-.1000E+01	-.1000E+01	-.1000E+01	-.1000E+01
222	-.1500E+01	-.1500E+01	-.1500E+01	-.1500E+01	-.1500E+01	-.1500E+01	-.1500E+01	-.1500E+01	-.1500E+01	-.1500E+01	-.1500E+01	-.1500E+01
223	-.8340E+00	-.8340E+00	-.8340E+00	-.8340E+00	-.8340E+00	-.8340E+00	-.8340E+00	-.8340E+00	-.8340E+00	-.8340E+00	-.8340E+00	-.8340E+00
224	-.3040E+03	-.3040E+03	-.3040E+03	-.3040E+03	-.3037E+03	-.3037E+03	-.3018E+03	-.2997E+03	-.3040E+03	-.3040E+03	-.3040E+03	-.3040E+03
225	.2000E+01	.2000E+01	.2000E+01	.2000E+01	.2004E+01	.2006E+01	.2002E+01	.2002E+01	.2000E+01	.2000E+01	.2000E+01	.2000E+01
226	-.5000E+00	-.5000E+00	-.5000E+00	-.5000E+00	-.5000E+00	-.5000E+00	-.5000E+00	-.5000E+00	-.5001E+00	-.5000E+00	-.5000E+00	-.5000E+00
227	.1000E+01	.1000E+01	.1000E+01	.1000E+01	.1000E+01	.1000E+01	.1000E+01	.1000E+01	.9998E+00	.9998E+00	.9998E+00	.9998E+00

k1: .05

	Merit Function 1								Merit Function 2								Merit Function 3							
FN	nfp1	nf1	nfp2	nf2	nfp3	nf3	nfp4	nf4	nfp1	nf1	nfp2	nf2	nfp3	nf3	nfp4	nf4	nfp1	nf1	nfp2	nf2	nfp3	nf3	nfp4	nf4
1	57	22	57	22	57	22	57	22	88	37	88	37	88	37	88	37	64	25	64	25	64	25	64	25
2	50	21	49	20	54	25	54	25	50	21	49	20	2049	1580	2040	1573	50	21	49	20	54	25	54	25
3	19	6	25	8	19	6	19	6	13	8	13	8	13	8	13	8	19	6	25	8	19	6	19	6
4	7	2	7	2	7	2	7	2	2694	2093	2694	2093	2694	2093	2694	2093	7	2	7	2	7	2	7	2
5	24	9	24	9	24	9	24	9	24	9	24	9	24	9	24	9	27	10	27	10	27	10	27	10
6	26	9	29	10	25	8	25	8	26	9	29	10	25	8	25	8	22	7	64	31	25	8	25	8
7	42	17	42	17	43	18	32	13	50	17	54	21	50	17	50	17	689	342	783	388	679	338	462	239
8	17	6	17	6	17	6	17	6	16	5	16	5	16	5	16	5	16	5	16	5	16	5	16	5
9	32	17	23	12	32	17	29	16	32	17	23	12	32	17	54	27	29	16	23	12	29	16	36	19
10	35	12	35	12	35	12	35	12	35	12	35	12	35	12	35	12	588	293	588	293	588	293	1979	1378
201	15	6	15	6	15	6	15	6	15	6	15	6	15	6	15	6	15	6	15	6	15	6	15	6
202	44	21	44	21	44	21	44	21	44	21	44	21	44	21	44	21	44	21	44	21	44	21	44	21
203	36	13	36	13	36	13	36	13	36	13	36	13	36	13	36	13	36	13	36	13	36	13	36	13
204	22	9	22	9	22	9	22	9	22	9	22	9	22	9	22	9	22	9	22	9	22	9	22	9
205	42	15	42	15	42	15	42	15	42	15	42	15	42	15	42	15	42	15	42	15	42	15	42	15
206	25	10	25	10	25	10	25	10	25	10	25	10	25	10	25	10	25	10	25	10	25	10	25	10
207	39	14	39	14	39	14	39	14	39	14	39	14	39	14	39	14	39	14	39	14	39	14	39	14
208	119	48	119	48	119	48	119	48	119	48	119	48	119	48	119	48	119	48	119	48	119	48	119	48
209	457	186	457	186	457	186	457	186	457	186	457	186	457	186	457	186	457	186	457	186	457	186	457	186
210	35	18	35	18	35	18	35	18	35	18	35	18	35	18	35	18	35	18	35	18	35	18	35	18
211	77	32	76	31	77	32	77	32	77	32	76	31	77	32	77	32	77	32	76	31	77	32	77	32
212	41	16	42	17	42	17	42	17	41	16	42	17	42	17	42	17	41	16	42	17	42	17	42	17
213	326	113	401	138	401	138	401	138	326	113	401	138	401	138	401	138	326	113	401	138	401	138	401	138
214	107	54	101	52	115	58	115	58	107	54	101	52	115	58	115	58	107	54	101	52	115	58	115	58
215	22	7	19	6	22	7	22	7	24	9	24	9	24	9	35	18	323	160	323	160	323	160	323	160
216	109	56	73	36	38	17	45	20	47	20	44	19	44	19	44	19	1260	881	316	203	386	251	450	297
217	25	8	25	8	25	8	25	8	25	8	25	8	25	8	25	8	544	271	544	271	544	271	547	272
218	118	39	67	22	64	21	64	21	118	39	67	22	64	21	64	21	239	110	258	127	275	138	339	170
219	87	18	87	18	87	18	114	25	87	18	87	18	87	18	102	21	2141	940	2230	1029	1779	726	1611	638
220	191	64	175	58	175	58	202	67	191	64	175	58	175	58	202	67	191	64	175	58	175	58	202	67
221	79	26	79	26	79	26	79	26	79	26	79	26	79	26	79	26	79	26	79	26	79	26	79	26
222	19	6	19	6	19	6	19	6	22	9	22	9	22	9	22	9	304	151	304	151	304	151	304	151
223	30	11	31	14	30	11	33	14	33	14	31	14	33	14	29	10	211	102	211	102	211	102	244	119
224	13	4	13	4	13	4	13	4	2683	2082	2683	2082	2683	2082	2683	2082	13	4	13	4	13	4	13	4
225	19	6	19	6	19	6	19	6	2682	2081	2682	2081	1963	1522	1972	1529	19	6	19	6	19	6	19	6
226	36	15	23	8	30	15	31	16	36	15	23	8	30	15	31	16	332	167	303	150	303	150	325	164
227	17	6	17	6	17	6	17	6	17	6	17	6	17	6	17	6	347	208	347	208	347	208	405	238
ADD	2459	942	2409	914	2400	913	2451	930	10457	7174	10438	7165	11741	8178	11813	8206	8899	4372	8222	3867	7735	3564	9019	4614

k1: .1

	Ment Function 1				Ment Function 2				Ment Function 3			
FN	Z1	Z2	Z3	Z4	Z1	Z2	Z3	Z4	Z1	Z2	Z3	Z4
1	.5163E-12	.5163E-12	.5163E-12	.5163E-12	.7575E-14	.7575E-14	.7575E-14	.7575E-14	.3846E-13	.3846E-13	.3846E-13	.3846E-13
2	.5043E-01	.5043E-01	.5043E-01	.5043E-01	.5043E-01	.5043E-01	.5043E-01	.5043E-01	.5043E-01	.5043E-01	.5043E-01	.5043E-01
3	.2500E-27	.2501E-27	.2500E-27	.2500E-27	.1175E-02	.1175E-02	.1175E-02	.1175E-02	.2500E-27	.2501E-27	.2500E-27	.2500E-27
4	.2667E+01	.2667E+01	.2667E+01	.2667E+01	.2670E+01	.2670E+01	.2670E+01	.2670E+01	.2667E+01	.2667E+01	.2667E+01	.2667E+01
5	-.1913E+01	-.1913E+01	-.1913E+01	-.1913E+01	-.1913E+01	-.1913E+01	-.1913E+01	-.1913E+01	-.1913E+01	-.1913E+01	-.1913E+01	.1913E+01
6	.2503E-22	.2163E-22	.4017E-16	.1013E-14	.2503E-22	.2163E-22	.4017E-16	.1013E-14	.4844E-20	.6336E-23	.4017E-16	.1013E-14
7	-.1732E+01	-.1732E+01	-.1732E+01	-.1732E+01	-.1732E+01	-.1732E+01	-.1732E+01	-.1732E+01	-.1732E+01	-.1732E+01	-.1732E+01	-.1732E+01
8	-.1000E+01	-.1000E+01	-.1000E+01	-.1000E+01	-.1000E+01	-.1000E+01	-.1000E+01	-.1000E+01	-.1000E+01	-.1000E+01	-.1000E+01	-.1000E+01
9	-.5000E+00	-.5000E+00	-.5000E+00	-.5000E+00	-.5000E+00	-.5000E+00	-.5000E+00	-.5000E+00	-.5000E+00	-.5000E+00	-.5000E+00	.5000E+00
10	-.1000E+01	-.1000E+01	-.1000E+01	-.1000E+01	-.1000E+01	-.1000E+01	-.1000E+01	-.1000E+01	-.1000E+01	-.1000E+01	-.1000E+01	.9997E+00
201	.1229E-21	.1229E-21	.1229E-21	.1229E-21	.1229E-21	.1229E-21	.1229E-21	.1229E-21	.1229E-21	.1229E-21	.1229E-21	.1229E-21
202	.4898E+02	.4898E+02	.4898E+02	.4898E+02	.4898E+02	.4898E+02	.4898E+02	.4898E+02	.4898E+02	.4898E+02	.4898E+02	.4898E+02
203	.3197E-13	.3197E-13	.3197E-13	.3197E-13	.3197E-13	.3197E-13	.3197E-13	.3197E-13	.3197E-13	.3197E-13	.3197E-13	.3197E-13
204	.1836E+00	.1836E+00	.1836E+00	.1836E+00	.1836E+00	.1836E+00	.1836E+00	.1836E+00	.1836E+00	.1836E+00	.1836E+00	.1836E+00
205	.5621E-13	.5621E-13	.5621E-13	.5621E-13	.5621E-13	.5621E-13	.5621E-13	.5621E-13	.5621E-13	.5621E-13	.5621E-13	.5621E-13
206	.3334E-14	.3334E-14	.3334E-14	.3334E-14	.3334E-14	.3334E-14	.3334E-14	.3334E-14	.3334E-14	.3334E-14	.3334E-14	.3334E-14
207	.1491E-16	.1491E-16	.1491E-16	.1491E-16	.1491E-16	.1491E-16	.1491E-16	.1491E-16	.1491E-16	.1491E-16	.1491E-16	.1491E-16
208	.1922E-15	.1922E-15	.1922E-15	.1922E-15	.1922E-15	.1922E-15	.1922E-15	.1922E-15	.1922E-15	.1922E-15	.1922E-15	.1922E-15
209	.7030E-12	.7030E-12	.7030E-12	.7030E-12	.7030E-12	.7030E-12	.7030E-12	.7030E-12	.7030E-12	.7030E-12	.7030E-12	.7030E-12
210	.2460E+01	.2460E+01	.2460E+01	.2460E+01	.2460E+01	.2460E+01	.2460E+01	.2460E+01	.2460E+01	.2460E+01	.2460E+01	.2460E+01
211	.6503E-13	.3595E-16	.6503E-13	.6503E-13	.6503E-13	.3595E-16	.6503E-13	.6503E-13	.6503E-13	.3595E-16	.6503E-13	.6503E-13
212	.8223E-15	.7835E-14	.2995E-14	.2995E-14	.8223E-15	.7835E-14	.2995E-14	.2995E-14	.8223E-15	.7835E-14	.2995E-14	.2995E-14
213	.3199E-18	.1644E-23	.1644E-23	.1644E-23	.3199E-18	.1644E-23	.1644E-23	.1644E-23	.3199E-18	.1644E-23	.1644E-23	.1644E-23
214	.3286E-02	.2998E-02	.3464E-02	.3464E-02	.3286E-02	.2998E-02	.3464E-02	.3464E-02	.3286E-02	.2998E-02	.3464E-02	.3464E-02
215	-.2804E-17	.4756E-23	-.2804E-17	-.6468E-14	-.3074E-10	-.2040E-13	-.3074E-10	-.3561E-14	-.8739E-04	-.8740E-04	-.8739E-04	-.8741E-04
216	.9994E+00	.9994E+00	.9994E+00	.9994E+00	.9994E+00	.9994E+00	.9994E+00	.9994E+00	.9994E+00	.9994E+00	.9994E+00	.9994E+00
217	-.8000E+00	-.8000E+00	-.8000E+00	-.8000E+00	-.8000E+00	-.8000E+00	-.8000E+00	-.8000E+00	-.8000E+00	-.8000E+00	-.8000E+00	-.8000E+00
218	-.6536E-25	-.1797E-25	.5364E-25	.5364E-25	-.6536E-25	-.1797E-25	.5364E-25	.5364E-25	-.3761E-19	-.2923E-11	-.1174E-20	-.1405E-21
219	-.1000E+01	-.1000E+01	-.1000E+01	-.1000E+01	-.1000E+01	-.1000E+01	-.1000E+01	-.1000E+01	-.1038E+01	-.1000E+01	.1006E+01	-.9986E+00
220	.1000E+01	.1000E+01	.1000E+01	.1000E+01	.1000E+01	.1000E+01	.1000E+01	.1000E+01	.1000E+01	.1000E+01	.1000E+01	.1000E+01
221	-.1000E+01	-.1000E+01	-.1000E+01	-.1000E+01	-.1000E+01	-.1000E+01	-.1000E+01	-.1000E+01	-.1000E+01	-.1000E+01	-.1000E+01	-.1000E+01
222	-.1500E+01	-.1500E+01	-.1500E+01	-.1500E+01	-.1500E+01	-.1500E+01	-.1500E+01	-.1500E+01	-.1500E+01	-.1500E+01	-.1500E+01	-.1500E+01
223	-.8340E+00	-.8340E+00	-.8340E+00	-.8340E+00	-.8340E+00	-.8340E+00	-.8340E+00	-.8340E+00	-.8340E+00	-.8340E+00	-.8340E+00	-.8340E+00
224	-.3040E+03	-.3040E+03	-.3040E+03	-.3040E+03	-.3037E+03	-.3037E+03	-.3013E+03	-.2997E+03	-.3040E+03	-.3040E+03	-.3040E+03	-.3040E+03
225	.2000E+01	.2000E+01	.2000E+01	.2000E+01	.2004E+01	.2006E+01	.2002E+01	.2002E+01	.2000E+01	.2000E+01	.2000E+01	.2000E+01
226	-.5000E+00	-.5000E+00	-.5000E+00	-.5000E+00	-.5000E+00	-.5000E+00	-.5000E+00	-.5000E+00	-.5000E+00	-.5000E+00	-.5000E+00	-.5000E+00
227	.1000E+01	.1000E+01	.1000E+01	.1000E+01	.1000E+01	.1000E+01	.1000E+01	.1000E+01	.9998E+00	.9998E+00	.9998E+00	.9998E+00

k1: .1

	Merit Function 1								Merit Function 2								Merit Function 3							
FN	nfp1	nf1	nfp2	nf2	nfp3	nf3	nfp4	nf4	nfp1	nf1	nfp2	nf2	nfp3	nf3	nfp4	nf4	nfp1	nf1	nfp2	nf2	nfp3	nf3	nfp4	nf4
1	57	22	57	22	57	22	57	22	88	37	88	37	88	37	88	37	64	25	64	25	64	25	64	25
2	50	21	51	22	63	26	63	26	50	21	51	22	63	26	63	26	50	21	51	22	63	26	63	26
3	19	6	28	9	19	6	19	6	13	8	13	8	13	8	13	8	19	6	28	9	19	6	19	6
4	7	2	7	2	7	2	7	2	2694	2093	2694	2093	2694	2093	2694	2093	7	2	7	2	7	2	7	2
5	24	9	24	9	24	9	24	9	24	9	24	9	24	9	24	9	27	10	27	10	27	10	27	10
6	29	10	29	10	25	8	25	8	29	10	29	10	25	8	25	8	84	55	76	37	25	8	25	8
7	35	14	42	17	35	14	30	11	52	19	54	23	50	17	47	16	676	337	648	321	665	332	697	362
8	17	6	17	6	17	6	17	6	16	5	16	5	16	5	16	5	16	5	16	5	16	5	16	5
9	32	17	22	9	32	17	29	16	32	17	22	9	32	17	53	28	29	16	30	15	29	16	36	19
10	35	12	35	12	35	12	35	12	35	12	35	12	35	12	35	12	588	293	588	293	588	293	825	444
201	15	6	15	6	15	6	15	6	15	6	15	6	15	6	15	6	15	6	15	6	15	6	15	6
202	44	21	44	21	44	21	44	21	44	21	44	21	44	21	44	21	44	21	44	21	44	21	44	21
203	36	13	36	13	36	13	36	13	36	13	36	13	36	13	36	13	36	13	36	13	36	13	36	13
204	22	9	22	9	22	9	22	9	22	9	22	9	22	9	22	9	22	9	22	9	22	9	22	9
205	42	15	42	15	42	15	42	15	42	15	42	15	42	15	42	15	42	15	42	15	42	15	42	15
206	25	10	25	10	25	10	25	10	25	10	25	10	25	10	25	10	25	10	25	10	25	10	25	10
207	3	1	3	1	3	1	3	1	3	1	3	1	3	1	3	1	3	1	3	1	3	1	3	
208	119	48	119	48	119	48	119	48	119	48	119	48	119	48	119	48	119	48	119	48	119	48	119	48
209	457	186	457	186	457	186	457	186	457	186	457	186	457	186	457	186	457	186	457	186	457	186	457	186
210	35	18	35	18	35	18	35	18	35	18	35	18	35	18	35	18	35	18	35	18	35	18	35	18
211	77	32	76	31	77	32	77	32	77	32	76	31	77	32	77	32	77	32	76	31	77	32	77	32
212	41	16	40	17	43	18	43	18	41	16	40	17	43	18	43	18	41	16	40	17	43	18	43	18
213	326	113	401	138	401	138	401	138	326	113	401	138	401	138	401	138	326	113	401	138	401	138	401	138
214	107	54	104	53	104	53	104	53	107	54	104	53	104	53	104	53	107	54	104	53	104	53	104	53
215	22	7	22	7	22	7	22	7	24	9	25	10	24	9	35	18	323	160	323	160	323	160	323	160
216	49	22	69	36	37	16	36	15	47	20	44	19	44	19	44	19	253	166	762	515	158	101	108	63
217	25	8	25	8	25	8	25	8	25	8	25	8	25	8	25	8	544	271	544	271	544	271	547	272
218	118	39	67	22	64	21	64	21	118	39	67	22	64	21	64	21	239	110	757	376	275	138	339	170
219	87	18	87	18	87	18	114	25	87	18	87	18	87	18	102	21	2295	1094	1601	748	2164	963	1750	737
220	175	58	184	61	175	58	206	69	175	58	184	61	175	58	206	69	175	58	184	61	175	58	202	67
221	79	26	79	26	79	26	79	26	79	26	79	26	79	26	79	26	79	26	79	26	79	26	79	26
222	19	6	19	6	19	6	19	6	22	9	22	9	22	9	22	9	304	151	304	151	304	151	304	151
223	30	11	31	14	30	11	33	14	33	14	31	14	33	14	29	10	211	102	211	102	211	102	200	97
224	13	4	13	4	13	4	13	4	2683	2082	2683	2082	2683	2082	2683	2082	13	4	13	4	13	4	13	4
225	19	6	19	6	19	6	19	6	2682	2081	2682	2081	1954	1515	1972	1529	19	6	19	6	19	6	19	6
226	35	14	23	8	24	9	30	15	35	14	23	8	24	9	30	15	117	64	299	148	299	148	378	197
227	17	6	17	6	17	6	17	6	17	6	17	6	17	6	17	6	347	208	347	208	347	208	405	238
ADD	2378	899	2422	919	2384	899	2442	921	10445	7170	10450	7171	9730	6607	9825	6656	7864	3745	8433	4094	7873	3640	7905	3676

k1: .15

	Merit Function 1				Merit Function 2				Merit Function 3			
FN	Z1	Z2	Z3	Z4	Z1	Z2	Z3	Z4	Z1	Z2	Z3	Z4
1	.5163E-12	.3717E-12	.5163E-12	.5163E-12	.7575E-14	.1846E-15	.7575E-14	.7575E-14	.3846E-13	.3846E-13	.3846E-13	.3846E-13
2	.5043E-01	.5043E-01	.5043E-01	.5043E-01	.5043E-01	.5043E-01	.5043E-01	.5043E-01	.5043E-01	.5043E-01	.5043E-01	.5043E-01
3	.2500E-27	.2501E-27	.2500E-27	.2500E-27	.1175E-02	.1175E-02	.1175E-02	.1175E-02	.2500E-27	.2501E-27	.2500E-27	.2500E-27
4	.2667E+01	.2667E+01	.2667E+01	.2667E+01	.2670E+01	.2670E+01	.2670E+01	.2670E+01	.2667E+01	.2667E+01	.2667E+01	.2667E+01
5	-.1913E+01	-.1913E+01	-.1913E+01	-.1913E+01	-.1913E+01	-.1913E+01	-.1913E+01	-.1913E+01	-.1913E+01	-.1913E+01	-.1913E+01	-.1913E+01
6	.2398E-22	.2759E-22	.1264E-12	.1013E-14	.2398E-22	.2759E-22	.1264E-12	.1013E-14	.6898E-15	.7805E-22	.1264E-12	.1013E-14
7	-.1732E+01	-.1732E+01	-.1732E+01	-.1732E+01	-.1732E+01	-.1732E+01	-.1732E+01	-.1732E+01	-.1732E+01	-.1732E+01	-.1732E+01	-.1732E+01
8	-.1000E+01	-.1000E+01	-.1000E+01	-.1000E+01	-.1000E+01	-.1000E+01	-.1000E+01	-.1000E+01	-.1000E+01	-.1000E+01	-.1000E+01	-.1000E+01
9	-.5000E+00	-.5000E+00	-.5000E+00	-.5000E+00	-.5000E+00	-.5000E+00	-.5000E+00	-.5000E+00	-.5000E+00	-.5000E+00	-.5000E+00	.5000E+00
10	-.1000E+01	-.1000E+01	-.1000E+01	-.1000E+01	-.1000E+01	-.1000E+01	-.1000E+01	-.1000E+01	-.1000E+01	-.1000E+01	-.1000E+01	-.1000E+01
201	.1229E-21	.1229E-21	.1229E-21	.1229E-21	.1229E-21	.1229E-21	.1229E-21	.1229E-21	.1229E-21	.1229E-21	.1229E-21	.1229E-21
202	.4898E+02	.4898E+02	.4898E+02	.4898E+02	.4898E+02	.4898E+02	.4898E+02	.4898E+02	.4898E+02	.4898E+02	.4898E+02	.4898E+02
203	.3197E-13	.3197E-13	.3197E-13	.3197E-13	.3197E-13	.3197E-13	.3197E-13	.3197E-13	.3197E-13	.3197E-13	.3197E-13	.3197E-13
204	.1836E+00	.1836E+00	.1836E+00	.1836E+00	.1836E+00	.1836E+00	.1836E+00	.1836E+00	.1836E+00	.1836E+00	.1836E+00	.1836E+00
205	.5621E-13	.5621E-13	.5621E-13	.5621E-13	.5621E-13	.5621E-13	.5621E-13	.5621E-13	.5621E-13	.5621E-13	.5621E-13	.5621E-13
206	.3334E-14	.3334E-14	.3334E-14	.3334E-14	.3334E-14	.3334E-14	.3334E-14	.3334E-14	.3334E-14	.3334E-14	.3334E-14	.3334E-14
207	.1491E-16	.1491E-16	.1491E-16	.1491E-16	.1491E-16	.1491E-16	.1491E-16	.1491E-16	.1491E-16	.1491E-16	.1491E-16	.1491E-16
208	.1922E-15	.1922E-15	.1922E-15	.1922E-15	.1922E-15	.1922E-15	.1922E-15	.1922E-15	.1922E-15	.1922E-15	.1922E-15	.1922E-15
209	.7030E-12	.9661E-13	.7030E-12	.7030E-12	.7030E-12	.9661E-13	.7030E-12	.7030E-12	.7030E-12	.9661E-13	.7030E-12	.7030E-12
210	.2460E+01	.2460E+01	.2460E+01	.2460E+01	.2460E+01	.2460E+01	.2460E+01	.2460E+01	.2460E+01	.2460E+01	.2460E+01	.2460E+01
211	.6503E-13	.2825E-16	.6503E-13	.6503E-13	.6503E-13	.2825E-16	.6503E-13	.6503E-13	.6503E-13	.2825E-16	.6503E-13	.6503E-13
212	.8223E-15	.3621E-17	.2570E-13	.2570E-13	.8223E-15	.3621E-17	.2570E-13	.2570E-13	.8223E-15	.3621E-17	.2570E-13	.2570E-13
213	.3199E-18	.1644E-23	.1644E-23	.1644E-23	.3199E-18	.1644E-23	.1644E-23	.1644E-23	.3199E-18	.1644E-23	.1644E-23	.1644E-23
214	.3286E-02	.1812E-02	.2273E-02	.2273E-02	.3286E-02	.1812E-02	.2273E-02	.2273E-02	.3286E-02	.1812E-02	.2273E-02	.2273E-02
215	-.2804E-17	.1092E-21	-.2804E-17	-.6468E-14	-.3074E-10	-.1305E-10	-.3074E-10	-.3561E-14	-.8739E-04	-.8740E-04	-.8739E-04	-.8742E-04
216	.9994E+00	.9994E+00	.9994E+00	.9994E+00	.9994E+00	.9994E+00	.9994E+00	.9994E+00	.9994E+00	.9994E+00	.9994E+00	.9994E+00
217	-.8000E+00	-.8000E+00	-.8000E+00	-.8000E+00	-.8000E+00	-.8000E+00	-.8000E+00	-.8000E+00	-.8000E+00	-.8000E+00	-.8000E+00	-.8000E+00
218	-.6536E-25	.1565E-26	.5364E-25	.5364E-25	-.6536E-25	.1565E-26	.5364E-25	.5364E-25	-.3761E-19	-.2038E-10	-.1174E-20	-.1405E-21
219	-.1000E+01	-.1000E+01	-.1000E+01	-.1000E+01	-.1000E+01	-.1000E+01	-.1000E+01	-.1000E+01	-.1000E+01	-.1000E+01	-.1000E+01	-.9990E+00
220	.1000E+01	.1000E+01	.1000E+01	.1000E+01	.1000E+01	.1000E+01	.1000E+01	.1000E+01	.1000E+01	.1000E+01	.1000E+01	.1000E+01
221	-.1000E+01	-.1000E+01	-.1000E+01	-.1000E+01	-.1000E+01	-.1000E+01	-.1000E+01	-.1000E+01	-.1000E+01	-.1000E+01	-.1000E+01	-.1000E+01
222	-.1500E+01	-.1500E+01	-.1500E+01	-.1500E+01	-.1500E+01	-.1500E+01	-.1500E+01	-.1500E+01	-.1500E+01	-.1500E+01	-.1500E+01	-.1500E+01
223	-.8340E+00	-.8340E+00	-.8340E+00	-.8340E+00	-.8340E+00	-.8340E+00	-.8340E+00	-.8340E+00	-.8340E+00	-.8340E+00	-.8340E+00	-.8340E+00
224	-.3040E+03	-.3040E+03	-.3040E+03	-.3040E+03	-.3037E+03	-.3037E+03	-.3021E+03	-.2997E+03	-.3040E+03	-.3040E+03	-.3040E+03	-.3040E+03
225	.2000E+01	.2000E+01	.2000E+01	.2000E+01	.2005E+01	.2006E+01	.2002E+01	.2002E+01	.2000E+01	.2000E+01	.2000E+01	.2000E+01
226	-.5000E+00	-.5000E+00	-.5000E+00	-.5000E+00	-.5000E+00	-.5000E+00	-.5000E+00	-.5000E+00	-.5000E+00	-.5000E+00	-.5000E+00	-.4876E+00
227	.1000E+01	.1000E+01	.1000E+01	.1000E+01	.1000E+01	.1000E+01	.1000E+01	.1000E+01	.9998E+00	.9998E+00	.9998E+00	.9998E+00

k1: .15

	Merit Function 1								Merit Function 2								Merit Function 3							
I-N	nfp1	nf1	nfp2	nf2	nfp3	nf3	nfp4	nf4	nfp1	nf1	nfp2	nf2	nfp3	nf3	nfp4	nf4	nfp1	nf1	nfp2	nf2	nfp3	nf3	nfp4	nf4
1	57	22	54	21	57	22	57	22	88	37	82	35	88	37	88	37	64	25	64	25	64	25	64	25
2	50	21	58	25	24	11	24	11	50	21	58	25	24	11	24	11	50	21	58	25	24	11	24	11
3	19	6	31	10	19	6	19	6	13	8	13	8	13	8	13	8	19	6	31	10	19	6	19	6
4	7	2	7	2	7	2	7	2	2694	2093	2694	2093	2694	2093	2694	2093	7	2	7	2	7	2	7	2
5	24	9	24	9	24	9	24	9	24	9	24	9	24	9	24	9	27	10	27	10	27	10	27	10
6	30	11	26	9	22	7	25	8	30	11	26	9	22	7	25	8	88	45	80	39	22	7	25	8
7	32	13	34	13	35	14	29	10	46	15	47	18	46	15	46	15	696	353	511	254	712	365	630	325
8	17	6	17	6	17	6	17	6	16	5	16	5	16	5	16	5	16	5	16	5	16	5	16	5
9	32	17	31	14	32	17	29	16	32	17	31	14	32	17	57	30	29	16	31	14	29	16	36	19
10	35	12	35	12	35	12	35	12	35	12	35	12	35	12	35	12	588	293	588	293	588	293	1011	550
201	15	6	15	6	15	6	15	6	15	6	15	6	15	6	15	6	15	6	15	6	15	6	15	6
202	44	21	44	21	44	21	44	21	44	21	44	21	44	21	44	21	44	21	44	21	44	21	44	21
203	36	13	36	13	36	13	36	13	36	13	36	13	36	13	36	13	36	13	36	13	36	13	36	13
204	22	9	22	9	22	9	22	9	22	9	22	9	22	9	22	9	22	9	22	9	22	9	22	9
205	42	15	42	15	42	15	42	15	42	15	42	15	42	15	42	15	42	15	42	15	42	15	42	15
206	25	10	25	10	25	10	25	10	25	10	25	10	25	10	25	10	25	10	25	10	25	10	25	10
207	39	14	39	14	39	14	39	14	39	14	39	14	39	14	39	14	39	14	39	14	39	14	39	14
208	119	48	119	48	119	48	119	48	119	48	119	48	119	48	119	48	119	48	119	48	119	48	119	48
209	457	186	442	181	457	186	457	186	457	186	442	181	457	186	457	186	457	186	442	181	457	186	457	186
210	35	18	35	18	35	18	35	18	35	18	35	18	35	18	35	18	35	18	35	18	35	18	35	18
211	77	32	75	30	77	32	77	32	77	32	75	30	77	32	77	32	77	32	75	30	77	32	77	32
212	41	16	47	20	43	18	43	18	41	16	47	20	43	18	43	18	41	16	47	20	43	18	43	18
213	326	113	401	138	401	138	401	138	326	113	401	138	401	138	401	138	326	113	401	138	401	138	401	138
214	107	54	114	59	121	60	121	60	107	54	114	59	121	60	121	60	107	54	114	59	121	60	121	60
215	22	7	22	7	22	7	22	7	24	9	24	9	24	9	35	18	323	160	323	160	323	160	323	160
216	42	19	70	37	38	17	38	17	47	20	44	19	44	19	44	19	137	80	401	224	518	345	133	78
217	25	8	25	8	25	8	25	8	25	8	25	8	25	8	25	8	544	271	544	271	544	271	547	272
218	118	39	70	23	64	21	64	21	118	39	70	23	64	21	64	21	239	110	785	390	275	138	339	170
219	87	18	87	18	87	18	114	25	87	18	87	18	87	18	102	21	2145	944	2168	967	2145	944	1934	805
220	196	69	187	62	175	58	217	76	196	69	187	62	175	58	217	76	189	64	187	62	175	58	208	69
221	79	26	79	26	79	26	79	26	79	26	79	26	79	26	79	26	79	26	79	26	79	26	79	26
222	19	6	19	6	19	6	19	6	22	9	22	9	22	9	22	9	304	151	304	151	304	151	304	151
223	30	11	31	14	30	11	33	14	33	14	31	14	33	14	29	10	211	102	211	102	211	102	28	11
224	13	4	13	4	13	4	13	4	2683	2082	2683	2082	2683	2082	2683	2082	13	4	13	4	13	4	13	4
225	19	6	19	6	19	6	19	6	2682	2081	2682	2081	1954	1515	1972	1529	19	6	19	6	19	6	19	6
226	35	14	25	12	24	9	24	9	35	14	25	12	24	9	24	9	334	167	295	146	303	150	116	67
227	17	6	17	6	17	6	17	6	17	6	17	6	17	6	17	6	347	208	347	208	347	208	405	238
ADD	2390	907	2437	932	2360	891	2426	915	10461	7178	10458	7179	9701	6596	9811	6650	7853	3624	8545	3976	8240	3891	7783	3606

APPENDIX B

VARIABLE METRIC MATRIX UPDATE PERFORMANCE

This section presents a computer printout of the optimization performance for the four different variable metric matrix updates using the Powell merit function. k1 is the value of the variable metric matrix update parameter. FN is the problem number. Zn is the solution cost for the update n. nfpn is the number of cost function evaluations including cost function evaluations required for partial derivative calculations. nfn is the number of cost function evaluations not including evaluations required for partial derivative calculations. The data is presented in the following order:

k1

FN Z1 Z2 Z3 Z4

. . .

k1

FN nfp1 nf1 nfp2 nf2 nfp3 nf3 nfp4 nf4

. . .

k1: .05

FN	Z1	Z2	Z3	Z4
1	.5163E-12	.5163E-12	.5163E-12	.5163E-12
2	.5043E-01	.5043E-01	.5043E-01	.5043E-01
3	.2500E-27	.2505E-27	.2500E-27	.2500E-27
4	.2667E+01	.2667E+01	.2667E+01	.2667E+01
5	-.1913E+01	-.1913E+01	-.1913E+01	-.1913E+01
6	.2486E-22	.2284E-22	.3326E-18	.1013E-14
7	-.1732E+01	-.1732E+01	-.1732E+01	-.1732E+01
8	-.1000E+01	-.1000E+01	-.1000E+01	-.1000E+01
9	-.5000E+00	-.5000E+00	-.5000E+00	-.5000E+00
10	-.1000E+01	-.1000E+01	-.1000E+01	-.1000E+01
201	.1229E-21	.1229E-21	.1229E-21	.1229E-21
202	.4898E+02	.4898E+02	.4898E+02	.4898E+02
203	.3197E-13	.3197E-13	.3197E-13	.3197E-13
204	.1836E+00	.1836E+00	.1836E+00	.1836E+00
205	.5621E-13	.5621E-13	.5621E-13	.5621E-13
206	.3334E-14	.3334E-14	.3334E-14	.3334E-14
207	.1491E-16	.1491E-16	.1491E-16	.1491E-16
208	.1922E-15	.1922E-15	.1922E-15	.1922E-15
209	.7030E-12	.7030E-12	.7030E-12	.7030E-12
210	.2460E+01	.2460E+01	.2460E+01	.2460E+01
211	.6503E-13	.2117E-15	.6503E-13	.6503E-13
212	.8223E-15	.3959E-14	.1481E-14	.1481E-14
213	.3199E-18	.1644E-23	.1644E-23	.1644E-23
214	.3286E-02	.4938E-02	.3391E-02	.3391E-02
215	-.2804E-17	-.2537E-10	-.2804E-17	-.6468E-14
216	.9994E+00	.9994E+00	.9994E+00	.9994E+00
217	-.8000E+00	-.8000E+00	-.8000E+00	-.8000E+00
218	-.6536E-25	-.6223E-25	.5364E-25	.5364E-25
219	-.1000E+01	-.1000E+01	-.1000E+01	-.1000E+01
220	.1000E+01	.1000E+01	.1000E+01	.1000E+01
221	-.1000E+01	-.1000E+01	-.1000E+01	-.1000E+01
222	-.1500E+01	-.1500E+01	-.1500E+01	-.1500E+01
223	-.8340E+00	-.8340E+00	-.8340E+00	-.8340E+00
224	-.3040E+03	-.3040E+03	-.3040E+03	-.3040E+03
225	.2000E+01	.2000E+01	.2000E+01	.2000E+01
226	-.5000E+00	-.5000E+00	-.5000E+00	-.5000E+00
227	.1000E+01	.1000E+01	.1000E+01	.1000E+01

k1: .05

FN	nfp1	nf1	nfp2	nf2	nfp3	nf3	nfp4	nf4
1	57	22	57	22	57	22	57	22
2	50	21	49	20	54	25	54	25
3	19	6	25	8	19	6	19	6
4	7	2	7	2	7	2	7	2
5	24	9	24	9	24	9	24	9
6	26	9	29	10	25	8	25	8
7	42	17	42	17	43	18	32	13
8	17	6	17	6	17	6	17	6
9	32	17	23	12	32	17	29	16
10	35	12	35	12	35	12	35	12
201	15	6	15	6	15	6	15	6
202	44	21	44	21	44	21	44	21
203	36	13	36	13	36	13	36	13
204	22	9	22	9	22	9	22	9
205	42	15	42	15	42	15	42	15
206	25	10	25	10	25	10	25	10
207	39	14	39	14	39	14	39	14
208	119	48	119	48	119	48	119	48
209	457	186	457	186	457	186	457	186
210	35	18	35	18	35	18	35	18
211	77	32	76	31	77	32	77	32
212	41	16	42	17	42	17	42	17
213	326	113	401	138	401	138	401	138
214	107	54	101	52	115	58	115	58
215	22	7	19	6	22	7	22	7
216	109	56	73	36	38	17	45	20
217	25	8	25	8	25	8	25	8
218	118	39	67	22	64	21	64	21
219	87	18	87	18	87	18	114	25
220	191	64	175	58	175	58	202	67
221	79	26	79	26	79	26	79	26
222	19	6	19	6	19	6	19	6
223	30	11	31	14	30	11	33	14
224	13	4	13	4	13	4	13	4
225	19	6	19	6	19	6	19	6
226	36	15	23	8	30	15	31	16
227	17	6	17	6	17	6	17	6
ADD	2459	942	2409	914	2400	913	2451	930

k1: .1

FN	Z1	Z2	Z3	Z4
1	.5163E-12	.5163E-12	.5163E-12	.5163E-12
2	.5043E-01	.5043E-01	.5043E-01	.5043E-01
3	.2500E-27	.2501E-27	.2500E-27	.2500E-27
4	.2667E+01	.2667E+01	.2667E+01	.2667E+01
5	-.1913E+01	-.1913E+01	-.1913E+01	-.1913E+01
6	.2503E-22	.2163E-22	.4017E-16	.1013E-14
7	-.1732E+01	-.1732E+01	-.1732E+01	-.1732E+01
8	-.1000E+01	-.1000E+01	-.1000E+01	-.1000E+01
9	-.5000E+00	-.5000E+00	-.5000E+00	-.5000E+00
10	-.1000E+01	-.1000E+01	-.1000E+01	-.1000E+01
201	.1229E-21	.1229E-21	.1229E-21	.1229E-21
202	.4898E+02	.4898E+02	.4898E+02	.4898E+02
203	.3197E-13	.3197E-13	.3197E-13	.3197E-13
204	.1836E+00	.1836E+00	.1836E+00	.1836E+00
205	.5621E-13	.5621E-13	.5621E-13	.5621E-13
206	.3334E-14	.3334E-14	.3334E-14	.3334E-14
207	.1491E-16	.1491E-16	.1491E-16	.1491E-16
208	.1922E-15	.1922E-15	.1922E-15	.1922E-15
209	.7030E-12	.7030E-12	.7030E-12	.7030E-12
210	.2460E+01	.2460E+01	.2460E+01	.2460E+01
211	.6503E-13	.3595E-16	.6503E-13	.6503E-13
212	.8223E-15	.7835E-14	.2995E-14	.2995E-14
213	.3199E-18	.1644E-23	.1644E-23	.1644E-23
214	.3286E-02	.2998E-02	.3464E-02	.3464E-02
215	-.2804E-17	.4756E-23	-.2804E-17	-.6468E-14
216	.9994E+00	.9994E+00	.9994E+00	.9994E+00
217	-.8000E+00	-.8000E+00	-.8000E+00	-.8000E+00
218	-.6536E-25	-.1797E-25	.5364E-25	.5364E-25
219	-.1000E+01	-.1000E+01	-.1000E+01	-.1000E+01
220	.1000E+01	.1000E+01	.1000E+01	.1000E+01
221	-.1000E+01	-.1000E+01	-.1000E+01	-.1000E+01
222	-.1500E+01	-.1500E+01	-.1500E+01	-.1500E+01
223	-.8340E+00	-.8340E+00	-.8340E+00	-.8340E+00
224	-.3040E+03	-.3040E+03	-.3040E+03	-.3040E+03
225	.2000E+01	.2000E+01	.2000E+01	.2000E+01
226	-.5000E+00	-.5000E+00	-.5000E+00	-.5000E+00
227	.1000E+01	.1000E+01	.1000E+01	.1000E+01

k1: .1

FN	nfp1	nf1	nfp2	nf2	nfp3	nf3	nfp4	nf4
1	57	22	57	22	57	22	57	22
2	50	21	51	22	63	26	63	26
3	19	6	28	9	19	6	19	6
4	7	2	7	2	7	2	7	2
5	24	9	24	9	24	9	24	9
6	29	10	29	10	25	8	25	8
7	35	14	42	17	35	14	30	11
8	17	6	17	6	17	6	17	6
9	32	17	22	9	32	17	29	16
10	35	12	35	12	35	12	35	12
201	15	6	15	6	15	6	15	6
202	44	21	44	21	44	21	44	21
203	36	13	36	13	36	13	36	13
204	22	9	22	9	22	9	22	9
205	42	15	42	15	42	15	42	15
206	25	10	25	10	25	10	25	10
207	39	14	39	14	39	14	39	14
208	119	48	119	48	119	48	119	48
209	457	186	457	186	457	186	457	186
210	35	18	35	18	35	18	35	18
211	77	32	76	31	77	32	77	32
212	41	16	40	17	43	18	43	18
213	326	113	401	138	401	138	401	138
214	107	54	104	53	104	53	104	53
215	22	7	22	7	22	7	22	7
216	49	22	69	36	37	16	36	15
217	25	8	25	8	25	8	25	8
218	118	39	67	22	64	21	64	21
219	87	18	87	18	87	18	114	25
220	175	58	184	61	175	58	206	69
221	79	26	79	26	79	26	79	26
222	19	6	19	6	19	6	19	6
223	30	11	31	14	30	11	33	14
224	13	4	13	4	13	4	13	4
225	19	6	19	6	19	6	19	6
226	35	14	23	8	24	9	30	15
227	17	6	17	6	17	6	17	6
ADD	2378	899	2422	919	2384	899	2442	921

k1: .15

FN	Z1	Z2	Z3	Z4
1	.5163E-12	.3717E-12	.5163E-12	.5163E-12
2	.5043E-01	.5043E-01	.5043E-01	.5043E-01
3	.2500E-27	.2501E-27	.2500E-27	.2500E-27
4	.2667E+01	.2667E+01	.2667E+01	.2667E+01
5	-.1913E+01	-.1913E+01	-.1913E+01	-.1913E+01
6	.2398E-22	.2759E-22	.1264E-12	.1013E-14
7	-.1732E+01	-.1732E+01	-.1732E+01	-.1732E+01
8	-.1000E+01	-.1000E+01	-.1000E+01	-.1000E+01
9	-.5000E+00	-.5000E+00	-.5000E+00	-.5000E+00
10	-.1000E+01	-.1000E+01	-.1000E+01	-.1000E+01
201	.1229E-21	.1229E-21	.1229E-21	.1229E-21
202	.4898E+02	.4898E+02	.4898E+02	.4898E+02
203	.3197E-13	.3197E-13	.3197E-13	.3197E-13
204	.1836E+00	.1836E+00	.1836E+00	.1836E+00
205	.5621E-13	.5621E-13	.5621E-13	.5621E-13
206	.3334E-14	.3334E-14	.3334E-14	.3334E-14
207	.1491E-16	.1491E-16	.1491E-16	.1491E-16
208	.1922E-15	.1922E-15	.1922E-15	.1922E-15
209	.7030E-12	.9661E-13	.7030E-12	.7030E-12
210	.2460E+01	.2460E+01	.2460E+01	.2460E+01
211	.6503E-13	.2825E-16	.6503E-13	.6503E-13
212	.8223E-15	.3621E-17	.2570E-13	.2570E-13
213	.3199E-18	.1644E-23	.1644E-23	.1644E-23
214	.3286E-02	.1812E-02	.2273E-02	.2273E-02
215	-.2804E-17	.1092E-21	-.2804E-17	-.6468E-14
216	.9994E+00	.9994E+00	.9994E+00	.9994E+00
217	-.8000E+00	-.8000E+00	-.8000E+00	-.8000E+00
218	-.6536E-25	.1565E-26	.5364E-25	.5364E-25
219	-.1000E+01	-.1000E+01	-.1000E+01	-.1000E+01
220	.1000E+01	.1000E+01	.1000E+01	.1000E+01
221	-.1000E+01	-.1000E+01	-.1000E+01	-.1000E+01
222	-.1500E+01	-.1500E+01	-.1500E+01	-.1500E+01
223	-.8340E+00	-.8340E+00	-.8340E+00	-.8340E+00
224	-.3040E+03	-.3040E+03	-.3040E+03	-.3040E+03
225	.2000E+01	.2000E+01	.2000E+01	.2000E+01
226	-.5000E+00	-.5000E+00	-.5000E+00	-.5000E+00
227	.1000E+01	.1000E+01	.1000E+01	.1000E+01

k1: .15

FN	nfp1	nf1	nfp2	nf2	nfp3	nf3	nfp4	nf4
1	57	22	54	21	57	22	57	22
2	50	21	58	25	24	11	24	11
3	19	6	31	10	19	6	19	6
4	7	2	7	2	7	2	7	2
5	24	9	24	9	24	9	24	9
6	30	11	26	9	22	7	25	8
7	32	13	34	13	35	14	29	10
8	17	6	17	6	17	6	17	6
9	32	17	31	14	32	17	29	16
10	35	12	35	12	35	12	35	12
201	15	6	15	6	15	6	15	6
202	44	21	44	21	44	21	44	21
203	36	13	36	13	36	13	36	13
204	22	9	22	9	22	9	22	9
205	42	15	42	15	42	15	42	15
206	25	10	25	10	25	10	25	10
207	39	14	39	14	39	14	39	14
208	119	48	119	48	119	48	119	48
209	457	186	442	181	457	186	457	186
210	35	18	35	18	35	18	35	18
211	77	32	75	30	77	32	77	32
212	41	16	47	20	43	18	43	18
213	326	113	401	138	401	138	401	138
214	107	54	114	59	121	60	121	60
215	22	7	22	7	22	7	22	7
216	42	19	70	37	38	17	38	17
217	25	8	25	8	25	8	25	8
218	118	39	70	23	64	21	64	21
219	87	18	87	18	87	18	114	25
220	196	69	187	62	175	58	217	76
221	79	26	79	26	79	26	79	26
222	19	6	19	6	19	6	19	6
223	30	11	31	14	30	11	33	14
224	13	4	13	4	13	4	13	4
225	19	6	19	6	19	6	19	6
226	35	14	25	12	24	9	24	9
227	17	6	17	6	17	6	17	6
ADD	2390	907	2437	932	2360	891	2426	915

k1: .2

FN	Z1	Z2	Z3	Z4
1	.5163E-12	.1551E-16	.5163E-12	.5163E-12
2	.5043E-01	.5043E-01	.5043E-01	.5043E-01
3	.2500E-27	.2500E-27	.2500E-27	.2500E-27
4	.2667E+01	.2667E+01	.2667E+01	.2667E+01
5	-.1913E+01	-.1913E+01	-.1913E+01	-.1913E+01
6	.6246E-21	.4594E-14	.1798E-17	.1013E-14
7	-.1732E+01	-.1732E+01	-.1732E+01	-.1732E+01
8	-.1000E+01	-.1000E+01	-.1000E+01	-.1000E+01
9	-.5000E+00	-.5000E+00	-.5000E+00	-.5000E+00
10	-.1000E+01	-.1000E+01	-.1000E+01	-.1000E+01
201	.1229E-21	.1229E-21	.1229E-21	.1229E-21
202	.4898E+02	.4898E+02	.4898E+02	.4898E+02
203	.3197E-13	.3197E-13	.3197E-13	.3197E-13
204	.1836E+00	.1836E+00	.1836E+00	.1836E+00
205	.5621E-13	.5621E-13	.5621E-13	.5621E-13
206	.3334E-14	.3334E-14	.3334E-14	.3334E-14
207	.1491E-16	.1491E-16	.1491E-16	.1491E-16
208	.1922E-15	.1922E-15	.1922E-15	.1922E-15
209	.7030E-12	.9218E-13	.7030E-12	.7030E-12
210	.2460E+01	.2460E+01	.2460E+01	.2460E+01
211	.6503E-13	.2838E-14	.6503E-13	.6503E-13
212	.8223E-15	.5525E-12	.9410E-18	.9410E-18
213	.3199E-18	.7771E-23	.1644E-23	.1644E-23
214	.3286E-02	.2346E-02	.4017E-02	.4017E-02
215	-.2804E-17	-.1856E-14	-.2804E-17	-.6468E-14
216	.9994E+00	.9994E+00	.9994E+00	.9994E+00
217	-.8000E+00	-.8000E+00	-.8000E+00	-.8000E+00
218	-.6536E-25	.6243E-25	.5364E-25	.5364E-25
219	-.1000E+01	-.1000E+01	-.1000E+01	-.1000E+01
220	.1000E+01	.1000E+01	.1000E+01	.1000E+01
221	-.1000E+01	-.1000E+01	-.1000E+01	-.1000E+01
222	-.1500E+01	-.1500E+01	-.1500E+01	-.1500E+01
223	-.8340E+00	-.8340E+00	-.8340E+00	-.8340E+00
224	-.3040E+03	-.3040E+03	-.3040E+03	-.3040E+03
225	.2000E+01	.2000E+01	.2000E+01	.2000E+01
226	-.5000E+00	-.5000E+00	-.5000E+00	-.5000E+00
227	.1000E+01	.1000E+01	.1000E+01	.1000E+01

k1: .2

FN	nfp1	nf1	nfp2	nf2	nfp3	nf3	nfp4	nf4
1	57	22	60	23	57	22	57	22
2	50	21	54	23	48	21	48	21
3	19	6	34	11	19	6	19	6
4	7	2	7	2	7	2	7	2
5	24	9	24	9	24	9	24	9
6	30	11	26	9	25	8	25	8
7	34	13	40	15	35	14	29	10
8	17	6	17	6	17	6	17	6
9	32	17	28	13	32	17	29	16
10	35	12	35	12	35	12	35	12
201	15	6	15	6	15	6	15	6
202	44	21	44	21	44	21	44	21
203	36	13	36	13	36	13	36	13
204	22	9	22	9	22	9	22	9
205	42	15	42	15	42	15	42	15
206	25	10	25	10	25	10	25	10
207	39	14	39	14	39	14	39	14
208	119	48	119	48	119	48	119	48
209	457	186	452	185	457	186	457	186
210	35	18	35	18	35	18	35	18
211	77	32	74	29	77	32	77	32
212	41	16	43	18	52	23	52	23
213	326	113	359	124	401	138	401	138
214	107	54	106	57	103	54	103	54
215	22	7	22	7	22	7	22	7
216	42	19	72	39	49	22	45	20
217	25	8	25	8	25	8	25	8
218	118	39	70	23	64	21	64	21
219	87	18	87	18	87	18	114	25
220	187	62	193	64	175	58	208	69
221	79	26	79	26	79	26	79	26
222	19	6	19	6	19	6	19	6
223	30	11	31	14	30	11	33	14
224	13	4	13	4	13	4	13	4
225	19	6	19	6	19	6	19	6
226	28	11	26	13	24	9	24	9
227	17	6	17	6	17	6	17	6
ADD	2376	897	2409	924	2389	906	2439	920

k1: .25

FN	Z1	Z2	Z3	Z4
1	.5163E-12	.5037E-11	.5163E-12	.5163E-12
2	.5043E-01	.5043E-01	.5043E-01	.5043E-01
3	.2500E-27	.2500E-27	.2500E-27	.2500E-27
4	.2667E+01	.2667E+01	.2667E+01	.2667E+01
5	-.1913E+01	-.1913E+01	-.1913E+01	-.1913E+01
6	.2520E-22	.8878E-23	.2501E-22	.1013E-14
7	-.1732E+01	-.1732E+01	-.1732E+01	-.1732E+01
8	-.1000E+01	-.1000E+01	-.1000E+01	-.1000E+01
9	-.5000E+00	-.5000E+00	-.5000E+00	-.5000E+00
10	-.1000E+01	-.1000E+01	-.1000E+01	-.1000E+01
201	.1229E-21	.1229E-21	.1229E-21	.1229E-21
202	.4898E+02	.4898E+02	.4898E+02	.4898E+02
203	.3197E-13	.3197E-13	.3197E-13	.3197E-13
204	.1836E+00	.1836E+00	.1836E+00	.1836E+00
205	.5621E-13	.5621E-13	.5621E-13	.5621E-13
206	.3334E-14	.3334E-14	.3334E-14	.3334E-14
207	.1491E-16	.1709E-16	.1491E-16	.1491E-16
208	.1922E-15	.1922E-15	.1922E-15	.1922E-15
209	.7030E-12	.9591E-13	.7030E-12	.7030E-12
210	.2460E+01	.2460E+01	.2460E+01	.2460E+01
211	.6503E-13	.3584E-16	.6503E-13	.6503E-13
212	.8223E-15	.8270E-14	.3466E-16	.3466E-16
213	.3199E-18	.1093E-16	.1644E-23	.1644E-23
214	.3286E-02	.4895E-02	.2624E-02	.2624E-02
215	-.2804E-17	-.5392E-12	-.2804E-17	-.6468E-14
216	.9994E+00	.9994E+00	.9994E+00	.9994E+00
217	-.8000E+00	-.8000E+00	-.8000E+00	-.8000E+00
218	-.6536E-25	.1988E-25	.5364E-25	.5364E-25
219	-.1000E+01	-.1000E+01	-.1000E+01	-.1000E+01
220	.1000E+01	.1000E+01	.1000E+01	.1000E+01
221	-.1000E+01	-.1000E+01	-.1000E+01	-.1000E+01
222	-.1500E+01	-.1500E+01	-.1500E+01	-.1500E+01
223	-.8340E+00	-.8340E+00	-.8340E+00	-.8340E+00
224	-.3040E+03	-.3040E+03	-.3040E+03	-.3040E+03
225	.2000E+01	.2000E+01	.2000E+01	.2000E+01
226	-.5000E+00	-.5000E+00	-.5000E+00	-.5000E+00
227	.1000E+01	.1000E+01	.1000E+01	.1000E+01

k1: .25

FN	nfp1	nf1	nfp2	nf2	nfp3	nf3	nfp4	nf4
1	57	22	57	22	57	22	57	22
2	50	21	61	26	56	23	56	23
3	19	6	40	13	19	6	19	6
4	7	2	7	2	7	2	7	2
5	24	9	24	9	24	9	24	9
6	33	12	29	10	28	9	25	8
7	31	12	34	11	35	14	29	10
8	17	6	17	6	17	6	17	6
9	32	17	31	14	32	17	29	16
10	35	12	35	12	35	12	35	12
201	15	6	15	6	15	6	15	6
202	44	21	44	21	44	21	44	21
203	36	13	36	13	36	13	36	13
204	22	9	22	9	22	9	22	9
205	42	15	42	15	42	15	42	15
206	25	10	25	10	25	10	25	10
207	39	14	39	14	39	14	39	14
208	119	48	119	48	119	48	119	48
209	457	186	440	177	457	186	457	186
210	35	18	35	18	35	18	35	18
211	77	32	80	31	77	32	77	32
212	41	16	42	17	51	22	51	22
213	326	113	278	97	401	138	401	138
214	107	54	93	46	99	52	99	52
215	22	7	22	7	22	7	22	7
216	46	21	74	39	43	20	49	22
217	25	8	25	8	25	8	25	8
218	118	39	73	24	64	21	64	21
219	87	18	87	18	87	18	114	25
220	184	61	199	66	175	58	208	69
221	79	26	79	26	79	26	79	26
222	19	6	19	6	19	6	19	6
223	30	11	31	14	30	11	33	14
224	13	4	13	4	13	4	13	4
225	19	6	19	6	19	6	19	6
226	28	11	23	8	25	10	24	9
227	17	6	17	6	17	6	17	6
ADD	2377	898	2326	879	2390	905	2446	921

k1: .30

FN	Z1	Z2	Z3	Z4
1	.5163E-12	.1677E-15	.5163E-12	.5163E-12
2	.5043E-01	.5043E-01	.5043E-01	.5043E-01
3	.2500E-27	.2500E-27	.2500E-27	.2500E-27
4	.2667E+01	.2667E+01	.2667E+01	.2667E+01
5	-.1913E+01	-.1913E+01	-.1913E+01	-.1913E+01
6	.2500E-22	.8315E-19	.2501E-22	.1013E-14
7	-.1732E+01	-.1732E+01	-.1732E+01	-.1732E+01
8	-.1000E+01	-.1000E+01	-.1000E+01	-.1000E+01
9	-.5000E+00	-.5000E+00	-.5000E+00	-.5000E+00
10	-.1000E+01	-.1000E+01	-.1000E+01	-.1000E+01
201	.1229E-21	.1229E-21	.1229E-21	.1229E-21
202	.4898E+02	.4898E+02	.4898E+02	.4898E+02
203	.3197E-13	.3197E-13	.3197E-13	.3197E-13
204	.1836E+00	.1836E+00	.1836E+00	.1836E+00
205	.5621E-13	.5621E-13	.5621E-13	.5621E-13
206	.3334E-14	.3334E-14	.3334E-14	.3334E-14
207	.1491E-16	.2134E-20	.1491E-16	.1491E-16
208	.1922E-15	.1447E-16	.1922E-15	.1922E-15
209	.7030E-12	.1310E-12	.7030E-12	.7030E-12
210	.2460E+01	.2460E+01	.2460E+01	.2460E+01
211	.6503E-13	.2369E-16	.6503E-13	.6503E-13
212	.8223E-15	.2094E-15	.1340E-14	.1340E-14
213	.3199E-18	.8506E-30	.1644E-23	.1644E-23
214	.3286E-02	.2288E-02	.1994E-02	.1994E-02
215	-.2804E-17	-.1025E-10	-.2804E-17	-.6468E-14
216	.9994E+00	.9994E+00	.9994E+00	.9994E+00
217	-.8000E+00	-.8000E+00	-.8000E+00	-.8000E+00
218	-.6536E-25	-.1944E-25	.5364E-25	.5364E-25
219	-.1000E+01	-.1000E+01	-.1000E+01	-.1000E+01
220	.1000E+01	.1000E+01	.1000E+01	.1000E+01
221	-.1000E+01	-.1000E+01	-.1000E+01	-.1000E+01
222	-.1500E+01	-.1500E+01	-.1500E+01	-.1500E+01
223	-.8340E+00	-.8340E+00	-.8340E+00	-.8340E+00
224	-.3040E+03	-.3040E+03	-.3040E+03	-.3040E+03
225	.2000E+01	.2000E+01	.2000E+01	.2000E+01
226	-.5000E+00	-.5000E+00	-.5000E+00	-.5000E+00
227	.1000E+01	.1000E+01	.1000E+01	.1000E+01

k1: .30

FN	nfp1	nf1	nfp2	nf2	nfp3	nf3	nfp4	nf4
1	57	22	61	24	57	22	57	22
2	50	21	61	26	55	24	55	24
3	19	6	43	14	19	6	19	6
4	7	2	7	2	7	2	7	2
5	24	9	24	9	24	9	24	9
6	33	12	29	10	28	9	25	8
7	31	12	33	12	30	11	29	10
8	17	6	17	6	17	6	17	6
9	32	17	31	14	32	17	29	16
10	35	12	35	12	35	12	35	12
201	15	6	15	6	15	6	15	6
202	44	21	44	21	44	21	44	21
203	36	13	36	13	36	13	36	13
204	22	9	22	9	22	9	22	9
205	42	15	42	15	42	15	42	15
206	25	10	25	10	25	10	25	10
207	39	14	39	14	39	14	39	14
208	119	48	124	51	119	48	119	48
209	457	186	434	175	457	186	457	186
210	35	18	35	18	35	18	35	18
211	77	32	73	28	77	32	77	32
212	41	16	42	17	43	18	43	18
213	326	113	365	126	401	138	401	138
214	107	54	114	59	110	55	110	55
215	22	7	22	7	22	7	22	7
216	49	22	72	39	47	22	48	21
217	25	8	25	8	25	8	25	8
218	118	39	73	24	64	21	64	21
219	87	18	87	18	87	18	114	25
220	188	63	205	68	175	58	208	69
221	79	26	79	26	79	26	79	26
222	19	6	19	6	19	6	19	6
223	30	11	31	14	30	11	33	14
224	13	4	13	4	13	4	13	4
225	19	6	19	6	19	6	19	6
226	28	11	23	10	28	11	29	12
227	17	6	17	6	17	6	17	6
ADD	2384	901	2436	927	2394	905	2452	923

k1: .35

FN	Z1	Z2	Z3	Z4
1	.5163E-12	.1244E-16	.5163E-12	.5163E-12
2	.5043E-01	.5043E-01	.5043E-01	.5043E-01
3	.2500E-27	.2500E-27	.2500E-27	.2500E-27
4	.2667E+01	.2667E+01	.2667E+01	.2667E+01
5	-.1913E+01	-.1913E+01	-.1913E+01	-.1913E+01
6	.2500E-22	.1298E-17	.2501E-22	.1013E-14
7	-.1732E+01	-.1732E+01	-.1732E+01	-.1732E+01
8	-.1000E+01	-.1000E+01	-.1000E+01	-.1000E+01
9	-.5000E+00	-.5000E+00	-.5000E+00	-.5000E+00
10	-.1000E+01	-.1000E+01	-.1000E+01	-.1000E+01
201	.1229E-21	.1229E-21	.1229E-21	.1229E-21
202	.4898E+02	.4898E+02	.4898E+02	.4898E+02
203	.3197E-13	.3197E-13	.3197E-13	.3197E-13
204	.1836E+00	.1836E+00	.1836E+00	.1836E+00
205	.5621E-13	.5621E-13	.5621E-13	.5621E-13
206	.3334E-14	.3334E-14	.3334E-14	.3334E-14
207	.1491E-16	.2753E-19	.1491E-16	.1491E-16
208	.1922E-15	.1817E-13	.1922E-15	.1922E-15
209	.7030E-12	.9004E-13	.7030E-12	.7030E-12
210	.2460E+01	.2460E+01	.2460E+01	.2460E+01
211	.6503E-13	.3032E-16	.6503E-13	.6503E-13
212	.8223E-15	.7043E-15	.2556E-14	.2556E-14
213	.3199E-18	.6220E-19	.1644E-23	.1644E-23
214	.3286E-02	.3057E-02	.3651E-02	.3651E-02
215	-.2804E-17	-.1091E-16	-.2804E-17	-.6468E-14
216	.9994E+00	.9994E+00	.9994E+00	.9994E+00
217	-.8000E+00	-.8000E+00	-.8000E+00	-.8000E+00
218	-.6536E-25	-.5756E-25	.5364E-25	.5364E-25
219	-.1000E+01	-.1000E+01	-.1000E+01	-.1000E+01
220	.1000E+01	.1000E+01	.1000E+01	.1000E+01
221	-.1000E+01	-.1000E+01	-.1000E+01	-.1000E+01
222	-.1500E+01	-.1500E+01	-.1500E+01	-.1500E+01
223	-.8340E+00	-.8340E+00	-.8340E+00	-.8340E+00
224	-.3040E+03	-.3040E+03	-.3040E+03	-.3040E+03
225	.2000E+01	.2000E+01	.2000E+01	.2000E+01
226	-.5000E+00	-.5000E+00	-.5000E+00	-.5000E+00
227	.1000E+01	.1000E+01	.1000E+01	.1000E+01

k1: .35

FN	nfp1	nf1	nfp2	nf2	nfp3	nf3	nfp4	nf4
1	57	22	64	25	57	22	57	22
2	50	21	54	23	67	28	67	28
3	19	6	46	15	19	6	19	6
4	7	2	7	2	7	2	7	2
5	24	9	24	9	24	9	24	9
6	33	12	29	10	28	9	25	8
7	33	14	32	11	30	11	29	10
8	17	6	17	6	17	6	17	6
9	32	17	28	9	32	17	29	16
10	35	12	35	12	35	12	35	12
201	15	6	15	6	15	6	15	6
202	44	21	44	21	44	21	44	21
203	36	13	36	13	36	13	36	13
204	22	9	22	9	22	9	22	9
205	42	15	42	15	42	15	42	15
206	25	10	25	10	25	10	25	10
207	39	14	39	14	39	14	39	14
208	119	48	106	41	119	48	119	48
209	457	186	430	173	457	186	457	186
210	35	18	35	18	35	18	35	18
211	77	32	80	31	77	32	77	32
212	41	16	41	16	43	18	43	18
213	326	113	227	80	401	138	401	138
214	107	54	104	53	100	51	100	51
215	22	7	25	8	22	7	22	7
216	45	20	71	38	47	20	45	18
217	25	8	25	8	25	8	25	8
218	118	39	73	24	64	21	64	21
219	87	18	87	18	87	18	114	25
220	193	68	211	70	175	58	217	72
221	79	26	79	26	79	26	79	26
222	19	6	19	6	19	6	19	6
223	30	11	31	14	30	11	33	14
224	13	4	13	4	13	4	13	4
225	19	6	19	6	19	6	19	6
226	28	11	19	6	27	10	27	10
227	17	6	17	6	17	6	17	6
ADD	2387	906	2271	856	2395	902	2458	921

k1: .40

FN	Z1	Z2	Z3	Z4
1	.5163E-12	.2558E-14	.5163E-12	.5163E-12
2	.5043E-01	.5043E-01	.5043E-01	.5043E-01
3	.2500E-27	.3940E-26	.2500E-27	.2500E-27
4	.2667E+01	.2667E+01	.2667E+01	.2667E+01
5	-.1913E+01	-.1913E+01	-.1913E+01	-.1913E+01
6	.2363E-22	.1061E-19	.2501E-22	.1013E-14
7	-.1732E+01	-.1732E+01	-.1732E+01	-.1732E+01
8	-.1000E+01	-.1000E+01	-.1000E+01	-.1000E+01
9	-.5000E+00	-.5000E+00	-.5000E+00	-.5000E+00
10	-.1000E+01	-.1000E+01	-.1000E+01	-.1000E+01
201	.1229E-21	.1229E-21	.1229E-21	.1229E-21
202	.4898E+02	.4898E+02	.4898E+02	.4898E+02
203	.3197E-13	.3197E-13	.3197E-13	.3197E-13
204	.1836E+00	.1836E+00	.1836E+00	.1836E+00
205	.5621E-13	.5621E-13	.5621E-13	.5621E-13
206	.3334E-14	.3334E-14	.3334E-14	.3334E-14
207	.1491E-16	.6191E-16	.1491E-16	.1491E-16
208	.1922E-15	.4770E-14	.1922E-15	.1922E-15
209	.7030E-12	.1121E-12	.7030E-12	.7030E-12
210	.2460E+01	.2460E+01	.2460E+01	.2460E+01
211	.6503E-13	.1050E-16	.6503E-13	.6503E-13
212	.8223E-15	.7338E-17	.1034E-11	.1034E-11
213	.3199E-18	.1694E-21	.1644E-23	.1644E-23
214	.3286E-02	.2056E-02	.4277E-02	.4277E-02
215	-.2804E-17	.4963E-23	-.2804E-17	-.6468E-14
216	.9994E+00	.9994E+00	.9994E+00	.4897E+02
217	-.8000E+00	-.8000E+00	-.8000E+00	-.8000E+00
218	-.6536E-25	-.3938E-26	.5364E-25	.5364E-25
219	-.1000E+01	-.1000E+01	-.1000E+01	-.1000E+01
220	.1000E+01	.1000E+01	.1000E+01	.1000E+01
221	-.1000E+01	-.1000E+01	-.1000E+01	-.1000E+01
222	-.1500E+01	-.1500E+01	-.1500E+01	-.1500E+01
223	-.8340E+00	-.8340E+00	-.8340E+00	-.8340E+00
224	-.3040E+03	-.3040E+03	-.3040E+03	-.3040E+03
225	.2000E+01	.2000E+01	.2000E+01	.2000E+01
226	-.5000E+00	-.5000E+00	-.5000E+00	-.5000E+00
227	.1000E+01	.1000E+01	.1000E+01	.1000E+01

k1: .40

FN	nfp1	nf1	nfp2	nf2	nfp3	nf3	nfp4	nf4
1	57	22	64	25	57	22	57	22
2	50	21	49	20	53	24	53	24
3	19	6	49	16	19	6	19	6
4	7	2	7	2	7	2	7	2
5	24	9	24	9	24	9	24	9
6	33	12	29	10	28	9	25	8
7	31	12	33	12	29	10	29	10
8	17	6	17	6	17	6	17	6
9	32	17	31	14	32	17	29	16
10	35	12	35	12	35	12	35	12
201	15	6	15	6	15	6	15	6
202	44	21	44	21	44	21	44	21
203	36	13	36	13	36	13	36	13
204	22	9	22	9	22	9	22	9
205	42	15	42	15	42	15	42	15
206	25	10	25	10	25	10	25	10
207	39	14	39	14	39	14	39	14
208	119	48	101	40	119	48	119	48
209	457	186	403	160	457	186	457	186
210	35	18	35	18	35	18	35	18
211	77	32	79	30	77	32	77	32
212	41	16	40	15	40	17	40	17
213	326	113	251	88	401	138	401	138
214	107	54	106	55	108	57	108	57
215	22	7	22	7	22	7	22	7
216	44	19	70	35	42	19	54	23
217	25	8	25	8	25	8	25	8
218	118	39	76	25	64	21	64	21
219	87	18	87	18	87	18	114	25
220	186	63	220	73	175	58	224	75
221	79	26	79	26	79	26	79	26
222	19	6	19	6	19	6	19	6
223	30	11	31	14	30	11	33	14
224	13	4	13	4	13	4	13	4
225	19	6	19	6	19	6	19	6
226	28	11	25	12	27	10	29	12
227	17	6	17	6	17	6	17	6
ADD	2377	898	2279	860	2380	901	2467	932

k1: .45

FN	Z1	Z2	Z3	Z4
1	.5163E-12	.1577E-15	.5163E-12	.5163E-12
2	.5043E-01	.5043E-01	.5043E-01	.5043E-01
3	.2500E-27	.2500E-27	.2500E-27	.2500E-27
4	.2667E+01	.2667E+01	.2667E+01	.2667E+01
5	-.1913E+01	-.1913E+01	-.1913E+01	-.1913E+01
6	.2265E-22	.1758E-17	.2500E-22	.1013E-14
7	-.1732E+01	-.1732E+01	-.1732E+01	-.1732E+01
8	-.1000E+01	-.1000E+01	-.1000E+01	-.1000E+01
9	-.5000E+00	-.5000E+00	-.5000E+00	-.5000E+00
10	-.1000E+01	-.1000E+01	-.1000E+01	-.1000E+01
201	.1229E-21	.1229E-21	.1229E-21	.1229E-21
202	.4898E+02	.4898E+02	.4898E+02	.4898E+02
203	.3197E-13	.3197E-13	.3197E-13	.3197E-13
204	.1836E+00	.1836E+00	.1836E+00	.1836E+00
205	.5621E-13	.1062E-15	.5621E-13	.5621E-13
206	.3334E-14	.3334E-14	.3334E-14	.3334E-14
207	.1491E-16	.1078E-17	.1491E-16	.1491E-16
208	.1922E-15	.1123E-16	.1922E-15	.1922E-15
209	.7030E-12	.1209E-12	.7030E-12	.7030E-12
210	.2460E+01	.2460E+01	.2460E+01	.2460E+01
211	.6503E-13	.3722E-16	.6503E-13	.6503E-13
212	.8223E-15	.8343E-17	.2688E-12	.2688E-12
213	.3199E-18	.2124E-20	.1644E-23	.1644E-23
214	.3286E-02	.6899E-02	.1559E-02	.1559E-02
215	-.2804E-17	-.1384E-11	-.2804E-17	-.6468E-14
216	.9994E+00	.9994E+00	.9994E+00	.4897E+02
217	-.8000E+00	-.8000E+00	-.8000E+00	-.8000E+00
218	-.6536E-25	.2088E-25	.5364E-25	.5364E-25
219	-.1000E+01	-.1000E+01	-.1000E+01	-.1000E+01
220	.1000E+01	.1000E+01	.1000E+01	.1000E+01
221	-.1000E+01	-.1000E+01	-.1000E+01	-.1000E+01
222	-.1500E+01	-.1500E+01	-.1500E+01	-.1500E+01
223	-.8340E+00	-.8340E+00	-.8340E+00	-.8340E+00
224	-.3040E+03	-.3040E+03	-.3040E+03	-.3040E+03
225	.2000E+01	.2000E+01	.2000E+01	.2000E+01
226	-.5000E+00	-.5000E+00	-.5000E+00	-.5000E+00
227	.1000E+01	.1000E+01	.1000E+01	.1000E+01

k1: .45

FN	nfp1	nf1	nfp2	nf2	nfp3	nf3	nfp4	nf4
1	57	22	67	26	57	22	57	22
2	50	21	54	21	59	26	59	26
3	19	6	55	18	19	6	19	6
4	7	2	7	2	7	2	7	2
5	24	9	24	9	24	9	24	9
6	33	12	29	10	28	9	25	8
7	33	12	30	11	29	10	26	9
8	17	6	17	6	17	6	17	6
9	32	17	37	16	32	17	29	16
10	35	12	35	12	35	12	35	12
201	15	6	15	6	15	6	15	6
202	44	21	44	21	44	21	44	21
203	36	13	36	13	36	13	36	13
204	22	9	22	9	22	9	22	9
205	42	15	39	14	42	15	42	15
206	25	10	25	10	25	10	25	10
207	39	14	42	15	39	14	39	14
208	119	48	119	46	119	48	119	48
209	457	186	414	163	457	186	457	186
210	35	18	35	18	35	18	35	18
211	77	32	83	32	77	32	77	32
212	41	16	38	15	39	16	39	16
213	326	113	242	85	401	138	401	138
214	107	54	72	41	115	60	115	60
215	22	7	22	7	22	7	22	7
216	52	23	61	30	50	23	53	22
217	25	8	25	8	25	8	25	8
218	118	39	76	25	64	21	64	21
219	87	18	87	18	87	18	114	25
220	184	61	229	76	175	58	264	93
221	79	26	79	26	79	26	79	26
222	19	6	19	6	19	6	19	6
223	30	11	22	7	30	11	33	14
224	13	4	13	4	13	4	13	4
225	19	6	19	6	19	6	19	6
226	28	11	19	6	27	10	27	10
227	17	6	17	6	17	6	17	6
ADD	2385	900	2269	844	2400	909	2513	950

k1: .5

FN	Z1	Z2	Z3	Z4
1	.5163E-12	.3181E-16	.5163E-12	.5163E-12
2	.5043E-01	.5043E-01	.5043E-01	.5043E-01
3	.2500E-27	.2500E-27	.2500E-27	.2500E-27
4	.2667E+01	.2667E+01	.2667E+01	.2667E+01
5	-.1913E+01	-.1913E+01	-.1913E+01	-.1913E+01
6	.2975E-20	.2472E-17	.2344E-21	.1013E-14
7	-.1732E+01	-.1732E+01	-.1732E+01	-.1732E+01
8	-.1000E+01	-.1000E+01	-.1000E+01	-.1000E+01
9	-.5000E+00	-.5000E+00	-.5000E+00	-.5000E+00
10	-.1000E+01	-.1000E+01	-.1000E+01	-.1000E+01
201	.1229E-21	.1229E-21	.1229E-21	.1229E-21
202	.4898E+02	.4898E+02	.4898E+02	.4898E+02
203	.3197E-13	.3197E-13	.3197E-13	.3197E-13
204	.1836E+00	.1836E+00	.1836E+00	.1836E+00
205	.5621E-13	.7209E-18	.5621E-13	.5621E-13
206	.3334E-14	.3334E-14	.3334E-14	.3334E-14
207	.1491E-16	.1266E-20	.1491E-16	.1491E-16
208	.1922E-15	.1755E-14	.1922E-15	.1922E-15
209	.7030E-12	.8302E-13	.7030E-12	.7030E-12
210	.2460E+01	.2460E+01	.2460E+01	.2460E+01
211	.6503E-13	.4602E-14	.6503E-13	.6503E-13
212	.8223E-15	.1851E-11	.1189E-14	.1189E-14
213	.3199E-18	.5672E-18	.1644E-23	.1644E-23
214	.3286E-02	.3615E-02	.2113E-02	.2113E-02
215	-.2804E-17	-.2763E-11	-.2804E-17	-.6468E-14
216	.9994E+00	.9994E+00	.9994E+00	.4897E+02
217	-.8000E+00	-.8000E+00	-.8000E+00	-.8000E+00
218	-.6536E-25	-.1272E-25	.5364E-25	.5364E-25
219	-.1000E+01	-.1000E+01	-.1000E+01	-.1000E+01
220	.1000E+01	.1000E+01	.1000E+01	.1000E+01
221	-.1000E+01	-.1000E+01	-.1000E+01	-.1000E+01
222	-.1500E+01	-.1500E+01	-.1500E+01	-.1500E+01
223	-.8340E+00	-.8340E+00	-.8340E+00	-.8340E+00
224	-.3040E+03	-.3040E+03	-.3040E+03	-.3040E+03
225	.2000E+01	.2000E+01	.2000E+01	.2000E+01
226	-.5000E+00	-.5000E+00	-.5000E+00	-.5000E+00
227	.1000E+01	.1000E+01	.1000E+01	.1000E+01

k1: .5

FN	nfp1	nf1	nfp2	nf2	nfp3	nf3	nfp4	nf4
1	57	22	69	26	57	22	57	22
2	50	21	54	21	53	24	53	24
3	19	6	61	20	19	6	19	6
4	7	2	7	2	7	2	7	2
5	24	9	24	9	24	9	24	9
6	26	9	29	10	25	8	25	8
7	32	11	32	13	30	11	29	10
8	17	6	17	6	17	6	17	6
9	32	17	37	14	32	17	29	16
10	35	12	35	12	35	12	35	12
201	15	6	15	6	15	6	15	6
202	44	21	44	21	44	21	44	21
203	36	13	36	13	36	13	36	13
204	22	9	22	9	22	9	22	9
205	42	15	39	14	42	15	42	15
206	25	10	25	10	25	10	25	10
207	39	14	42	15	39	14	39	14
208	119	48	103	40	119	48	119	48
209	457	186	444	171	457	186	457	186
210	35	18	35	18	35	18	35	18
211	77	32	83	32	77	32	77	32
212	41	16	35	14	39	16	39	16
213	326	113	227	80	401	138	401	138
214	107	54	82	43	110	55	110	55
215	22	7	22	7	22	7	22	7
216	41	18	56	27	45	20	52	23
217	25	8	25	8	25	8	25	8
218	118	39	79	26	64	21	64	21
219	87	18	87	18	87	18	114	25
220	187	62	238	79	175	58	220	77
221	79	26	79	26	79	26	79	26
222	19	6	19	6	19	6	19	6
223	30	11	25	8	30	11	33	14
224	13	4	13	4	13	4	13	4
225	19	6	19	6	19	6	19	6
226	27	10	20	7	27	10	27	10
227	17	6	17	6	17	6	17	6
ADD	2368	891	2296	847	2382	899	2460	929

k1: .55

FN	Z1	Z2	Z3	Z4
1	.5163E-12	.9042E-17	.5163E-12	.5163E-12
2	.5043E-01	.5043E-01	.5043E-01	.5043E-01
3	.2500E-27	.2500E-27	.2500E-27	.2500E-27
4	.2667E+01	.2667E+01	.2667E+01	.2667E+01
5	-.1913E+01	-.1913E+01	-.1913E+01	-.1913E+01
6	.2500E-22	.3050E-18	.2165E-21	.1013E-14
7	-.1732E+01	-.1732E+01	-.1732E+01	-.1732E+01
8	-.1000E+01	-.1000E+01	-.1000E+01	-.1000E+01
9	-.5000E+00	-.5000E+00	-.5000E+00	-.5000E+00
10	-.1000E+01	-.1000E+01	-.1000E+01	-.1000E+01
201	.1229E-21	.1229E-21	.1229E-21	.1229E-21
202	.4898E+02	.4898E+02	.4898E+02	.4898E+02
203	.3197E-13	.3197E-13	.3197E-13	.3197E-13
204	.1836E+00	.1836E+00	.1836E+00	.1836E+00
205	.5621E-13	.4775E-19	.5621E-13	.5621E-13
206	.3334E-14	.3334E-14	.3334E-14	.3334E-14
207	.1491E-16	.2047E-14	.1491E-16	.1491E-16
208	.1922E-15	.2270E-14	.1922E-15	.1922E-15
209	.7030E-12	.1053E-12	.7030E-12	.7030E-12
210	.2460E+01	.2460E+01	.2460E+01	.2460E+01
211	.6503E-13	.4279E-16	.6503E-13	.6503E-13
212	.8223E-15	.3834E-14	.5124E-14	.5124E-14
213	.3199E-18	.3809E-20	.1644E-23	.1644E-23
214	.3286E-02	.2033E-02	.2818E-02	.2818E-02
215	-.2804E-17	-.5244E-11	-.2804E-17	-.6468E-14
216	.9994E+00	.9994E+00	.9994E+00	.4897E+02
217	-.8000E+00	-.8000E+00	-.8000E+00	-.8000E+00
218	-.6536E-25	-.5585E-26	.5364E-25	.5364E-25
219	-.1000E+01	-.1000E+01	-.1000E+01	-.1000E+01
220	.1000E+01	.1000E+01	.1000E+01	.1000E+01
221	-.1000E+01	-.1000E+01	-.1000E+01	-.1000E+01
222	-.1500E+01	-.1500E+01	-.1500E+01	-.1500E+01
223	-.8340E+00	-.8340E+00	-.8340E+00	-.8340E+00
224	-.3040E+03	-.3040E+03	-.3040E+03	-.3040E+03
225	.2000E+01	.2000E+01	.2000E+01	.2000E+01
226	-.5000E+00	-.5000E+00	-.5000E+00	-.5000E+00
227	.1000E+01	.1000E+01	.1000E+01	.1000E+01

k1: .55

FN	nfp1	nf1	nfp2	nf2	nfp3	nf3	nfp4	nf4
1	57	22	73	28	57	22	57	22
2	50	21	55	22	67	28	67	28
3	19	6	70	23	19	6	19	6
4	7	2	7	2	7	2	7	2
5	24	9	24	9	24	9	24	9
6	29	10	26	9	25	8	25	8
7	32	11	30	11	30	11	29	10
8	17	6	17	6	17	6	17	6
9	32	17	41	18	32	17	29	16
10	35	12	35	12	35	12	35	12
201	15	6	15	6	15	6	15	6
202	44	21	44	21	44	21	44	21
203	36	13	36	13	36	13	36	13
204	22	9	22	9	22	9	22	9
205	42	15	40	15	42	15	42	15
206	25	10	25	10	25	10	25	10
207	39	14	42	15	39	14	39	14
208	119	48	116	45	119	48	119	48
209	457	186	437	170	457	186	457	186
210	35	18	35	18	35	18	35	18
211	77	32	88	33	77	32	77	32
212	41	16	40	15	41	16	41	16
213	326	113	263	92	401	138	401	138
214	107	54	99	50	110	57	110	57
215	22	7	22	7	22	7	22	7
216	42	19	56	27	57	26	54	27
217	25	8	25	8	25	8	25	8
218	118	39	82	27	64	21	64	21
219	87	18	87	18	87	18	114	25
220	187	62	247	82	175	58	218	73
221	79	26	79	26	79	26	79	26
222	19	6	19	6	19	6	19	6
223	30	11	32	13	30	11	33	14
224	13	4	13	4	13	4	13	4
225	19	6	19	6	19	6	19	6
226	27	10	20	7	27	10	27	10
227	17	6	17	6	17	6	17	6
ADD	2372	893	2398	889	2410	911	2476	935

k1: .6

FN	Z1	Z2	Z3	Z4
1	.5163E-12	.5891E-17	.5163E-12	.5163E-12
2	.5043E-01	.5043E-01	.5043E-01	.5043E-01
3	.2500E-27	.3513E-26	.2500E-27	.2500E-27
4	.2667E+01	.2667E+01	.2667E+01	.2667E+01
5	-.1913E+01	-.1913E+01	-.1913E+01	-.1913E+01
6	.2485E-22	.9694E-22	.3450E-21	.1013E-14
7	-.1732E+01	-.1732E+01	-.1732E+01	-.1732E+01
8	-.1000E+01	-.1000E+01	-.1000E+01	-.1000E+01
9	-.5000E+00	-.5000E+00	-.5000E+00	-.5000E+00
10	-.1000E+01	-.1000E+01	-.1000E+01	-.1000E+01
201	.1229E-21	.1229E-21	.1229E-21	.1229E-21
202	.4898E+02	.4898E+02	.4898E+02	.4898E+02
203	.3197E-13	.3197E-13	.3197E-13	.3197E-13
204	.1836E+00	.1836E+00	.1836E+00	.1836E+00
205	.5621E-13	.4759E-16	.5621E-13	.5621E-13
206	.3334E-14	.3334E-14	.3334E-14	.3334E-14
207	.1491E-16	.6232E-16	.1491E-16	.1491E-16
208	.1922E-15	.1039E-16	.1922E-15	.1922E-15
209	.7030E-12	.1393E-12	.7030E-12	.7030E-12
210	.2460E+01	.2460E+01	.2460E+01	.2460E+01
211	.6503E-13	.4734E-17	.6503E-13	.6503E-13
212	.8223E-15	.1004E-10	.6839E-13	.6839E-13
213	.3199E-18	.1361E-25	.1644E-23	.1644E-23
214	.3286E-02	.2768E-02	.2795E-02	.2795E-02
215	-.2804E-17	-.9518E-11	-.2804E-17	-.6468E-14
216	.9994E+00	.9994E+00	.9994E+00	.9994E+00
217	-.8000E+00	-.8000E+00	-.8000E+00	-.8000E+00
218	-.6536E-25	.5584E-25	.5364E-25	.5364E-25
219	-.1000E+01	-.1000E+01	-.1000E+01	-.1000E+01
220	.1000E+01	.1000E+01	.1000E+01	.1000E+01
221	-.1000E+01	-.1000E+01	-.1000E+01	-.1000E+01
222	-.1500E+01	-.1500E+01	-.1500E+01	-.1500E+01
223	-.8340E+00	-.8340E+00	-.8340E+00	-.8340E+00
224	-.3040E+03	-.3040E+03	-.3040E+03	-.3040E+03
225	.2000E+01	.2000E+01	.2000E+01	.2000E+01
226	-.5000E+00	-.5000E+00	-.5000E+00	-.5000E+00
227	.1000E+01	.1000E+01	.1000E+01	.1000E+01

k1: .6

FN	nfp1	nf1	nfp2	nf2	nfp3	nf3	nfp4	nf4
1	57	22	81	30	57	22	57	22
2	50	21	26	11	49	22	49	22
3	19	6	76	25	19	6	19	6
4	7	2	7	2	7	2	7	2
5	24	9	24	9	24	9	24	9
6	29	10	30	11	25	8	25	8
7	36	15	29	10	29	10	29	10
8	17	6	17	6	17	6	17	6
9	32	17	37	16	32	17	29	16
10	35	12	35	12	35	12	35	12
201	15	6	15	6	15	6	15	6
202	44	21	44	21	44	21	44	21
203	36	13	36	13	36	13	36	13
204	22	9	22	9	22	9	22	9
205	42	15	43	16	42	15	42	15
206	25	10	25	10	25	10	25	10
207	39	14	46	17	39	14	39	14
208	119	48	140	55	119	48	119	48
209	457	186	474	181	457	186	457	186
210	35	18	35	18	35	18	35	18
211	77	32	88	33	77	32	77	32
212	41	16	38	15	36	15	36	15
213	326	113	353	122	401	138	401	138
214	107	54	97	48	107	56	107	56
215	22	7	22	7	22	7	22	7
216	49	22	56	27	52	23	56	25
217	25	8	25	8	25	8	25	8
218	118	39	82	27	64	21	64	21
219	87	18	87	18	87	18	114	25
220	190	63	262	87	175	58	226	79
221	79	26	79	26	79	26	79	26
222	19	6	19	6	19	6	19	6
223	30	11	28	9	30	11	33	14
224	13	4	13	4	13	4	13	4
225	19	6	19	6	19	6	19	6
226	27	10	20	7	27	10	27	10
227	17	6	17	6	17	6	17	6
ADD	2386	901	2547	934	2378	899	2460	931

k1: .65

FN	Z1	Z2	Z3	Z4
1	.5163E-12	.9059E-17	.5163E-12	.5163E-12
2	.5043E-01	.5043E-01	.5043E-01	.5043E-01
3	.2500E-27	.2867E-27	.2500E-27	.2500E-27
4	.2667E+01	.2667E+01	.2667E+01	.2667E+01
5	-.1913E+01	-.1913E+01	-.1913E+01	-.1913E+01
6	.2172E-22	.1305E-13	.9420E-19	.1013E-14
7	-.1732E+01	-.1732E+01	-.1732E+01	-.1732E+01
8	-.1000E+01	-.1000E+01	-.1000E+01	-.1000E+01
9	-.5000E+00	-.5000E+00	-.5000E+00	-.5000E+00
10	-.1000E+01	-.1000E+01	-.1000E+01	-.1000E+01
201	.1229E-21	.1229E-21	.1229E-21	.1229E-21
202	.4898E+02	.4898E+02	.4898E+02	.4898E+02
203	.3197E-13	.3197E-13	.3197E-13	.3197E-13
204	.1836E+00	.1836E+00	.1836E+00	.1836E+00
205	.5621E-13	.1550E-14	.5621E-13	.5621E-13
206	.3334E-14	.3334E-14	.3334E-14	.3334E-14
207	.1491E-16	.1709E-19	.1491E-16	.1491E-16
208	.1922E-15	.6882E-16	.1922E-15	.1922E-15
209	.7030E-12	.9210E-13	.7030E-12	.7030E-12
210	.2460E+01	.2460E+01	.2460E+01	.2460E+01
211	.6503E-13	.3570E-16	.6503E-13	.6503E-13
212	.8223E-15	.7638E-16	.2276E-15	.2276E-15
213	.3199E-18	.2995E-26	.1644E-23	.1644E-23
214	.3286E-02	.2186E-02	.4847E-02	.4847E-02
215	-.2804E-17	-.1682E-10	-.2804E-17	-.6468E-14
216	.9994E+00	.9994E+00	.9994E+00	.9994E+00
217	-.8000E+00	-.8000E+00	-.8000E+00	-.8000E+00
218	-.6536E-25	-.5021E-25	.5364E-25	.5364E-25
219	-.1000E+01	-.1000E+01	-.1000E+01	-.1000E+01
220	.1000E+01	.1000E+01	.1000E+01	.1000E+01
221	-.1000E+01	-.1000E+01	-.1000E+01	-.1000E+01
222	-.1500E+01	-.1500E+01	-.1500E+01	-.1500E+01
223	-.8340E+00	-.8340E+00	-.8340E+00	-.8340E+00
224	-.3040E+03	-.3040E+03	-.3040E+03	-.3040E+03
225	.2000E+01	.2000E+01	.2000E+01	.2000E+01
226	-.5000E+00	-.5000E+00	-.5000E+00	-.5000E+00
227	.1000E+01	.1000E+01	.1000E+01	.1000E+01

k1: .65

FN	nfp1	nf1	nfp2	nf2	nfp3	nf3	nfp4	nf4
1	57	22	85	32	57	22	57	22
2	50	21	26	11	59	24	59	24
3	19	6	88	29	19	6	19	6
4	7	2	7	2	7	2	7	2
5	24	9	24	9	24	9	24	9
6	29	10	30	11	25	8	25	8
7	30	11	35	16	31	12	29	10
8	17	6	17	6	17	6	17	6
9	32	17	44	19	32	17	29	16
10	35	12	37	12	35	12	35	12
201	15	6	15	6	15	6	15	6
202	44	21	51	24	44	21	44	21
203	36	13	36	13	36	13	36	13
204	22	9	22	9	22	9	22	9
205	42	15	43	16	42	15	42	15
206	25	10	25	10	25	10	25	10
207	39	14	49	18	39	14	39	14
208	119	48	134	51	119	48	119	48
209	457	186	463	174	457	186	457	186
210	35	18	35	18	35	18	35	18
211	77	32	105	40	77	32	77	32
212	41	16	38	15	36	15	36	15
213	326	113	401	138	401	138	401	138
214	107	54	107	56	82	45	82	45
215	22	7	22	7	22	7	22	7
216	53	24	57	28	51	22	42	17
217	25	8	25	8	25	8	25	8
218	118	39	85	28	64	21	64	21
219	87	18	87	18	87	18	114	25
220	187	62	280	93	175	58	226	79
221	79	26	79	26	79	26	79	26
222	19	6	19	6	19	6	19	6
223	30	11	37	12	30	11	33	14
224	13	4	13	4	13	4	13	4
225	19	6	19	6	19	6	19	6
226	27	10	20	7	27	10	27	10
227	17	6	17	6	17	6	17	6
ADD	2381	898	2677	984	2364	891	2431	914

k1: .70

FN	Z1	Z2	Z3	Z4
1	.5163E-12	.3884E-13	.5163E-12	.5163E-12
2	.5043E-01	.5043E-01	.5043E-01	.5043E-01
3	.2500E-27	.2256E-27	.2500E-27	.2500E-27
4	.2667E+01	.2667E+01	.2667E+01	.2667E+01
5	-.1913E+01	-.1913E+01	-.1913E+01	-.1913E+01
6	.2043E-22	.8085E-13	.7516E-17	.1013E-14
7	-.1732E+01	-.1732E+01	-.1732E+01	-.1732E+01
8	-.1000E+01	-.1000E+01	-.1000E+01	-.1000E+01
9	-.5000E+00	-.5000E+00	-.5000E+00	-.5000E+00
10	-.1000E+01	-.1000E+01	-.1000E+01	-.1000E+01
201	.1229E-21	.1229E-21	.1229E-21	.1229E-21
202	.4898E+02	.4898E+02	.4898E+02	.4898E+02
203	.3197E-13	.1101E-15	.3197E-13	.3197E-13
204	.1836E+00	.1836E+00	.1836E+00	.1836E+00
205	.5621E-13	.9904E-20	.5621E-13	.5621E-13
206	.3334E-14	.3334E-14	.3334E-14	.3334E-14
207	.1491E-16	.1694E-13	.1491E-16	.1491E-16
208	.1922E-15	.1139E-17	.1922E-15	.1922E-15
209	.7030E-12	.8959E-13	.7030E-12	.7030E-12
210	.2460E+01	.2460E+01	.2460E+01	.2460E+01
211	.6503E-13	.4553E-16	.6503E-13	.6503E-13
212	.8223E-15	.1254E-13	.1271E-14	.1271E-14
213	.3199E-18	.8261E-26	.1644E-23	.1644E-23
214	.3286E-02	.3128E-02	.2794E-02	.2794E-02
215	-.2804E-17	-.2897E-10	-.2804E-17	-.6468E-14
216	.9994E+00	.9994E+00	.9994E+00	.9994E+00
217	-.8000E+00	-.8000E+00	-.8000E+00	-.8000E+00
218	-.6536E-25	-.1058E-25	.5364E-25	.5364E-25
219	-.1000E+01	-.1000E+01	-.1000E+01	-.1000E+01
220	.1000E+01	.1000E+01	.1000E+01	.1000E+01
221	-.1000E+01	-.1000E+01	-.1000E+01	-.1000E+01
222	-.1500E+01	-.1500E+01	-.1500E+01	-.1500E+01
223	-.8340E+00	-.8340E+00	-.8340E+00	-.8340E+00
224	-.3040E+03	-.3040E+03	-.3040E+03	-.3040E+03
225	.2000E+01	.2000E+01	.2000E+01	.2000E+01
226	-.5000E+00	-.5000E+00	-.5000E+00	-.5000E+00
227	.1000E+01	.1000E+01	.1000E+01	.1000E+01

k1: .70

FN	nfp1	nf1	nfp2	nf2	nfp3	nf3	nfp4	nf4
1	57	22	91	34	57	22	57	22
2	50	21	20	9	53	22	53	22
3	19	6	103	34	19	6	19	6
4	7	2	7	2	7	2	7	2
5	24	9	24	9	24	9	24	9
6	29	10	30	11	25	8	25	8
7	30	11	29	10	30	11	29	10
8	17	6	17	6	17	6	17	6
9	32	17	47	20	32	17	29	16
10	35	12	39	14	35	12	35	12
201	15	6	15	6	15	6	15	6
202	44	21	41	16	44	21	44	21
203	36	13	39	14	36	13	36	13
204	22	9	23	10	22	9	22	9
205	42	15	45	16	42	15	42	15
206	25	10	25	10	25	10	25	10
207	39	14	54	19	39	14	39	14
208	119	48	148	55	119	48	119	48
209	457	186	495	186	457	186	457	186
210	35	18	35	18	35	18	35	18
211	77	32	107	40	77	32	77	32
212	41	16	37	14	39	16	39	16
213	326	113	473	162	401	138	401	138
214	107	54	103	54	107	54	107	54
215	22	7	22	7	22	7	22	7
216	53	24	57	28	48	21	40	17
217	25	8	25	8	25	8	25	8
218	118	39	88	29	64	21	64	21
219	87	18	91	18	87	18	114	25
220	190	63	301	100	175	58	222	75
221	79	26	79	26	79	26	79	26
222	19	6	19	6	19	6	19	6
223	30	11	44	15	30	11	33	14
224	13	4	13	4	13	4	13	4
225	19	6	19	6	19	6	19	6
226	33	16	23	8	27	10	27	10
227	17	6	17	6	17	6	17	6
ADD	2390	905	2845	1030	2382	897	2447	918

k1: .75

FN	Z1	Z2	Z3	Z4
1	.5163E-12	.1659E-11	.5163E-12	.5163E-12
2	.5043E-01	.5043E-01	.5043E-01	.5043E-01
3	.2500E-27	.2500E-27	.2500E-27	.2500E-27
4	.2667E+01	.2667E+01	.2667E+01	.2667E+01
5	-.1913E+01	-.1913E+01	-.1913E+01	-.1913E+01
6	.2488E-22	.1166E-12	.6043E-15	.1013E-14
7	-.1732E+01	-.1732E+01	-.1732E+01	-.1732E+01
8	-.1000E+01	-.1000E+01	-.1000E+01	-.1000E+01
9	-.5000E+00	-.5000E+00	-.5000E+00	-.5000E+00
10	-.1000E+01	-.1000E+01	-.1000E+01	-.1000E+01
201	.1229E-21	.1229E-21	.1229E-21	.1229E-21
202	.4898E+02	.4898E+02	.4898E+02	.4898E+02
203	.3197E-13	.1683E-15	.3197E-13	.3197E-13
204	.1836E+00	.1836E+00	.1836E+00	.1836E+00
205	.5621E-13	.2443E-16	.5621E-13	.5621E-13
206	.3334E-14	.3334E-14	.3334E-14	.3334E-14
207	.1491E-16	.3995E-12	.1491E-16	.1491E-16
208	.1922E-15	.2426E-10	.1922E-15	.1922E-15
209	.7030E-12	.8994E-13	.7030E-12	.7030E-12
210	.2460E+01	.2460E+01	.2460E+01	.2460E+01
211	.6503E-13	.1272E-14	.6503E-13	.6503E-13
212	.8223E-15	.3342E-15	.1776E-12	.1776E-12
213	.3199E-18	.4726E-25	.1644E-23	.1644E-23
214	.3286E-02	.3564E-02	.4007E-02	.4007E-02
215	-.2804E-17	-.4904E-10	-.2804E-17	-.6468E-14
216	.9994E+00	.9994E+00	.9994E+00	.9994E+00
217	-.8000E+00	-.8000E+00	-.8000E+00	-.8000E+00
218	-.6536E-25	.3009E-25	.5364E-25	.5364E-25
219	-.1000E+01	-.1000E+01	-.1000E+01	-.1000E+01
220	.1000E+01	.1000E+01	.1000E+01	.1000E+01
221	-.1000E+01	-.1000E+01	-.1000E+01	-.1000E+01
222	-.1500E+01	-.1500E+01	-.1500E+01	-.1500E+01
223	-.8340E+00	-.8340E+00	-.8340E+00	-.8340E+00
224	-.3040E+03	-.3040E+03	-.3040E+03	-.3040E+03
225	.2000E+01	.2000E+01	.2000E+01	.2000E+01
226	-.5000E+00	-.5000E+00	-.5000E+00	-.5000E+00
227	.1000E+01	.1000E+01	.1000E+01	.1000E+01

k1: .75

FN	nfp1	nf1	nfp2	nf2	nfp3	nf3	nfp4	nf4
1	57	22	99	36	57	22	57	22
2	50	21	51	20	48	21	48	21
3	19	6	127	42	19	6	19	6
4	7	2	7	2	7	2	7	2
5	24	9	24	9	24	9	24	9
6	29	10	30	11	25	8	25	8
7	33	12	29	10	30	11	29	10
8	17	6	17	6	17	6	17	6
9	32	17	49	20	32	17	29	16
10	35	12	39	14	35	12	35	12
201	15	6	15	6	15	6	15	6
202	44	21	56	25	44	21	44	21
203	36	13	39	14	36	13	36	13
204	22	9	23	10	22	9	22	9
205	42	15	45	16	42	15	42	15
206	25	10	25	10	25	10	25	10
207	39	14	54	19	39	14	39	14
208	119	48	153	56	119	48	119	48
209	457	186	576	213	457	186	457	186
210	35	18	35	18	35	18	35	18
211	77	32	128	47	77	32	77	32
212	41	16	40	15	39	16	39	16
213	326	113	566	193	401	138	401	138
214	107	54	105	52	98	51	98	51
215	22	7	22	7	22	7	22	7
216	49	22	60	29	48	21	40	17
217	25	8	25	8	25	8	25	8
218	118	39	94	31	64	21	64	21
219	87	18	86	17	87	18	114	25
220	190	63	334	111	175	58	218	73
221	79	26	79	26	79	26	79	26
222	19	6	19	6	19	6	19	6
223	30	11	47	16	30	11	33	14
224	13	4	13	4	13	4	13	4
225	19	6	19	6	19	6	19	6
226	27	10	23	8	27	10	27	10
227	17	6	17	6	17	6	17	6
ADD	2383	898	3170	1139	2368	893	2429	912

k1: .80

FN	Z1	Z2	Z3	Z4
1	.5163E-12	.8498E-14	.5163E-12	.5163E-12
2	.5043E-01	.5043E-01	.5043E-01	.5043E-01
3	.2500E-27	.2498E-27	.2500E-27	.2500E-27
4	.2667E+01	.2667E+01	.2667E+01	.2667E+01
5	-.1913E+01	-.1913E+01	-.1913E+01	-.1913E+01
6	.2500E-22	.4621E-20	.2339E-13	.1013E-14
7	-.1732E+01	-.1732E+01	-.1732E+01	-.1732E+01
8	-.1000E+01	-.1000E+01	-.1000E+01	-.1000E+01
9	-.5000E+00	-.5000E+00	-.5000E+00	-.5000E+00
10	-.1000E+01	-.1000E+01	-.1000E+01	-.1000E+01
201	.1229E-21	.1229E-21	.1229E-21	.1229E-21
202	.4898E+02	.4898E+02	.4898E+02	.4898E+02
203	.3197E-13	.2873E-12	.3197E-13	.3197E-13
204	.1836E+00	.1836E+00	.1836E+00	.1836E+00
205	.5621E-13	.2421E-14	.5621E-13	.5621E-13
206	.3334E-14	.3334E-14	.3334E-14	.3334E-14
207	.1491E-16	.2265E-14	.1491E-16	.1491E-16
208	.1922E-15	.1811E-13	.1922E-15	.1922E-15
209	.7030E-12	.9024E-13	.7030E-12	.7030E-12
210	.2460E+01	.2460E+01	.2460E+01	.2460E+01
211	.6503E-13	.1026E-11	.6503E-13	.6503E-13
212	.8223E-15	.5120E-15	.2624E-15	.2624E-15
213	.3199E-18	.3353E-24	.1644E-23	.1644E-23
214	.3286E-02	.1348E-02	.3208E-02	.3208E-02
215	-.2804E-17	-.7418E-12	-.2804E-17	-.6468E-14
216	.9994E+00	.9994E+00	.9994E+00	.9994E+00
217	-.8000E+00	-.8000E+00	-.8000E+00	-.8000E+00
218	-.6536E-25	.3383E-25	.5364E-25	.5364E-25
219	-.1000E+01	-.1000E+01	-.1000E+01	-.1000E+01
220	.1000E+01	.1000E+01	.1000E+01	.1000E+01
221	-.1000E+01	-.1000E+01	-.1000E+01	-.1000E+01
222	-.1500E+01	-.1500E+01	-.1500E+01	-.1500E+01
223	-.8340E+00	-.8340E+00	-.8340E+00	-.8340E+00
224	-.3040E+03	-.3040E+03	-.3040E+03	-.3040E+03
225	.2000E+01	.2000E+01	.2000E+01	.2000E+01
226	-.5000E+00	-.5000E+00	-.5000E+00	-.5000E+00
227	.1000E+01	.1000E+01	.1000E+01	.1000E+01

k1: .80

FN	nfp1	nf1	nfp2	nf2	nfp3	nf3	nfp4	nf4
1	57	22	117	42	57	22	57	22
2	50	21	26	11	51	22	51	22
3	19	6	157	52	19	6	19	6
4	7	2	7	2	7	2	7	2
5	24	9	24	9	24	9	24	9
6	29	10	29	10	25	8	25	8
7	30	11	28	9	30	11	30	11
8	17	6	17	6	17	6	17	6
9	32	17	58	23	32	17	29	16
10	35	12	38	13	35	12	35	12
201	15	6	15	6	15	6	15	6
202	44	21	43	16	44	21	44	21
203	36	13	36	13	36	13	36	13
204	22	9	22	9	22	9	22	9
205	42	15	48	17	42	15	42	15
206	25	10	25	10	25	10	25	10
207	39	14	61	22	39	14	39	14
208	119	48	177	64	119	48	119	48
209	457	186	591	212	457	186	457	186
210	35	18	35	18	35	18	35	18
211	77	32	152	55	77	32	77	32
212	41	16	40	15	42	17	42	17
213	326	113	701	238	401	138	401	138
214	107	54	84	47	148	75	148	75
215	22	7	22	7	22	7	22	7
216	53	24	60	29	52	23	40	17
217	25	8	25	8	25	8	25	8
218	118	39	100	33	64	21	64	21
219	87	18	101	24	87	18	114	25
220	190	63	379	126	175	58	215	72
221	79	26	79	26	79	26	79	26
222	19	6	19	6	19	6	19	6
223	30	11	50	17	30	11	33	14
224	13	4	13	4	13	4	13	4
225	19	6	19	6	19	6	19	6
226	27	10	23	8	27	10	27	10
227	17	6	17	6	17	6	17	6
ADD	2384	899	3438	1219	2428	921	2483	938

k1: .85

FN	Z1	Z2	Z3	Z4
1	.5163E-12	.8448E-17	.5163E-12	.5163E-12
2	.5043E-01	.5043E-01	.5043E-01	.5043E-01
3	.2500E-27	.2500E-27	.2500E-27	.2500E-27
4	.2667E+01	.2667E+01	.2667E+01	.2667E+01
5	-.1913E+01	-.1913E+01	-.1913E+01	-.1913E+01
6	.4190E-12	.6324E-22	.1502E-13	.1013E-14
7	-.1732E+01	-.1732E+01	-.1732E+01	-.1732E+01
8	-.1000E+01	-.1000E+01	-.1000E+01	-.1000E+01
9	-.5000E+00	-.5000E+00	-.5000E+00	-.5000E+00
10	-.1000E+01	-.1000E+01	-.1000E+01	-.1000E+01
201	.1229E-21	.1229E-21	.1229E-21	.1229E-21
202	.4898E+02	.4898E+02	.4898E+02	.4898E+02
203	.3197E-13	.6900E-12	.3197E-13	.3197E-13
204	.1836E+00	.1836E+00	.1836E+00	.1836E+00
205	.5621E-13	.2705E-17	.5621E-13	.5621E-13
206	.3334E-14	.3334E-14	.3334E-14	.3334E-14
207	.1491E-16	.3344E-15	.1491E-16	.1491E-16
208	.1922E-15	.2793E-14	.1922E-15	.1922E-15
209	.7030E-12	.1493E-12	.7030E-12	.7030E-12
210	.2460E+01	.2460E+01	.2460E+01	.2460E+01
211	.6503E-13	.3576E-16	.6503E-13	.6503E-13
212	.8223E-15	.3425E-17	.3981E-16	.3981E-16
213	.3199E-18	.8337E-23	.1644E-23	.1644E-23
214	.3286E-02	.2982E-02	.2826E-02	.2826E-02
215	-.2804E-17	-.5320E-13	-.2804E-17	-.6468E-14
216	.9994E+00	.9994E+00	.9994E+00	.9994E+00
217	-.8000E+00	-.8000E+00	-.8000E+00	-.8000E+00
218	-.6536E-25	-.3433E-25	.5364E-25	.5364E-25
219	-.1000E+01	-.1000E+01	-.1000E+01	-.1000E+01
220	.1000E+01	.1000E+01	.1000E+01	.1000E+01
221	-.1000E+01	-.1000E+01	-.1000E+01	-.1000E+01
222	-.1500E+01	-.1500E+01	-.1500E+01	-.1500E+01
223	-.8340E+00	-.8340E+00	-.8340E+00	-.8340E+00
224	-.3040E+03	-.3040E+03	-.3040E+03	-.3040E+03
225	.2000E+01	.2000E+01	.2000E+01	.2000E+01
226	-.5000E+00	-.5000E+00	-.5000E+00	-.5000E+00
227	.1000E+01	.1000E+01	.1000E+01	.1000E+01

k1: .85

FN	nfp1	nf1	nfp2	nf2	nfp3	nf3	nfp4	nf4
1	57	22	147	52	57	22	57	22
2	50	21	26	11	48	21	48	21
3	19	6	211	70	19	6	19	6
4	7	2	7	2	7	2	7	2
5	24	9	24	9	24	9	24	9
6	23	8	32	11	25	8	25	8
7	34	13	28	9	30	11	30	11
8	17	6	17	6	17	6	17	6
9	32	17	72	25	32	17	29	16
10	35	12	34	11	35	12	35	12
201	15	6	15	6	15	6	15	6
202	44	21	46	17	44	21	44	21
203	36	13	36	13	36	13	36	13
204	22	9	25	10	22	9	22	9
205	42	15	64	23	42	15	42	15
206	25	10	25	10	25	10	25	10
207	39	14	72	25	39	14	39	14
208	119	48	258	93	119	48	119	48
209	457	186	815	292	457	186	457	186
210	35	18	35	18	35	18	35	18
211	77	32	182	65	77	32	77	32
212	41	16	38	15	42	17	42	17
213	326	113	907	306	401	138	401	138
214	107	54	104	49	111	54	111	54
215	22	7	22	7	22	7	22	7
216	53	24	63	30	56	25	40	17
217	25	8	25	8	25	8	25	8
218	118	39	109	36	64	21	64	21
219	87	18	81	16	87	18	114	25
220	190	63	454	151	175	58	214	71
221	79	26	79	26	79	26	79	26
222	19	6	19	6	19	6	19	6
223	30	11	69	24	30	11	33	14
224	13	4	13	4	13	4	13	4
225	19	6	19	6	19	6	19	6
226	27	10	19	6	27	10	27	10
227	17	6	17	6	17	6	17	6
ADD	2382	899	4209	1474	2392	901	2442	915

k1: .90

FN	Z1	Z2	Z3	Z4
1	.5163E-12	.5965E-13	.5163E-12	.5163E-12
2	.5043E-01	.5043E-01	.5043E-01	.5043E-01
3	.2500E-27	.2500E-27	.2500E-27	.2500E-27
4	.2667E+01	.2667E+01	.2667E+01	.2667E+01
5	-.1913E+01	-.1913E+01	-.1913E+01	-.1913E+01
6	.2500E-22	.2461E-22	.6414E-14	.1013E-14
7	-.1732E+01	-.1732E+01	-.1732E+01	-.1732E+01
8	-.1000E+01	-.1000E+01	-.1000E+01	-.1000E+01
9	-.5000E+00	-.5000E+00	-.5000E+00	-.5000E+00
10	-.1000E+01	-.1000E+01	-.1000E+01	-.1000E+01
201	.1229E-21	.1229E-21	.1229E-21	.1229E-21
202	.4898E+02	.4898E+02	.4898E+02	.4898E+02
203	.3197E-13	.2065E-15	.3197E-13	.3197E-13
204	.1836E+00	.1836E+00	.1836E+00	.1836E+00
205	.5621E-13	.1052E-13	.5621E-13	.5621E-13
206	.3334E-14	.3334E-14	.3334E-14	.3334E-14
207	.1491E-16	.6625E-15	.1491E-16	.1491E-16
208	.1922E-15	.2651E-11	.1922E-15	.1922E-15
209	.7030E-12	.9018E-03	.7030E-12	.7030E-12
210	.2460E+01	.2460E+01	.2460E+01	.2460E+01
211	.6503E-13	.3681E-15	.6503E-13	.6503E-13
212	.8223E-15	.1755E-20	.1162E-14	.1162E-14
213	.3199E-18	.2774E-13	.1644E-23	.1644E-23
214	.3286E-02	.2672E-02	.5394E-02	.5394E-02
215	-.2804E-17	-.1144E-14	-.2804E-17	-.6468E-14
216	.9994E+00	.9994E+00	.9994E+00	.9994E+00
217	-.8000E+00	-.8000E+00	-.8000E+00	-.8000E+00
218	-.6536E-25	-.2055E-25	.5364E-25	.5364E-25
219	-.1000E+01	-.1000E+01	-.1000E+01	-.1000E+01
220	.1000E+01	.1000E+01	.1000E+01	.1000E+01
221	-.1000E+01	-.1000E+01	-.1000E+01	-.1000E+01
222	-.1500E+01	-.1500E+01	-.1500E+01	-.1500E+01
223	-.8340E+00	-.8340E+00	-.8340E+00	-.8340E+00
224	-.3040E+03	-.3040E+03	-.3040E+03	-.3040E+03
225	.2000E+01	.2000E+01	.2000E+01	.2000E+01
226	-.5000E+00	-.5000E+00	-.5000E+00	-.5000E+00
227	.1000E+01	.1000E+01	.1000E+01	.1000E+01

k1: .90

FN	nfp1	nf1	nfp2	nf2	nfp3	nf3	nfp4	nf4
1	57	22	201	70	57	22	57	22
2	50	21	28	11	53	22	53	22
3	19	6	319	106	19	6	19	6
4	7	2	7	2	7	2	7	2
5	24	9	24	9	24	9	24	9
6	29	10	35	12	25	8	25	8
7	30	11	29	10	33	12	31	12
8	17	6	17	6	17	6	17	6
9	32	17	94	35	32	17	29	16
10	35	12	34	11	35	12	35	12
201	15	6	15	6	15	6	15	6
202	44	21	61	26	44	21	44	21
203	36	13	60	21	36	13	36	13
204	22	9	25	10	22	9	22	9
205	42	15	85	30	42	15	42	15
206	25	10	25	10	25	10	25	10
207	39	14	96	33	39	14	39	14
208	119	48	260	91	119	48	119	48
209	457	186	927	326	457	186	457	186
210	35	18	32	17	35	18	35	18
211	77	32	233	82	77	32	77	32
212	41	16	43	16	42	17	42	17
213	326	113	907	306	401	138	401	138
214	107	54	112	55	98	49	98	49
215	22	7	22	7	22	7	22	7
216	49	22	72	33	48	21	46	19
217	25	8	25	8	25	8	25	8
218	118	39	127	42	64	21	64	21
219	87	18	82	17	87	18	114	25
220	193	64	598	199	175	58	214	71
221	79	26	79	26	79	26	79	26
222	19	6	19	6	19	6	19	6
223	30	11	80	27	30	11	33	14
224	13	4	13	4	13	4	13	4
225	19	6	19	6	19	6	19	6
226	27	10	22	7	27	10	27	10
227	17	6	17	6	17	6	17	6
ADD	2383	898	4844	1689	2379	894	2441	914

k1: .95

FN	Z1	Z2	Z3	Z4
1	.5163E-12	.2752E-10	.5163E-12	.5163E-12
2	.5043E-01	.5043E-01	.5043E-01	.5043E-01
3	.2500E-27	.4116E-15	.2500E-27	.2500E-27
4	.2667E+01	.2667E+01	.2667E+01	.2667E+01
5	-.1913E+01	-.1913E+01	-.1913E+01	-.1913E+01
6	.2473E-22	.1360E-15	.4163E-14	.1013E-14
7	-.1732E+01	-.1732E+01	-.1732E+01	-.1732E+01
8	-.1000E+01	-.1000E+01	-.1000E+01	-.1000E+01
9	-.5000E+00	-.5000E+00	-.5000E+00	-.5000E+00
10	-.1000E+01	-.1000E+01	-.1000E+01	-.1000E+01
201	.1229E-21	.1229E-21	.1229E-21	.1229E-21
202	.4898E+02	.4898E+02	.4898E+02	.4898E+02
203	.3197E-13	.3868E-11	.3197E-13	.3197E-13
204	.1836E+00	.1836E+00	.1836E+00	.1836E+00
205	.5621E-13	.1141E-11	.5621E-13	.5621E-13
206	.3334E-14	.3334E-14	.3334E-14	.3334E-14
207	.1491E-16	.1464E-10	.1491E-16	.1491E-16
208	.1922E-15	.2002E-11	.1922E-15	.1922E-15
209	.7030E-12	.1959E+00	.7030E-12	.7030E-12
210	.2460E+01	.2460E+01	.2460E+01	.2460E+01
211	.6503E-13	.2964E-11	.6503E-13	.6503E-13
212	.8223E-15	.1306E-09	.2024E-14	.2024E-14
213	.3199E-18	.1869E-04	.1644E-23	.1644E-23
214	.3286E-02	.5193E-02	.2615E-02	.2615E-02
215	-.2804E-17	-.2950E-13	-.2804E-17	-.6468E-14
216	.9994E+00	.9994E+00	.9994E+00	.9994E+00
217	-.8000E+00	-.8000E+00	-.8000E+00	-.8000E+00
218	-.6536E-25	.1820E-25	.5364E-25	.5364E-25
219	-.1000E+01	-.1000E+01	-.1000E+01	-.1000E+01
220	.1000E+01	.2196E+02	.1000E+01	.1000E+01
221	-.1000E+01	-.1000E+01	-.1000E+01	-.1000E+01
222	-.1500E+01	-.1500E+01	-.1500E+01	-.1500E+01
223	-.8340E+00	-.8340E+00	-.8340E+00	-.8340E+00
224	-.3040E+03	-.3040E+03	-.3040E+03	-.3040E+03
225	.2000E+01	.2000E+01	.2000E+01	.2000E+01
226	-.5000E+00	-.5000E+00	-.5000E+00	-.5000E+00
227	.1000E+01	.1000E+01	.1000E+01	.1000E+01

k1: .95

FN	nfp1	nf1	nfp2	nf2	nfp3	nf3	nfp4	nf4
1	57	22	339	116	57	22	57	22
2	50	21	28	11	53	22	53	22
3	19	6	610	203	19	6	19	6
4	7	2	7	2	7	2	7	2
5	24	9	24	9	24	9	24	9
6	29	10	38	13	25	8	25	8
7	34	13	26	9	33	12	29	10
8	17	6	17	6	17	6	17	6
9	32	17	157	56	32	17	29	16
10	35	12	34	11	35	12	35	12
201	15	6	15	6	15	6	15	6
202	44	21	82	33	44	21	44	21
203	36	13	75	26	36	13	36	13
204	22	9	28	11	22	9	22	9
205	42	15	90	31	42	15	42	15
206	25	10	25	10	25	10	25	10
207	39	14	144	49	39	14	39	14
208	119	48	508	175	119	48	119	48
209	457	186	916	315	457	186	457	186
210	35	18	35	18	35	18	35	18
211	77	32	379	130	77	32	77	32
212	41	16	47	18	42	17	42	17
213	326	113	907	306	401	138	401	138
214	107	54	109	48	113	60	113	60
215	22	7	19	6	22	7	22	7
216	45	20	84	37	45	20	40	17
217	25	8	25	8	25	8	25	8
218	118	39	163	54	64	21	64	21
219	87	18	81	16	87	18	114	25
220	193	64	900	299	175	58	217	72
221	79	26	79	26	79	26	79	26
222	19	6	19	6	19	6	19	6
223	30	11	115	40	30	11	33	14
224	13	4	13	4	13	4	13	4
225	19	6	19	6	19	6	19	6
226	28	11	20	7	27	10	27	10
227	17	6	17	6	17	6	17	6
ADD	2384	899	6194	2127	2391	904	2451	922

k1: 1.

FN	Z1	Z2	Z3	Z4
1	.5163E-12	.1349E-02	.5163E-12	.5163E-12
2	.5043E-01	.5043E-01	.5043E-01	.5043E-01
3	.2500E-27	.9881E-03	.2500E-27	.2500E-27
4	.2667E+01	.2667E+01	.2667E+01	.2667E+01
5	-.1913E+01	-.1913E+01	-.1913E+01	-.1913E+01
6	.2115E-22	.5284E-10	.3410E-14	.1013E-14
7	-.1732E+01	-.1732E+01	-.1732E+01	-.1732E+01
8	-.1000E+01	-.1000E+01	-.1000E+01	-.1000E+01
9	-.5000E+00	-.5000E+00	-.5000E+00	-.5000E+00
10	-.1000E+01	-.1000E+01	-.1000E+01	-.1000E+01
201	.1229E-21	.1229E-21	.1229E-21	.1229E-21
202	.4898E+02	.4898E+02	.4898E+02	.4898E+02
203	.3197E-13	.1731E-09	.3197E-13	.3197E-13
204	.1836E+00	.1836E+00	.1836E+00	.1836E+00
205	.5621E-13	.1590E-08	.5621E-13	.5621E-13
206	.3334E-14	.3334E-14	.3334E-14	.3334E-14
207	.1491E-16	.4478E-08	.1491E-16	.1491E-16
208	.1922E-15	.5404E+00	.1922E-15	.1922E-15
209	.7030E-12	.2355E+01	.7030E-12	.7030E-12
210	.2460E+01	.2460E+01	.2460E+01	.2460E+01
211	.6503E-13	.6417E-02	.6503E-13	.6503E-13
212	.8223E-15	.8413E-18	.2539E-14	.2539E-14
213	.3199E-18	.1425E+03	.1644E-23	.1644E-23
214	.3286E-02	.3777E-02	.3744E-02	.3744E-02
215	-.2804E-17	-.5985E-17	-.2804E-17	-.6468E-14
216	.9994E+00	.9994E+00	.9994E+00	.9994E+00
217	-.8000E+00	-.8000E+00	-.8000E+00	-.8000E+00
218	-.6536E-25	-.3105E-26	.5364E-25	.5364E-25
219	-.1000E+01	-.1000E+01	-.1000E+01	-.1000E+01
220	.1000E+01	.3024E+02	.1000E+01	.1000E+01
221	-.1000E+01	-.1000E+01	-.1000E+01	-.1000E+01
222	-.1500E+01	-.1500E+01	-.1500E+01	-.1500E+01
223	-.8340E+00	-.8340E+00	-.8340E+00	-.8340E+00
224	-.3040E+03	-.3040E+03	-.3040E+03	-.3040E+03
225	.2000E+01	.2000E+01	.2000E+01	.2000E+01
226	-.5000E+00	-.5000E+00	-.5000E+00	-.5000E+00
227	.1000E+01	.1000E+01	.1000E+01	.1000E+01

k1: 1.

FN	nfp1	nf1	nfp2	nf2	nfp3	nf3	nfp4	nf4
1	57	22	905	304	57	22	57	22
2	50	21	28	11	59	24	59	24
3	19	6	900	299	19	6	19	6
4	7	2	7	2	7	2	7	2
5	24	9	24	9	24	9	24	9
6	29	10	71	24	25	8	25	8
7	34	13	29	10	32	13	30	11
8	17	6	17	6	17	6	17	6
9	32	17	622	207	32	17	29	16
10	35	12	34	11	35	12	35	12
201	15	6	15	6	15	6	15	6
202	44	21	130	45	44	21	44	21
203	36	13	114	39	36	13	36	13
204	22	9	31	12	22	9	22	9
205	42	15	283	96	42	15	42	15
206	25	10	25	10	25	10	25	10
207	39	14	432	145	39	14	39	14
208	119	48	906	305	119	48	119	48
209	457	186	910	309	457	186	457	186
210	35	18	35	18	35	18	35	18
211	77	32	906	305	77	32	77	32
212	41	16	43	16	42	17	42	17
213	326	113	907	306	401	138	401	138
214	107	54	86	41	92	47	92	47
215	22	7	16	5	22	7	22	7
216	41	18	157	62	45	20	51	22
217	25	8	25	8	25	8	25	8
218	118	39	352	117	64	21	64	21
219	87	18	86	17	87	18	114	25
220	193	64	900	299	175	58	254	87
221	79	26	79	26	79	26	79	26
222	19	6	19	6	19	6	19	6
223	30	11	271	94	30	11	33	14
224	13	4	13	4	13	4	13	4
225	19	6	19	6	19	6	19	6
226	27	10	16	5	27	10	27	10
227	17	6	17	6	17	6	17	6
ADD	2379	896	9430	3191	2375	894	2485	932

DISTRIBUTION LIST

Commander
Armament Research, Development and Engineering Center
U.S. Army Armament, Munitions and Chemical Command
ATTN: SMCAR-IMI-I (5)
SMCAR-CO
SMCAR-CCH-V, M. D. Nicolich
SMCAR-FSA-E, W. P. Dunn
SMCAR-FSN-T, A. Garica
SMCAR-TD
SMCAR-TDC
SMCAR-AE (3)
SMCAR-AEE (7)
Picatinny Arsenal, NJ 07806-5000

Commander
U.S. Army Armament, Munitions and Chemical Command
ATTN: AMSMC-GCL (D)
AMSMC-DSM-B
Picatinny Arsenal, NJ 07806-5000

Administrator
Defense Technical Information Center
ATTN: Accessions Division (2)
Cameron Station
Alexandria, VA 22304-6145

Director
U.S. Army Material Systems Analysis Activity
ATTN: AMXSY-MP
AMXSY-RW
Aberdeen Proving Ground, MD 21005-5066

Commander
Chemical Research, Development and Engineering Center
U.S. Army Armament, Munitions and Chemical Command
ATTN: SMCCR-MSI
AMSMC-DCG
AMSMC-DSM-A
Aberdeen Proving Ground, MD 21010-5423

Commander
Chemical Research, Development and Engineering Center
U.S. Army Armament, Munitions and Chemical Command
ATTN: SMCCR-RSP-A
SMCCR-SPS-IL
SMCCR-CO
SMCCR-MU
SMCCR-SPS-M
Aberdeen Proving Ground, MD 21010-5423

Director
Ballistic Research Laboratory
ATTN: AMXBR-OD-ST
SLCBR-TB-EE, D. Bowman
R. Frey
O. Lyman
J. Watson
SLCBR-TB-W, J. Harrison
M. Lampson
J. Kineke
G. Randers-Pehrson
SLCBR-TB-P, K. D. Kimsey
S. Segletes
Aberdeen Proving Ground, MD 21005-5066

Chief
Benet Weapons Laboratory, CCAC
Armament Research, Development and Engineering Center
U.S. Army Armament, Munitions and Chemical Command
ATTN: SMCAR-CCB-TL
Watervliet, NY 12189-5000

Commander
U.S. Army Rock Island Arsenal
ATTN: SMCRI-TI, Technical Library
SMCAR-FSP-D
SMCAR-DS
SMCAR-ESP-L
Rock Island, IL 61299-6000

Director
U.S. Army TRADOC Systems Analysis Activity
ATTN: ATAA-SL
White Sands Missile Range, NM 88002

Commander
U.S. Army Materiel Command
ATTN: AMCDRA-ST
AMCCN-C
AMCLD, D. Vitali
5001 Eisenhower Avenue
Alexandria, VA 22333-0001

Commander
U.S. Army Laboratory Command
ATTN: AMSLC-DL
2800 Powder Mill Road
Adelphi, MD 20783-1145

Director
U.S. Army Aviation Research and Technology Center
ATTN: SAVRT-R, Library
M/S 219-3
Ames Research Center
Moffet Field, CA 94035-1000

Commander
U.S. Army Missile Command
ATTN: AMSMI-RD-CS-R (DOC)
Redstone Arsenal, AL 35898-5010

Commander
U.S. Army Tank-Automotive Command
ATTN: ASQNC-TAC-DIT (Technical Information Center)
Warren, MI 48397-5000

Commander
U.S. Army Field Artillery School
ATTN: ATSF-CSI
Fort Sill, OK 73503-5000

Commander
U.S. Army Infantry School
ATTN: ATSH-CD-CSO-OR
Fort Benning, GA 31905-5660

Director
U.S. Army Research Office
ATTN: Technical Library
P.O. Box 12211
4300 Miami Blvd
Research Triangle Park, NC 27709

Director
U.S. Army Materials Technology Laboratory
ATTN: Technical Library
SLCMT-MRT, A. Chou
J. McLaughlin
C. S. White
Watertown, MA 02172-0001

NIST
ATTN: C. S. Choi
Bldg 235, Reactor Radiation Division
Gaithersberg, MD 20899

Commander
U.S. Army Missile Command
ATTN: SFAE-FS-AM-E, C. Allen
SFAE-FS-HD-E-E-B, R. Bell
SFAE-FS-TO-E-S, G. Haynes
P. Hooper
AMSMI-RD-ST-WF, S. Hill
D. Lovelace
M. Schexnayder
Redstone Arsenal, AL 35898-5250

Chief of Navel Research
Office of Naval Technology
ATTN: ONT-23, A. J. Faulsditch
Ballston Towers
Arlington, VA 22217

Commander
Naval Weapons Center
ATTN: Code 385, A. Amster
Code 3835, K. J. Graham
Code 3261, E. Lundstrom
Code 6214, W. J. McCarter
Code 388, R. Reed, Jr.
Code 320, L. Smith
Code 3268, D. Thompson
Code 3263, T. T. Yee
Technical Library
China Lake, CA 93555

Commander
Naval Surface Weapons Center
ATTN: Code G34, L. Crabtree
J. C. Monolo
J. Vena
Code G22, C. R. Garnett
Code G30, M. Shamblem
Code H11, M. J. Sill
Code G33, L. F. Williams
Technical Library
Dahlgreen, VA 22448-5000

Commander
Naval Surface Weapons Center
ATTN: R12, B. A. Baudler
R. Garret
R. H. Moffet
J. Short
R13, R. R. Bernecker
J. W. Forbes
H. D. Jones
D. G. Tasker
E. Zimet
U43, R. Caminity
U12, H. Chen
A. A. Dare
R10A, C. Dickinson
U11, D. Harris
P. Marshall
G402, P. C. Haung

R10, S. J. Jacobs
R32, T. L. Jungling
R122, L. Roslund
R121, M. Stosz
L. Mensi
P. Walter
F. J. Zerilli
Technical Library
10901 New Hampshire Ave
Silver Spring, MD 20903-5000

Commander
NUSC Newport
ATTN: Code 8214, S. Dickinson
Newport, RI 02841

Commander
Air Force Armament Laboratory
ATTN: AFATL/DLJW, W. Cook
M. Nixon
AFATL/MNW, LT D. Lorey
R. D. Guba
J. Foster
ATAFTL-MNE, G. Parson
Technical Library
Eglin AFB, FL 32542-5434

Director
DARPA
ATTN: LTC J. Beno
J. Richardson
1400 Wilson Blvd
Arlington, VA 22209-2308

Director
DARPA
ATTN: T. Phillips
3701 North Fairfax Dr.
Arlington, VA 22203-1714

Director
Lawrence Livermore National Laboratory
University of California
P.O. Box 808
ATTN: L-122, O. J. Alford
B. R. Bowman
W. Dixon
R. Pierce
R. Rosinsky
D. Stewart
A. Vidlak
R. Whirley
L-35, R. B. Christensen
T. McAbee
C. Simonson
R. E. Tipton
L-11, M. Finger
L-282, L. Green
M. Murphey
R. Simpson
P. Souers
C. Tarver
L-290, A. Holt
J. E. Reaugh
L-874, R. M. Kuklo
L-352, D. Wood
Technical Library
Livermore, CA 94550

Director
Los Alamos National Laboratory
ATTN: MS F663, T. F. Adams
G. E. Cort
D. Mandell
MS J960, E. Fern
J. Hull
R. Karpp
MS 970, J. Goforth
S. Marsh
MS G740. R. Greiner
MS K557, R. Henninger
MS F669, J. V. Repa

MS B214, J. P. Ritchie
MS K574, A. Rollett
Technical Library
P.O. Box 1663
Los Alamos, NM 87545

Director
Sandia National Laboratory
ATTN: Division 2512, W. J. Andrzejewski
D. Marchi
Division 1431, M. G. Elrick
E. S. Hertel, Jr.
J. M. McGlaun
A. C. Robinson
Division 1433, D. E. Grady
Division 1551, R. Graham
R. Lafarge
Division 9122, J .Hickerson
R. O. Nellums
Division 1432, G. I. Kerley
M. E. Kipp
P. Yarrington
Technical Library
P.O. Box 5800
Albuquerque, NM 87185

Aerojet Ordnance Company
Experimental Technology Center
ATTN: G. Padgett
P. Wolf
1100 Bulloch Blvd
Socorro, NM 87801

Aerojet Precision Weapons
Dept. 5131/T-W
ATTN: D. Bender
J. Carleone
D. Donati
H. Hope
R. S. Kowell
1100 Hoyvale Dr.
Azusa, CA 91702

Alliant Techsystems, Inc.
ATTN: K. L. Christianson
T. Holmquist
G. R. Johnson
R. Stryk
MN 48-2700
7225 Northland Drive
Brooklyn Park, MN 55428

Applied Ordnance Technology, Inc.
ATTN: NIMIC, Eddie Norton
1000 Century Plaza, Suite 212, Box 24
10630 Little Patuxent Parkway
Columbia, MD 21044

Babcock & Wilcox
ATTN: K. Camplin
J. R. Mallory, Jr.
P.O. Box 1165
Lynchburg, VA 24506

Batelle Northwest
ATTN: J. B. Brown, Jr.
MSIN 3 K5-22
P.O. Box 999
Richmond, WA 99352

Battelle
ATTN: C. R. Hargreaves
B. D. Trott
L. E. Vescelius
505 Kin Ave
Columbus, OH 43201-2693

Boeing Corporation
ATTN: K. Housen, MS 87-60
T. M. Murray, MS 84-84
P. O. Box 3999
Seattle, WA 98124

California Research & Technology Corp.
ATTN: R. Brown
5117 Johnson Drive
Pleasonton, CA 94566

California Research & Technology Corp
ATTN: M. Mejerus
P.O. Box 2229
Princeton, NJ 08543-2229

Conventional Munitions Systems
ATTN: R. A. Snow
W. Schwartz
4904 Eisenhower Blvd, Suite 310
Tampa, FL 33634

Dyna East Corporation
ATTN: P. C. Chou
R. Ciccarelli
W. Flis
3201 Arch Street
Philadelphia, PA 19104

Enig Associates, Inc.
ATTN: J. W. Enig
11120 New Hampshire Ave.
Suite 500
Silver Spring, MD 20904-2633

Explosive Technology
ATTN: J. Kennedy
M. L. Knaebel
P.O. Box KK
Fairfield, CA 94533

Kaman Sciences Corporation
ATTN: D. Barnette
D. Elder
P. Russell
P.O. Box 7463
Colorado Springs, CO 80933-7463

General Dynamics
ATTN: J. Cuadros
P.O. Box 50-800
Mail Zone 601-87
Ontario, CA 91761-1085

General Research Corporation
ATTN: A. Charters
T. Menna
P.O. Box 6770
Santa Barbara, CA 93160-6770

Livermore Software Technology Corp.
ATTN: J. O. Hallquist
2876 Waverly Way
Livermore, CA 94550

Lockheed Missile & Space Co., Inc.
ATTN: S. Kusumi, 0-81-11, Bldg 157
J. Phillips, 0-54-50
P.O. Box 3504
Sunnyvale, CA 94088

Lockheed Missile & Space Co., Inc.
ATTN: R. A. Hoffmann
Santa Cruz Facility
Empire Grade Road
Santa Cruz, CA 95060

Mason & Hanger - Silas Mason Co.
ATTN: A. Larson
J. Leeper
Iowa Army Ammunition Plant
Middletown, IA 52638-9701

McDonnell-Douglas Helicopter
ATTN: L. R. Bird
L. A. Mason
5000 E. McDowell Road, MS 543-D216
Mesa, AZ 85205

Nuclear Metals Inc.
ATTN: J. Schreiber
2229 Main Street
Concord, MA 01742

Orlando Technology, Inc.
ATTN: J. D. Abrams
M. Gunger
D. Matuska
J. Osborn
R. D. Szczepanski
P.O. Box 855
Shalimar, FL 32579

Physics International
ATTN: R. Funston
L. Garnett
J. Hudson
2700 Merced Street
P.O. Box 5010
San Leandro, CA 94577

Martin Marietta
ATTN: J. Conner
K. Fitsgerald
P. O. Box 2788, MS 8733
Denton, TX 76202

Rockwell Missile Systems Division
ATTN: M. Buchbinder
D. M. Windeljohn
1800 Satellite Blvd.
Duluth, GA 30136

S-Cubed
ATTN: R. Sedgwick
P.O. Box 1620
LaJolla, CA 92038-1620

Schlumberger Perforating & Test
ATTN: M. T. Gonzalez
D. Markel
P.O. Box 1590
14910 Ariline Road
Rosharon, TX 77583-1590

Southwest Research Institute
ATTN: C. E. Anderson
J. D. Walker
A. Wenzel
P.O. Drawer 28255
San Antonio, TX 78228-0225